

ULTRAWIDEBAND CHANNEL SOUNDING STUDIES IN OUTDOOR AND OUTDOOR-INDOOR ENVIRONMENTS

BY

JOSEPH AJAY NEIL NORONHA

Thesis submitted to the Faculty of the
Virginia Polytechnic Institute and State University
In partial fulfillment of the requirements of the degree of

MASTER OF SCIENCE
in
Electrical Engineering

Dr. D. G. Sweeney (Chair)
Dr. R. M. Buehrer
Dr. J. H. Reed

June 7th, 2004
Virginia Polytechnic Institute and State University
Blacksburg, VA

Keywords: Ultrawideband (UWB), Pathloss, Penetration Loss, Delay Spread, Power Delay
Profile

ULTRAWIDEBAND CHANNEL SOUNDING STUDIES IN OUTDOOR AND OUTDOOR-INDOOR ENVIRONMENTS

Joseph Ajay Neil Noronha

Abstract

Ultrawideband (UWB) is one of the most promising communication technologies in recent times with the promise of high data rates and spectral reuse.

This work analyses the outdoor and outdoor-to-indoor propagating characteristics of the UWB pulse, which can be of the order of a few gigahertz in bandwidth. The aim of the thesis is to provide the parameters needed in order to develop a channel model for such cases. The channel model would then play an important role in determining physical layer (PHY) solutions to optimally exploit these characteristics.

The measurements carried out on the Virginia Tech campus are used to compute parameters such as path loss, penetration loss and delay statistics. These are carried out in multiple frequency bands and the results are compared across frequency bands to determine effect of different frequency levels on the parameters.

Finally the results are analyzed with respect to similar parameters obtained in other measurement campaigns in an attempt to evaluate the performance of Ultrawideband vis-à-vis narrowband systems.

Acknowledgements

First and foremost I would like to thank my Creator who has been most generous in every possible way. Without his presence in my life I would not have achieved anything.

I would like to place my sincere gratitude to Dr. Sweeney for being a great advisor, encouraging me to always aim higher and providing hours of unstinted support and assistance.

I am grateful to both Dr. Buehrer and Dr. Reed for their suggestions and support towards the successful completion of this work. I appreciate your taking time of a busy schedule to help me especially with the data analysis.

I would like to also thank Timothy Bielawa, Thomas Rondeau and Timothy Gallagher for their assistance in both the measurements and the data analysis that followed.

Last but not the least I owe a lot to my parents and sister for their sacrifices which has helped me to reach where I am today.

Contents

1	Introduction.....	1
2	The Ultrawideband Propagation Environment	5
3	Measurement System	10
3.1	Channel Sounder.....	10
3.1.1	Measurement Transmitter	10
3.1.2	Measurement System Receiver and Timing	11
3.1.3	UWB Antenna.....	12
3.2	Measurement Locations	13
3.3	Reference Measurements	16
3.4	Data Processing.....	18
4	Outdoor Ultrawideband Measurements	23
4.1	Pathloss	23
4.1.1	2-4 GHz.....	24
4.1.2	6-7 GHz.....	26
4.1.3	1-2 GHz.....	28
4.2	Power Delay Profile (PDP) and Time Dispersion Parameters.....	31
4.2.1	2-4 GHz.....	31
4.2.2	6-7 GHz.....	32
4.2.3	1-2 GHz.....	33
4.3	Characterization of Multipath Components.....	35
4.3.1	2-4 GHz.....	35
4.3.2	6-7 GHz.....	36
4.3.3	1-2 GHz.....	37
5	Outdoor-to-Indoor Measurements	39
5.1	Pathloss	39
5.1.1	200-400 MHz	39
5.1.2	6-7 GHz.....	44
5.2	Characterization of the Multipath	49
5.2.1	200-400 MHz	49
5.2.2	6-7 GHz.....	55
5.3	Penetration Loss.....	60
5.3.1	200-400 MHz	60
5.3.2	6-7 GHz.....	60
6	Evaluation of the Empirical Ultrawideband Parameters.....	62
6.1	Outdoor Measurements	62
6.1.1	Pathloss	63
6.1.2	Small Scale Time Parameters	64
6.2	Outdoor-to-Indoor Penetration Loss	66
7	Conclusion	70
8	Appendix.....	72
8.1	Appendix I - Sample Outdoor Setup with sets of received data	72
8.2	Appendix II – Outdoor-to-Indoor Measurement Locations.....	75
8.3	Appendix III - Outdoor Measurement Locations.....	77
9	References.....	80

List of Figures

Figure 1.1 FCC Spectral Mask for UWB for short-range communications [2].....	2
Figure 2.1 Pulse with high energy per pulse and low average energy ($T_f \gg T_p$).....	6
Figure 3.1 Channel Sounder	11
Figure 3.2 Timing Diagram	12
Figure 3.3 Received Time-Domain Waveform of the CBAS Link	12
Figure 3.4 Received Time-Domain Waveform of the Vivaldi Link.....	12
Figure 3.5 Antenna Pattern of the Vivaldi Aerial	13
Figure 3.6 Reference Pulse (1-2 GHz).....	14
Figure 3.7 Sample Measurement Location	15
Figure 3.8 Reference Pulse (200 – 400 MHz)	16
Figure 3.9 2.0- 4.0 GHz Reference Pulse	17
Figure 3.10 6.0 – 7.0 GHz Reference LOS Pulse. The displayed pulse is the 1.0 – 2.0 GHz the output of the 6.0 – 7.0 GHz downconverter.....	17
Figure 3.11 Reference Pulse 1-2 GHz	18
Figure 3.12 Grid used for the Measurements.....	19
Figure 3.13 Effect of Averaging on SNR	20
Figure 3.14 Outdoor-Indoor Penetration Loss Calculation Arrangement	22
Figure 4.1 Perry Street LOS.....	23
Figure 4.2: 2.0 – 4.0 GHz LOS Pathloss referenced to free space including all locations..	24
Figure 4.3 2.0 – 4.0 GHz NLOS Pathloss using all received energy for all locations.....	25
Figure 4.4 2.0 – 4.0 GHz NLOS Pathloss using only the strongest component for all locations	26
Figure 4.5 LOS Pathloss for all locations	27
Figure 4.6 NLOS Pathloss with total received energy for all locations.....	27
Figure 4.7 NLOS Pathloss with only strongest multipath for all locations	28
Figure 4.8 1.0 – 2.0 GHz Outdoor LOS Pathloss	29
Figure 4.9 1.0 – 2.0 GHz NLOS Pathloss including all multipath components	30
Figure 4.10 1.0 – 2.0 GHz NLOS Pathloss considering only the strongest multipath component.....	30
Figure 4.11 Burchard Hall 1, discrete clusters of multipath (inset – zoomed in version) ...	31
Figure 4.12 Burchard Hall 1, Clustering of Multipath in Time Domain	32
Figure 4.13 PDP at Cowgill Hall at 6.0198m. Note the early arriving pulse	33
Figure 4.14 Power delay profile at Cowgill Hall.....	34
Figure 4.15 Burchard Hall 1, Multipath Number and Energy at 10.34m NLOS.....	35
Figure 4.16 : Strongest Multipath is >50% of total Energy Received.....	36
Figure 4.17 Number and energy of observed multipath at Cowgill.	36
Figure 4.18 Comparison between strongest multipath component and total energy received at Burchard 1.....	37
Figure 4.19 Number and Strength of Multipath at Cowgill Hall.....	38
Figure 4.20: Largest Component and Total Energy of all Multipath at Cowgill Hall.....	38
Figure 5.1 Total Energy Pathloss in Modular Building.....	40
Figure 5.2 Pathloss of Strongest Multipath Component in Modular Building.....	40
Figure 5.3 Durham Hall Total Energy Pathloss.....	42

Figure 5.4 Durham Hall Pathloss with Strongest Multipath only.....	42
Figure 5.5 Randolph Hall Total Energy Pathloss	43
Figure 5.6 Randolph Hall Pathloss with Strongest Multipath only	43
Figure 5.7 Total Pathloss at Modular Building.....	44
Figure 5.8 Strongest Path Pathloss at Modular Building.....	45
Figure 5.9 Total pathloss at Durham Hall employing all measurements.....	46
Figure 5.10 Strongest multipath component pathloss at Durham Hall employing all measurements.....	47
Figure 5.11 Durham Hall pathloss at short range employing all multipath components	47
Figure 5.12 Durham Hall pathloss at long range employing all multipath components	48
Figure 5.13 Durham Hall pathloss at short range employing only the strongest component	48
Figure 5.14 Durham Hall pathloss at long range employing only the strongest component	49
Figure 5.15 Sample Power Delay Profile from the Modular Building.....	50
Figure 5.16: Sample Power Delay Profile from Durham Hall.....	50
Figure 5.17 Sample Power Delay Profile from Randolph Hall	51
Figure 5.18 Modular Building Multipath Time Distribution.....	52
Figure 5.19 Durham Hall Multipath Time Distribution.....	53
Figure 5.20 Randolph Hall Multipath Time Distribution	53
Figure 5.21 Comparison of Total Energy with Largest Multipath Component at the Modular Building.....	54
Figure 5.22 Comparison of Total Energy with Largest Multipath Component at Durham Hall.....	54
Figure 5.23 Comparison of Total Energy with Largest Multipath Component at Randolph Hall.....	55
Figure 5.24 Power Delay Profile at the Modular Building.....	56
Figure 5.25 Power Delay Profile at Durham Hall.....	56
Figure 5.26 Combining of successive multipath components	57
Figure 5.27 Plot of Energy and Number of Multipath Components in the Modular Building	58
Figure 5.28 Plot of Energy and Number of Multipath Components in Durham Hall	59
Figure 5.29 Relation of Total Energy and Strongest Multipath Component in the Modular Building.....	59
Figure 5.30 Relation of Total Energy and Strongest Multipath Component in Durham Hall	60
Figure 6.1 Variation in RMS Delay spread obtained for UWB versus other campaigns	65
Figure 6.2 Frequency selective transmission.....	67
Figure 6.3 Variation of penetration loss with frequency in propagation through different materials.....	69
Figure 6.4 Trend indicating variation of pathloss vs. frequency in different materials.....	70
Figure 8.1 Burchard Hall Measurement Locations.....	72
Figure 8.2 Burchard Hall measurement location. This picture is the transmitter location in the lower right of Figure 8.1	72
Figure 8.3 Location next to Cowgill Hall with a bounce path off Hancock. The Modular Building is to the left.....	73
Figure 8.4 Burchard Hall NLOS path.....	73

Figure 8.5 Cowgill Hall NLOS path. Multiple Multipath off Adjacent Walls - Canyon Environment..... 74

Figure 8.6 Burchard Hall NLOS, note the resolvable multipath components 74

Figure 8.7 Modular Building Transmitter and Receiver Locations. The transmitter location is the X to the right of the building and the receiver is placed a various locations down the center hall. The receiver locations are approximately 0.3 meters apart..... 75

Figure 8.8 Randolph Hall Transmitter and Receiver Locations. The transmitter location is the X in the right center and the receiver is placed a various locations down the center hall on the same level as the transmitter. The reference measurement was taken at the “REF” X at the center right. The receiver locations are approximately 0.3 meters apart..... 76

Figure 8.9 Durham Hall Transmitter and Receiver Locations. The transmitter location is the X in the lower right and the receiver is placed a various locations down the center hall on the same level as the transmitter. Two reference measurements were taken. These are located at REF 1 and REF 2 in the vestibule. The receiver locations are approximately 0.3 meters apart..... 76

Figure 8.10. Burchard hall Location 1 The receiver is placed next to the two air handlers on top of Burchard (green crosses), and it faces parallel to the path. The transmitter is placed on top of the unfinished stairwell (red cross, lower left) so that the path from the transmitter to receiver is blocked by the air handlers 77

Figure 8.11 Burchard 2 location. Transmitter is placed next to the skylight, facing the stairwell (red cross, center left). The receiver (green crosses) starts 1.5 meters back from the stairwell and moves in 1.5 meter increments. The receiver antenna is facing the stairwell. This gives a line of sight signal that is much weaker than the first multipath. Most of the received signal comes from the bounce off the stairwell 77

Figure 8.12 Burchard Hall Location 3. The transmitter (red cross, center) is placed between Burruss Hall and Burchard Hall, facing Burchard. The receiver (green crosses, lower center) moves along the same track as in Burchard 2, except that the antenna is now facing Burruss 78

Figure 8.13 Hancock Hall The transmitter (red cross, center) and receiver (green crosses, front center) are placed perpendicular to each other 7.2 meters apart. The receiver moves back 1.5 meters at a time eventually being blocked from the transmitter by Hancock Hall 78

Figure 8.14 Cowgill location. The transmitter (red cross, upper right) and the receiver (green crosses, center) are placed beside each other facing the wall of Hancock. The receiver is moved closer to Hancock 1.5 meters feet at a time. The first multi-path is the strongest as the line of sight signal is received in the side and back lobes of the receiver antenna 79

The figures have been taken with permission from the DARPA NETEX report on Ultrawideband Channel Sounding.

List of Tables

Table 3.1 Filters and Transmitter Power.....	10
Table 4.1 Outdoor Pathloss Exponents for 2.0 - 4.0 GHz	24
Table 4.2 Outdoor Pathloss Exponents for 6.0 - 7.0 GHz	26
Table 4.3 Outdoor Pathloss Exponents for 1.0 - 2.0 GHz	28
Table 4.4 Small Scale Time Parameters for 2.0 – 4.0 GHz outdoors	32
Table 4.5 Small Scale Time Parameters for 6.0 – 7.0 GHz	33
Table 4.6 Small Scale Time Parameters for outdoor 1.0 – 2.0 GHz.....	34
Table 5.1 Pathloss at Modular Building	40
Table 5.2 Path Loss exponents and Standard Deviation for Durham Hall and Randolph Hall	41
Table 5.3 6.0 – 7.0 GHz Pathloss Exponents.....	44
Table 5.4: Comparison of pathloss exponents in Durham Hall.....	45
Table 5.5 Small Scale Time Parameters	51
Table 5.6: Small Scale Time Parameters	57
Table 5.7 Summary of Penetration Loss (200 – 400 MHz).....	60
Table 5.8 Penetration Loss at 6.0 – 7.0 GHz	61
Table 6.1 Comparison of outdoor path loss exponents obtained by various researchers with our UWB path loss exponents in the 1.0 – 2.0 GHz band.	63
Table 6.2 Comparison of outdoor path loss exponents obtained by various researchers with our UWB path loss exponents in the 2.0 – 4.0 GHz band.	63
Table 6.3 Comparison of outdoor path loss exponents obtained by various researchers with our UWB path loss exponents in the 6.0 – 7.0 GHz band.	63
Table 6.4 Comparison of outdoor delay spread reported by various researchers with our UWB path loss exponents in the 1.0 – 2.0 GHz band.....	64
Table 6.5 Comparison of outdoor delay spread reported by various researchers with our UWB path loss exponents in the 2.0 – 4.0 GHz band.....	64
Table 6.6 Comparison of outdoor delay spread reported by various researchers with our UWB path loss exponents in the 6.0 – 7.0 GHz band.....	65
Table 6.7 Comparison of Measured Penetration Loss	66
Table 6.8 Comparison of Pathloss Exponents	69

1 Introduction

Ultrawideband (UWB) is a communications technology with the potential to provide high data-rate wireless services with relatively simple low power radio hardware. The Federal Communications Commission's (FCC) first report and order on February 14, 2002 [2], heralded the first attempt towards the standardization of a system for different applications with the allocated frequency bands being collocated with existing licensed spectrum. From a telecommunications standpoint, data rates of the order of gigabits per second were seen possible over short distances in the unlicensed regime. Given the enormous bandwidth available, UWB has attracted the attention of a large number of manufacturers with potential applications from short-distance, high data rate multimedia communications to medical imaging.

This has come at an opportune time when most of the RF spectrum (1 – 10 GHz) has already been partitioned and allocated to licensed operators – resulting in a drought of available spectrum. UWB seems to provide the very answer to this problem offering the possibility of both spectrum reuse and coexistence with existing narrowband systems. Furthermore, advances in VLSI technology have enabled on-chip implementations feasible making UWB systems a very attractive proposition.

The nomenclature of *Ultrawideband* was provided primarily by the Department of Defense (U.S.A) around 1989 in respect to impulse-based systems. In it's most basic form the FCC defined UWB as any system with a fractional bandwidth of greater than 20%, or a system with a bandwidth greater than 500MHz [2].

Specifically

$$\frac{f_H - f_L}{(f_H + f_L)/2} > 20\% \quad \text{Eqn. 1.1}$$

where f_H and f_L defined the upper and lower bounds of the 10dB bandwidth respectively. In addition, the FCC also prescribed a spectral mask (Figure 1.1) that would provide some level of interference protection to critical bands such as GPS. In the U.S.A

the frequencies between 3.1 – 10.6 GHz were allocated for short-range communication systems. Depending upon the application i.e. ranging or imaging the spectral mask was accordingly adjusted depending upon the potential interference provided by the intended application to existing users.

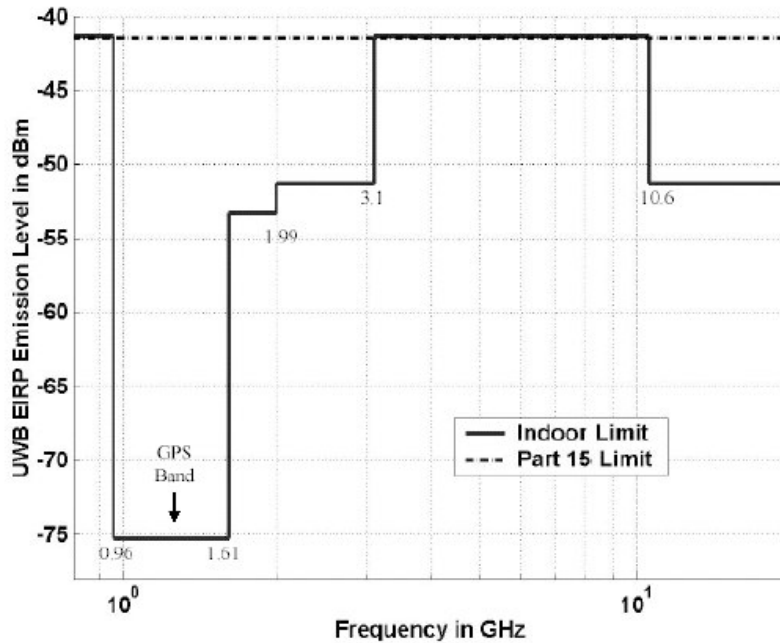


Figure 1.1 FCC Spectral Mask for UWB for short-range communications [2]

With these definitions in hand a great deal of work has been done in analyzing the UWB propagation environment [7] and in the use of sub-nanosecond pulses [6] to satisfy the given mask. Two flavors of UWB have since developed – Impulse UWB (I-UWB) which uses short pulses to transmit data and Multi-band OFDM-UWB, which makes use of spread spectrum techniques to spread the information across the available frequency band. The work carried out for this thesis is attuned towards the former, using sub-nanosecond pulses to sound and obtain the channel characteristics.

A bulk of the propagation studies [3] and corresponding channel models [7] which have been developed have catered largely to indoor environments, since UWB, in its present form is best suited for high data rate, short-range communications in dense multipath environments. This is due to the fine time resolution afforded by the sub-nanosecond pulses along with the power-limited regime under which it is allowed to operate.

This thesis analyzes the propagation mechanism of ultrawideband across different frequencies and environments. This research is primarily focused on outdoor and outdoor-to-indoor environments, which have not been studied as evident from the lack of available literature [8], [4]. There are several challenges in undertaking UWB outdoor channel sounding. There is a lack of dense, resolvable multipath as is available indoors, since the distances between reflecting surfaces are typically far greater as compared to indoor locations. The low maximum transmit power of -41 dBm/MHz severely restricts the maximum range. At the receiver, the large bandwidth required at the front end increases the noise bandwidth that reduces the sensitivity of the receiver. However there are several applications, both civil and military such as sensor networks and imaging that operate at low data rates in such environments. The work is primarily aimed at such applications where information about the channel would be a useful tool in the PHY design.

The thesis is comprised of the following sections. Chapter II serves as a literature review, and in doing so highlights the lack of results in UWB outdoor propagation. It also serves to introduce the parameters which are required for the development of a channel model, namely pathloss, power delay profile (PDP) and small-scale time parameters for the outdoor propagation and penetration loss for the outdoor-to-indoor propagation. The section further discusses how these parameters should be analyzed given that the measurements no longer use CW signals and the signals could potentially occupy bandwidths of the order of gigahertz.

Chapter III describes the hardware designed to undertake the measurements in the bands of 200-400 MHz, 1.0-2.0 GHz, 2.0-4.0 GHz and 6.0-7.0 GHz. It also throws light on the issue of antenna design for Ultrawideband systems. A description of the locations chosen for both outdoor channel sounding and buildings used for the penetration loss experiments is provided. The chapter discusses the post processing carried out on the obtained data with the necessary computations to obtain the channel parameters.

Chapter IV and V analyze the results obtained from the outdoor and outdoor-to-indoor propagation experiments respectively. This is done in sequential order for each individual frequency band under consideration. The pathloss, power delay profile and the small-scale time parameters are obtained for each frequency band. In Chapter V the penetration loss is also calculated in addition to the other channel parameters. At each stage the parameters

obtained are discussed with respect to the environment in which the measurements are taken to aid in interpreting the results. Additional results in terms of energy per multipath component are also provided.

In Chapter VI the parameters are compared against results, both narrowband and ultrawideband obtained in the available scientific literature. Given the paucity of published outdoor UWB literature this serves in part in an attempt to validate the results. At the same time differing results provide a tool to compare the UWB propagation characteristics vis-à-vis narrowband continuous wave (CW) parameters at similar frequencies.

Chapter VII concludes the thesis, highlighting the main points of the discussion and providing some pointers towards potential applications and possible future work to further this study.

2 The Ultrawideband Propagation Environment

Channel sounding is used to estimate parameters to develop a channel model. The signal that is transmitted propagates through the channel and experiences multiple echoes before reaching the receiver. These multipath components suffer different levels of delay and attenuation depending upon the path. The signal also experiences large scale fading in terms of pathloss. These measurements are statistically averaged to serve as parameters for the channel model.

Large-scale parameters are characterized in terms of pathloss that describes the average signal strength over a distance in terms of the pathloss exponent. It provides an estimate of the rate at which the signal fades over a large area. Traditional pathloss models have made use of Friis' free space propagation model where the wavelength λ was the frequency of transmission.

$$L = \left(\frac{4\pi l}{\lambda} \right)^2 \quad \text{Eqn. 2.1}$$

In the Friis equation the wavelength is factored in due to the gain of the antenna $G = \frac{4\pi A_e}{\lambda^2}$ where A_e is the effective aperture of the antenna. The pathloss is thus dependent on the frequency dependent gain of the antenna.

Siwiak [4] carried out studies in indoor environments taking the frequency as the center frequency of the UWB pulse. In computing the pathloss he considered the center frequency of the UWB pulse in determining the exponent. However given the bandwidth involved and the pulse shape dependent power spectral density it seems impractical to use the same for UWB systems as an accurate estimate of path loss. To better estimate of the pathloss exponent we determine the ratio of the total energy received over all frequencies of interest to the total energy received at a known reference distance. At the receiver this energy would include all the multipath components received above a predetermined threshold. In this manner since both the reference and received pulse have the same frequency dependent characteristic the common frequency component is eliminated in the pathloss computation.

The noise floor of the receiver defines the threshold. At the same time we also compute the pathloss due to the strongest path, which would typically be the LOS path.

$$\left[\frac{E_r}{E_{ref}} \right]_{average} = \left(\frac{d_{ref}}{d} \right)^n \quad \text{Eqn. 2.2}$$

where

$$E_r = \int_{f_1}^{f_2} E_r(f) df$$

- E_r Energy received at distance d
- E_{ref} Energy received at reference d_{ref} assuming free space propagation
- n Pathloss exponent
- f_1, f_2 Frequencies denoting upper and lower 10dB points

It is also important to note that when we consider energy in our discussions we refer to the total energy in a single pulse. Consider the following pulse stream as indicated in Figure 2.1.

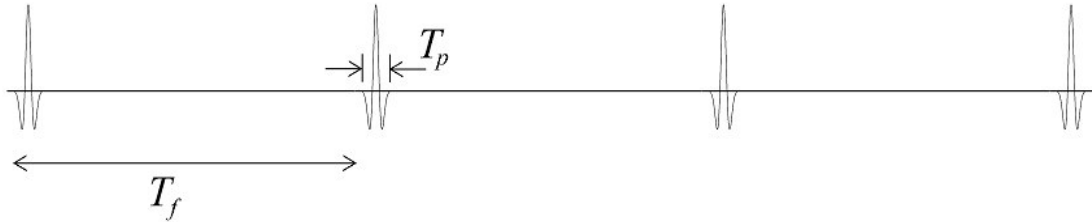


Figure 2.1 Pulse with high energy per pulse and low average energy ($T_f \gg T_p$)

Where

$$E_{total} = \int_0^{T_p} E(t) dt \quad \text{Eqn. 2.3}$$

$$E_{avg} = \frac{T_p}{T_f} E_{total} \quad \text{Eqn. 2.4}$$

This is unlike CW signals where average energy is considered. In I-UWB systems due to a low pulse repetition rate (T_f) as compared to the pulse time period (T_p) it would be

possible to have a low average energy while transmitting a high peak energy signal. In this case the total energy would be a better representation of the transmit energy.

The work by Cassioli [5] along with Siwiak [4], both carried out in indoor environments indicate that as compared to narrowband CW signals UWB would tend to have lower pathloss. However due to larger distances between reflecting surfaces at outdoor locations the total signal received above the threshold would be made up of fewer multipath components. This would lead to a greater pathloss. It is also seen that the UWB signal is not subjected to destructive interference of the incoming multipath at the receiver – the signals arriving as delayed resolvable echoes. This is also observed in outdoor channels.

The single work carried out specifically in UWB outdoor propagation is by Win [8] in a semi-rural environment. The study caters towards the penetration of UWB baseband (centered at 1.3 GHz) pulses through trees and provides results of time based small-scale parameters. It is observed that the delay statistics are in the order of tens of nanoseconds, which is evident due to the outdoor environment. In other studies [7], [5] undertaken towards the development of the UWB standard it is observed that few multipath components overlap each other resulting in reduced interference. These studies, which were carried out in indoor environments observe a pathloss less than two and delay statistics less than ten nanoseconds. At the same time the multipath is no longer continuous and there can be delay bins in which no multipath components fall and are empty. This can also be observed in outdoor environments since the arrival interval of the multipath is dependent on the difference in distance between the LOS pulse and reflected pulse. Assuming a pulse-width of 0.3ns corresponding to a bandwidth of 3 GHz destructive interference will occur if the differential delay is less than 0.15ns i.e. a path difference of 0.45m. This is not characteristic of outdoor propagation where the path differences are typically of greater orders of magnitude unless the receiver is surrounded by clutter.

RMS delay spread, power delay profile (PDP) and excess delay are the means of describing the primary characteristics of the multipath channel. Since the ultimate goal would be to develop a complete channel model we aim to provide the above-described parameters, which typically define the channel model. This would be based on the type of

environment (outdoor/ outdoor-to-indoor) and path (LOS/NLOS). As illustrated in [8] as the distance increases the delay spread could increase to reflect the different paths.

The mean excess delay is the first moment of the PDP while the rms delay spread is the square root of the second central moment of the PDP.

$$\begin{aligned} \bar{\tau} &= \frac{\sum_k a_k^2 \tau_k}{\sum_k a_k^2} \\ \bar{\tau}^2 &= \frac{\sum_k a_k^2 \tau_k^2}{\sum_k a_k^2} \\ \sigma_\tau &= \sqrt{\bar{\tau}^2 - (\bar{\tau})^2} \end{aligned} \tag{Eqn. 2.5}$$

Where

a_k Amplitude of the k^{th} multipath component.

τ_k Time delay of the k^{th} multipath component with respect to the first arriving multipath

The delays are measured with respect to the first arriving signal. Given the small pulse-width, it is intuitive that the multipath components will be specular. Another factor that is taken into account is the environment in which the multipath are received. In indoor environments [3] it is possible to detect the presence of a large number of multipath components due to the numerous paths obtained from reflections off the indoor surfaces. However in outdoor environments, the absence of reflecting surfaces along with decreased sensitivity at the receiver due to the large receiver noise bandwidth severely limits the number of multipath that can be detected .

There has been little research carried out in analyzing the outdoor-to-indoor penetration with respect to ultrawideband [41]. The sub-gigahertz band of 200-400 MHz is within the FCC band for imaging and sensing applications. This is also the military UHF communication band. The channel sounding in the band was suggested by our sponsors. UWB may have some unique advantages in this respect. The bandwidth available may overcome any frequency selective attenuation by surfaces as seen in narrowband CW

signals. At the same time the fine time resolution offered is useful in imaging applications. The 6-7 GHz band is also studied with regards to wireless LAN based applications. Given that commercial environments have different architectural features of windows, concrete and glass walls etc. the pulse can not only propagate through the walls but also penetrate through the other openings. The work by Durgin [29] serves as a tool of reference in the study of the penetration loss. Along with the penetration loss, the contribution of pathloss for such types of propagation is also studied. Finally an attempt is made to extrapolate the results based on the different frequency bands used similar to the attempt by Devasirvatham [23].

3 Measurement System

3.1 Channel Sounder

The channel measurements are taken with the VA Tech short pulse channel sounder. The sounder employs a pulse generator in the transmitter and a sliding correlator sampler for the receiver. A block diagram of the sounder is shown in Figure 3.1. It differs from conventional UWB systems in that the output is band-limited. This is consistent with the FCC definition of UWB. The FCC spectrum mask above 950 MHz assumes a bandpass system rather than a simple baseband impulse. This is accomplished using bandpass filters. Table 3.1 tabulates the available filters and the peak power available for each band. Each filter is a three-section filter with a Butterworth response since they provide a good impulse response.

Table 3.1 Filters and Transmitter Power

3dB BW	Peak Transmitter Power (W)
200 – 400 MHz	1.0
1000 – 2000 MHz	0.25
2.0 – 4.0 GHz	0.5
6.0 – 7.0 GHz	1.0

3.1.1 Measurement Transmitter

The transmitter operates at 200,000 pulses per second with 5 μ sec repetition time limiting the maximum range to approximately 1500 m. The total time of flight plus the delay of any multipath components must be less than 5 μ sec. The transmitter pulser employs a step recovery diode (SRD) [12]. It creates a 500 psec Gaussian monocycle, which is bandpass filtered and amplified. The clock for the transmitter is a 10 MHz oven controlled crystal oscillator (OCXO). The OCXO is operated from a battery backed up supply to insure long-term stability, and the transmitter and receiver oscillators are “zero beat” before each measurement run.

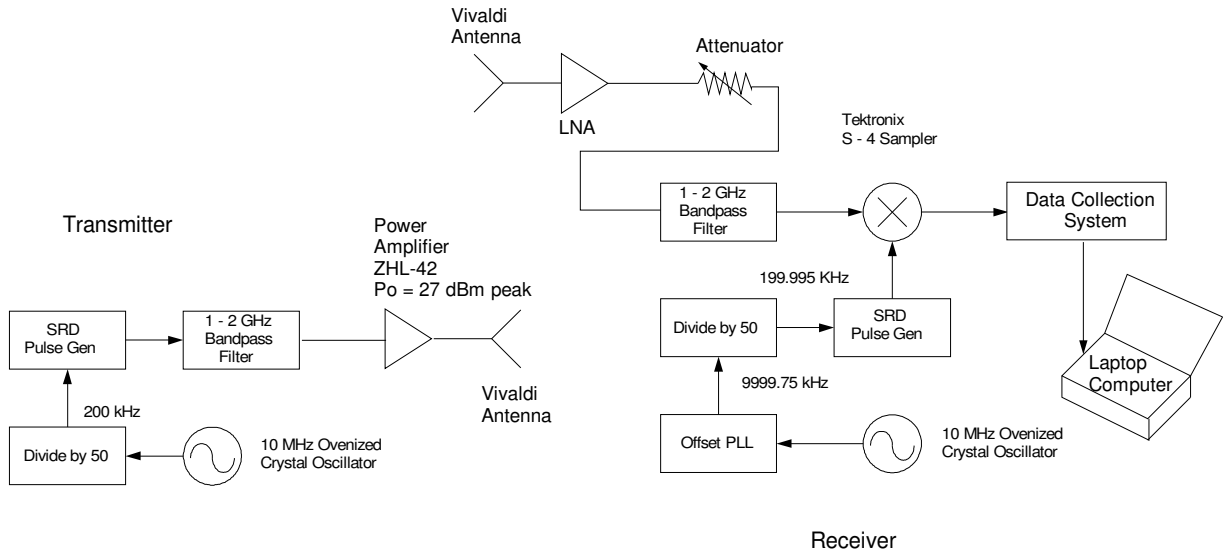


Figure 3.1 Channel Sounder

3.1.2 Measurement System Receiver and Timing

The receiver employs a high-speed sampler where the sampler operates at a slightly lower rate than the transmitter. The result is that the sampling instant progresses in time with respect to the transmitter pulse. The transmitter runs at 200,000 pulses per second (5μsec) and the receiver runs at 199,995 samples per second. The time between each receiver sample is 5μsec + 125 psec. The effective sampling rate is 8GHz. However, it requires 40,000 transmitter pulses for the receiver to step through the entire 5μsec between transmitter pulses. This time dilation requires 200ms being required to acquire one PDP. The time dilation factor can be computed as given in Eqn. 3.1.

$$TD = \frac{\alpha}{\alpha - \beta} = \frac{200,000}{200,000 - 199,995} = 40,000 \quad \text{Eqn. 3.1}$$

Time dilation factor

α : Transmitter pulse rate

β : Receiver sample rate

Figure 3.2 describes this effect graphically.

The receiver timing is controlled by an OCXO similar to the one in the transmitter.

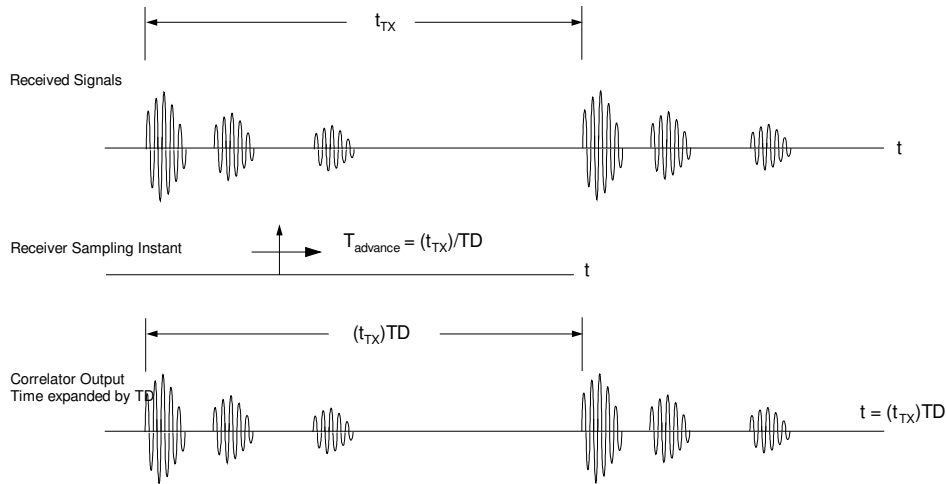


Figure 3.2 Timing Diagram

3.1.3 UWB Antenna

Other campaigns [13] have glossed over the importance of the antenna in developing a UWB propagation model, although antennas widely vary in their response towards an impulse. It is found that classical broadband antennas may not be useful for impulsive based applications. A comparison between the impulse response of the Archimedian spiral and a Vivaldi antenna is given in Figure 3.3 and Figure 3.4. The spiral has a wide 10:1 bandwidth. In the time domain it produces a ringing effect resulting in a large tail that is reflected in its impulse response.

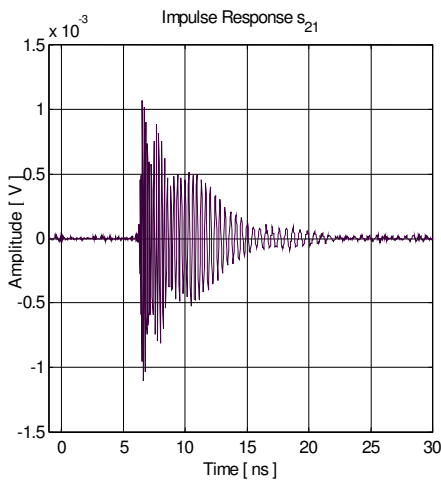


Figure 3.3 Received Time-Domain Waveform of the CBAS Link

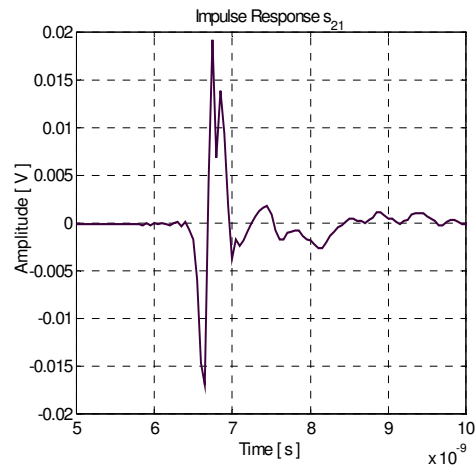


Figure 3.4 Received Time-Domain Waveform of the Vivaldi Link

The Vivaldi antenna however is both broadband in nature and produces an impulse response that is the first derivative of the input pulse. This distortion free pulse aids in characterizing the channel independent of the antenna.

A pair of Vivaldi antennas [14] are used for measurements above 1 GHz. They offer good impulse response and are non-dispersive as compared to other broadband radiating structures [15]. The limitation is that they are directional with a beam-width of ~40 degrees.

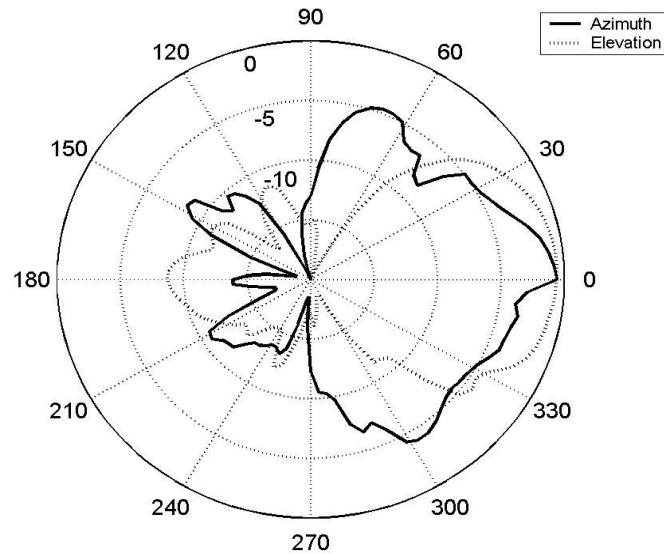


Figure 3.5 Antenna Pattern of the Vivaldi Aerial

The antenna pattern for the Vivaldi Aerial is shown in Figure 3.5. The 200 – 400 MHz measurements were conducted with omni-directional discone antennas.

3.2 Measurement Locations

Measurement locations were chosen to provide diverse propagation environments in order to develop a comprehensive database from which the UWB parameters could be developed. Before each measurement session a calibration is carried out by connecting the transmitter and receiver via coax cable with varying levels of attenuation to establish the linear operating range of the channel sounder and to provide for a reference waveform (Figure 3.6) for further analysis.

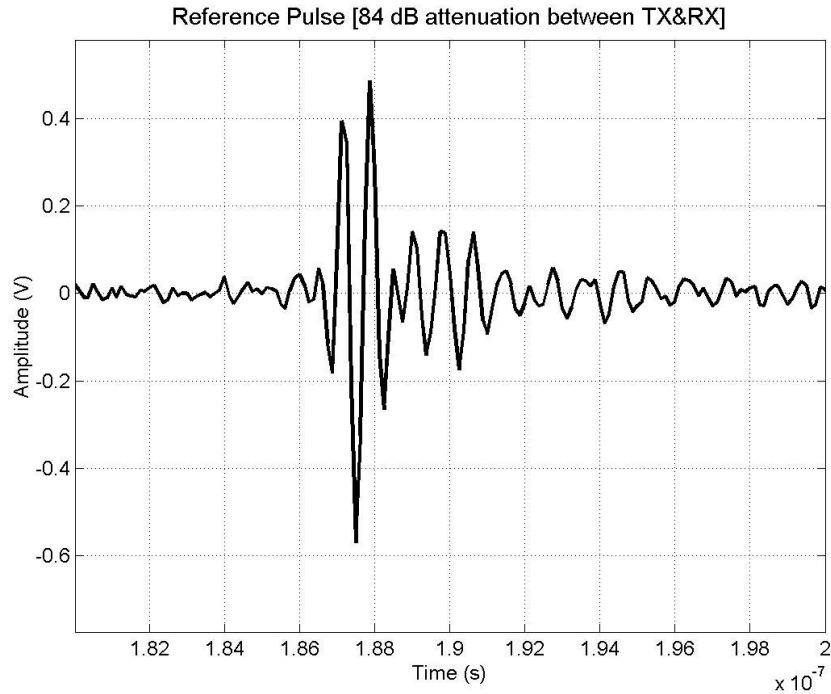


Figure 3.6 Reference Pulse (1-2 GHz)

Since the existing literature on other outdoor UWB models is limited [8], scenarios similar to other narrow band measurement campaigns were selected as typical environments. The idea is to conduct measurements in an environment with widely varying topologies and surfaces. Locations near Burchard Hall, Cowgill Hall, and Hancock Hall on the VA Tech campus are chosen for the outdoor measurements. Figure 3.7 is a drawing of Burchard Hall. The building space itself is underground and the roof is a concrete plaza with pyramidal glass skylights, columns, and low walls. There are a number of trees along the upper edge of the plaza. The area represents a rich multipath environment. Additional locations are chose behind Cowgill and Hancock Hall (8.1). Here the buildings where close together and formed a “canyon.”

Each location has up to 10 different distances measured between the transmitter and receiver. Both NLOS and LOS measurements are taken with an emphasis towards NLOS since they provide more multipath. The surfaces off which reflections are obtained varied from smooth walls to rough limestone surfaces at these locations.

Outdoor-to-indoor measurements are conducted in the Modular Building, a wood structure located behind Cowgill Hall, Durham Hall, and Randolph Hall. Durham and Randolph Hall are steel, brick, and stone buildings.

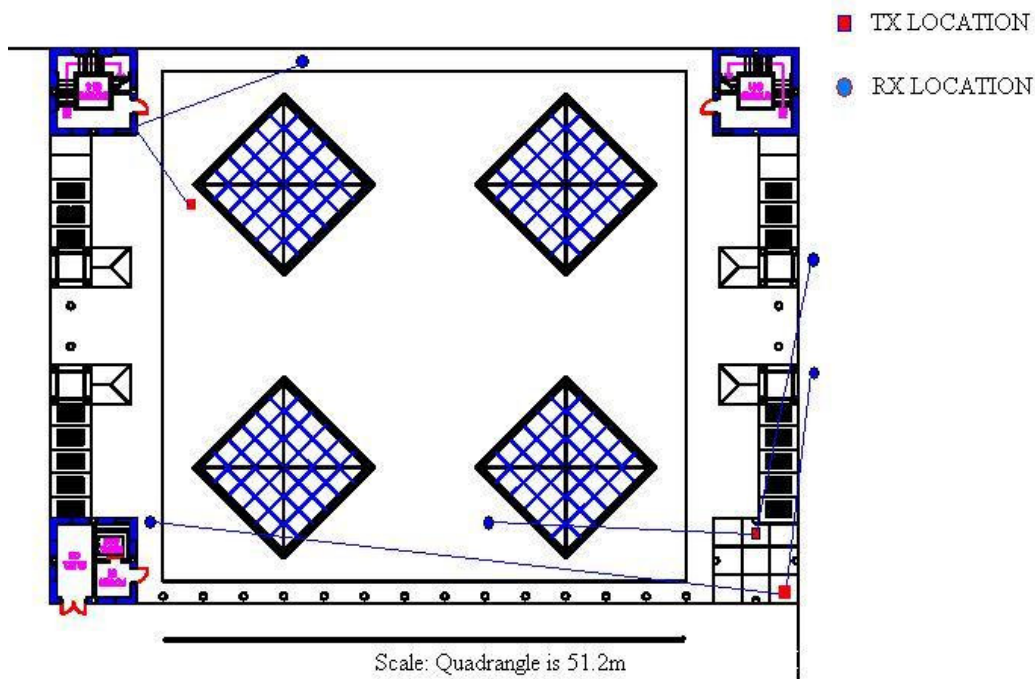


Figure 3.7 Sample Measurement Location

The requirement was for measurements in commercial environments and three buildings with differing structure and composition were chosen.

1. Modular Building houses the CWT RF lab and it was used for the preliminary measurements. The walls inside are made of drywall with wooden studs. The interior walls are about 2 meters high and they are open at the top in tall cubicles. The floor and the roof are wood. The exterior walls are wood studs with wood windows and doors and aluminum siding. It is similar to pre-fabricated building structures in commercial areas [8.2].

2. Randolph Hall is primarily a concrete and brick structure. It is a three-story building with classrooms, offices, and hallways. Initial experiments show that the signal did not directly penetrate several walls. It propagated via openings (doors etc.) down the hallways [8.2].

3. Durham Hall is similar in construction to Randolph. It is four stories tall and it contains of a large number of laboratories and offices. The outer structure is a combination of glass, limestone and concrete that enables the signal to pass through and propagate through the building. Heavy attenuation by the walls and the low transmit power greatly reduces direct through wall propagation. In order to determine building penetration, two

reference measurements are taken. One is taken just inside the glass doors in the vestibule. This measurement represents a minimum of penetration loss. The second reference measurement is taken behind the inner glass doors of the vestibule [8.2].

3.3 Reference Measurements

Reference measurements are taken in the far field. These measurements are used as a reference to compute the pathloss. The impulse response of the bandpass filter along with the frequency band under consideration determines the number of cycles in the reference pulse. For this set of measurements at each location a total of 5 pulses were averaged to improve the SNR.

1. The reference measurement at 200 – 400 MHz is an LOS measurement at a distance of 2.286m. This distance is chosen to ensure that the antennas are in the far field. The reference pulse is shown in Figure 3.8. The bandpass filters in the transmitter and receiver are approximately 200 MHz wide at the 3 dB points.
2. The reference measurement at 2.0 – 4.0 GHz is taken on Perry Street at a distance of 5.49m. The Perry Street location provides a clear LOS path with a minimum of reflections and the range ensures that the antennas are in the far field. The 2.0-4.0 GHz reference pulse is shown in Figure 3.9.

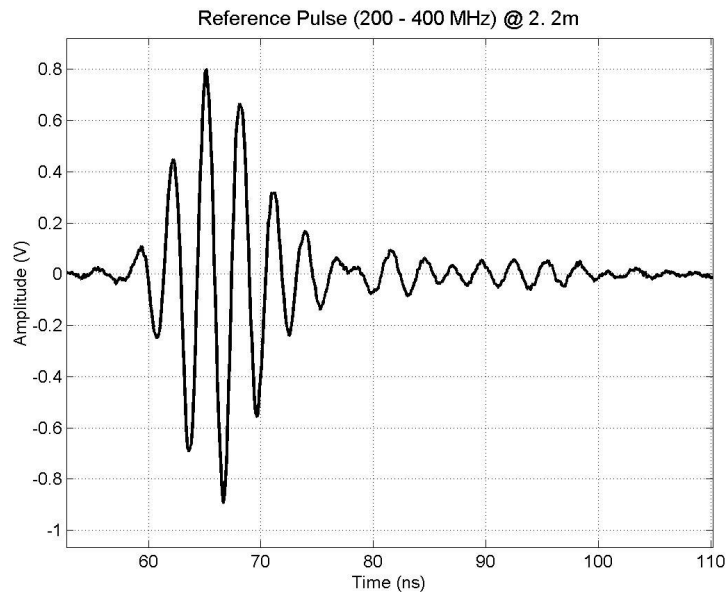


Figure 3.8 Reference Pulse (200 – 400 MHz)

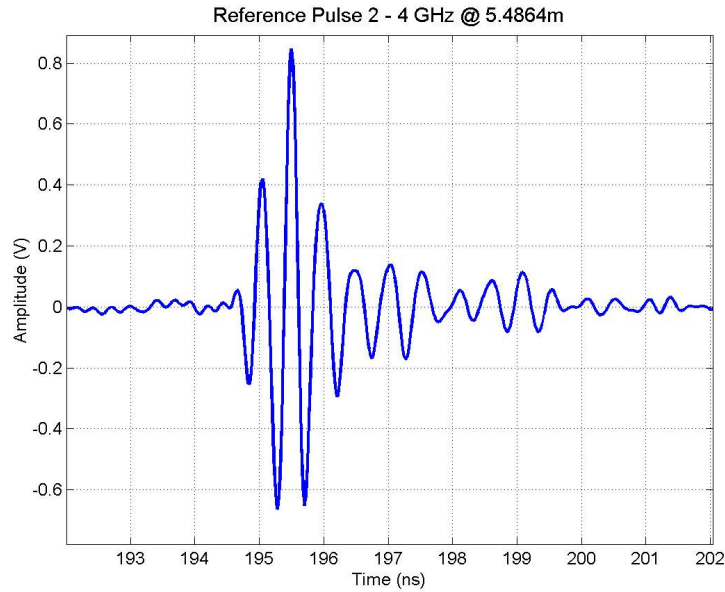


Figure 3.9 2.0- 4.0 GHz Reference Pulse

3. The reference pulse for the 6 - 7 GHz measurement is a LOS pulse taken on Perry Street at a distance of 3m. Although the pulse has a bandwidth of approximately 750 MHz, it exhibits a long “tail.” This is a function of the impulse response of the filters. The pulse is band-limited to 1.0 – 2.0 GHz and then is up-converted to 6.0 - 7.0 GHz. The result is that the pulse must pass through two additional filters in the process of up and down conversion. The reference pulse is shown in Figure 3.10.

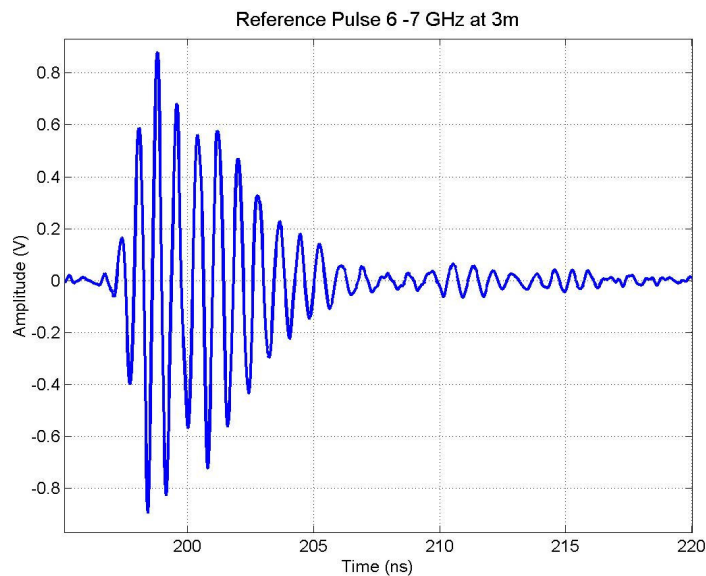


Figure 3.10 6.0 – 7.0 GHz Reference LOS Pulse. The displayed pulse is the 1.0 – 2.0 GHz the output of the 6.0 – 7.0 GHz downconverter

4. A reference measurement for the 1.0 – 2.0 GHz band is taken at a distance of 1.0m. The reference pulse is basically the impulse response of the bandpass filter and shows the presence of some ringing as can be seen in Figure 3.11.

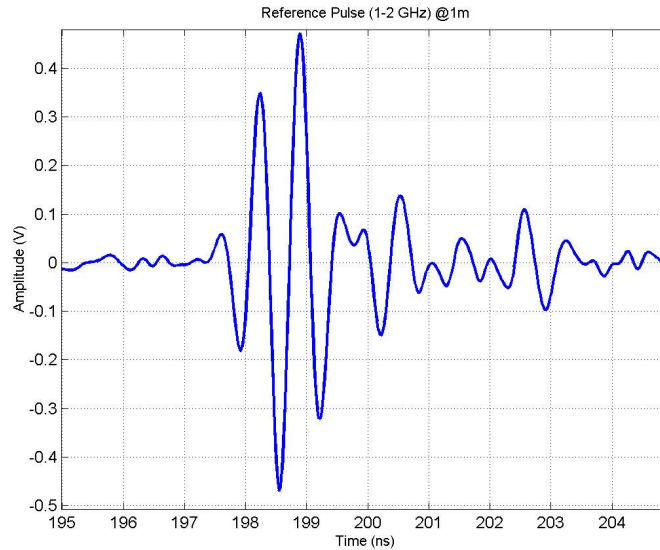


Figure 3.11 Reference Pulse 1-2 GHz

3.4 Data Processing

The collected data is post processed to obtain the pathloss exponent, delay spread, excess delay, and the distribution of multipath components. This section outlines data processing methodology.

1. Measurements are made at five different points approximately 0.3 meters apart at each measurement point. The outdoor-to-indoor measurements are taken in a straight line and the outdoor measurements are conducted in a square grid. The measurement grid is shown in Figure 3.12. The smaller size of the Vivaldi antennas permits the grid measurement. The larger Discone antennas used in the outdoor-to-indoor measurements do not lend themselves to a grid measurement and are moved along a linear track [14].

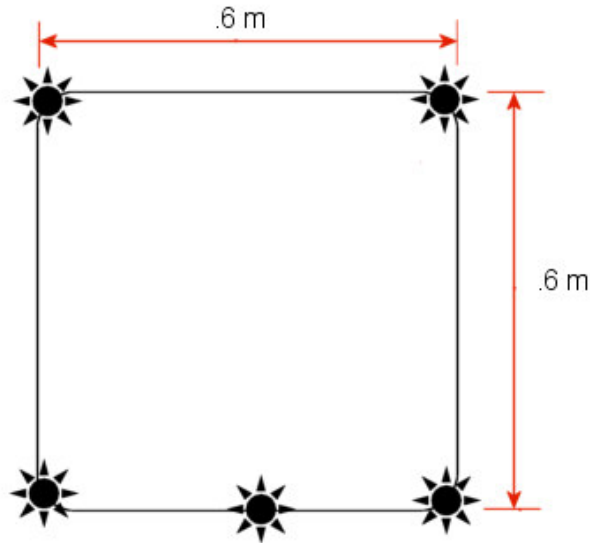


Figure 3.12 Grid used for the Measurements

2. Ten data samples from each measurement location are averaged together. The pulses are aligned using a simple peak detect algorithm that align the pulses using the strongest peak as a reference. The swept-time delay sliding correlator measurements are not absolute time but relative time measurements. The algorithm does not degrade the pulse. The averaging improves the signal to noise ratio (SNR). The effect of this averaging can be seen in Figure 3.13. Averaging 10 pulses results in a SNR improvement of 5.0 dB. Averaging requires that the channel is stationary over the duration of the measurement. To ensure that this assumption is valid, most of the measurements were taken after college working hours to provide a relatively static environment.

3. The averaged data is then up-sampled from the effective sample rate of 8.0GHz to 40GHz.

4. A threshold is empirically computed for each measurement by taking the last 1000 samples of the data. These last samples represent a range of approximately 1500 m. This is far beyond the expected range of any multipath components so the last 1000 samples contain only noise. The mean and standard deviation are calculated and the threshold is calculated using:

$$\text{Threshold} = \text{mean} + \alpha \times \text{std deviation} \quad \text{Eqn. 3.2}$$

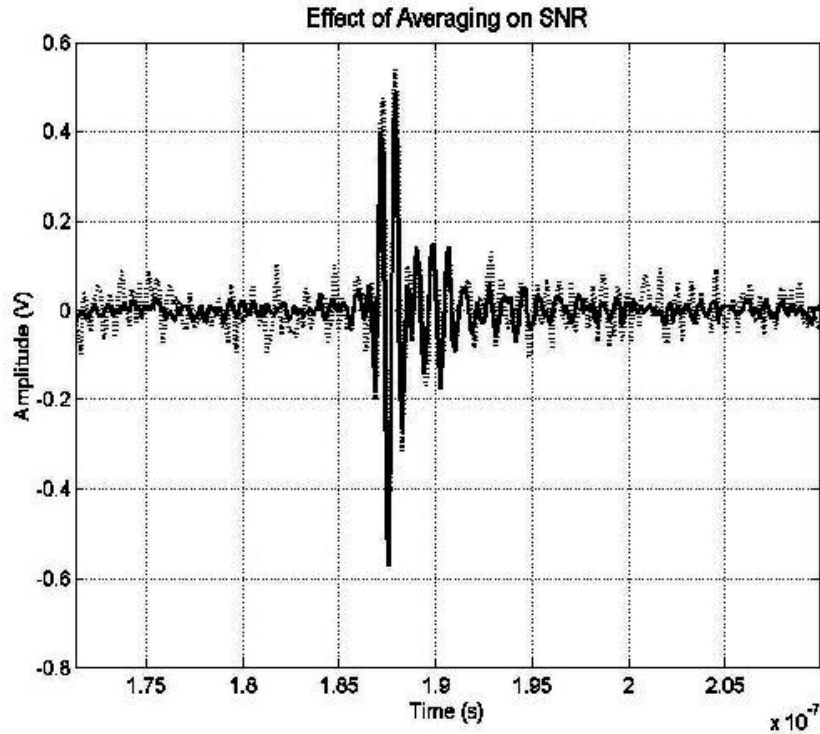


Figure 3.13 Effect of Averaging on SNR

The optimum threshold was found to be 3 standard deviations above the mean. This defines the noise floor for the receiver.

5. Using a clear LOS pulse in the desired frequency band as a reference, the number of samples comprising the ‘up-sampled’ pulse is determined. Given this knowledge, a power delay profile is obtained by stepping through the data with a correlation peak-searching algorithm to locate the presence of multipath components. The energy of each multipath component and time of arrival with respect to first arriving pulse is then calculated from the output of the correlation.

6. The path-loss exponent n and its standard deviation σ are calculated. The path-loss exponent was computed with respect to the reference measurement. Two primary path-loss exponents are computed: one for the total energy in the entire received signal and one for the strongest received pulse. The calculations are made for both the LOS and NLOS cases in the outdoor measurements.

7. For the outdoor-to-indoor measurements, the path-loss exponents are computed for each of the measurement sites.

The path loss analysis applies the minimum mean square error (MMSE) estimate to calculate the path loss exponent, n , and the standard deviation about the pathloss, σ . The sum of the square error is given by [16]:

$$J(n) = \sum_{i=1}^k (\rho_i - \varepsilon_i) \quad \text{Eqn. 3.3}$$

where

- k number of samples
- ρ_i the estimated received energy in dB
- ε_i the received energy in dB

Eqn. 3.3 is a function of n due to the estimated energy, which is found using:

$$\varepsilon_i = \rho_i(d_0) - 10n \log\left(\frac{d_i}{d_0}\right) + \alpha \quad \text{Eqn. 3.4}$$

- d_0 LOS reference distance
- n path loss exponent
- α receiver attenuation variation from the reference

The derivative of $J(n)$ is taken and the resulting equation set equal to zero to solve for n .

The sample variance is then determined from:

$$\sigma^2 = \frac{J(n)}{k} \quad \text{Eqn. 3.5}$$

8. The mean excess delay (τ), rms delay spread (σ) and the excess delay spread (at the 20dB level) are calculated to characterize the time parameters of the multipath channel. The energy in each multipath component and the time of arrival of each multipath is recorded.

9. For outdoor-to-indoor measurements the primary consideration is the attenuation offered by the external walls and the partitions of the building. In the present study, we evaluate the feasibility of UWB under the same circumstances.

We define the penetration loss as the difference in the mean signal level between the measurement taken at a fixed location outside and the reference measurement taken indoors on the opposite side of the wall in a straight LOS path to the receiver [17]. This is illustrated in Figure 3.14. A measurement is taken with the transmitter just inside and just

outside of the wall in question. Additional measurements are then taken leaving the transmitter fixed outside and moving the receiver to various points indoors. For outdoor-to-indoor measurements, the range is limited by the low average transmitter power and the additional loss in the wall.

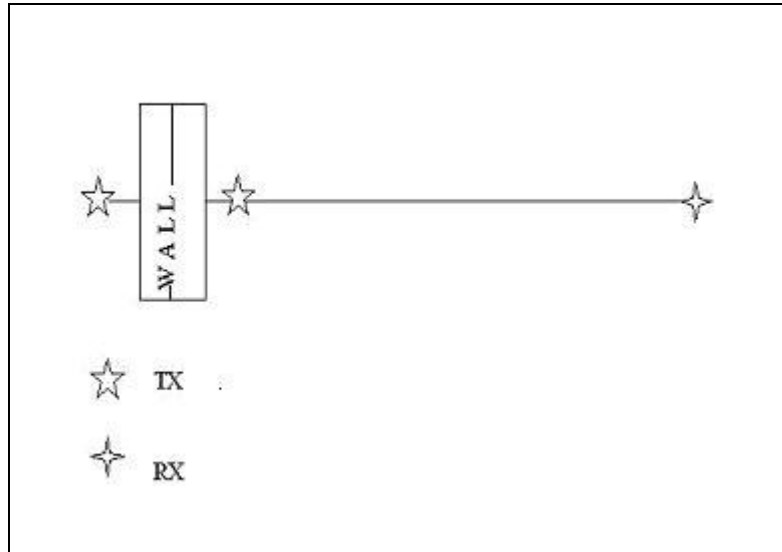


Figure 3.14 Outdoor-Indoor Penetration Loss Calculation Arrangement

Using the measurement setup, locations and data processing techniques discussed and extensive data set was accumulated to compute the channel parameters.

4 Outdoor Ultrawideband Measurements

The outdoor measurements are carried out at different locations around the Virginia Tech Campus in the frequency bands of 1-2 GHz, 2-4 GHz and 6-7 GHz. Limited receiver sensitivity results in the usage of directional antennas resulting in fewer multipath being obtained. The maximum range obtained (LOS) is dependent upon the peak transmitted power at each frequency band and is a maximum of ~250m at the 6.0-7.0 GHz band.

A line of sight (LOS) reference measurement is carried out in an open, low reflection, area on Perry Street. This LOS measurement is used as the loss reference for the pathloss exponent calculations since it is possible to isolate the clear LOS path from the other reflections.



Figure 4.1 Perry Street LOS

4.1 Pathloss

The pathloss exponent is calculated with both the LOS or NLOS measurements. The pathloss exponent and standard deviation are computed for LOS paths, for NLOS paths

including the total received energy, and for NLOS paths where only the strongest multipath is considered.

4.1.1 2-4 GHz

The LOS pathloss approaches the free space pathloss and the results of the LOS measurements are shown in Figure 4.2. Figure 4.3 and Figure 4.4 show the pathloss over the different NLOS locations. Figure 4.3 is the NLOS pathloss considering the entire received energy and Figure 4.4 is the pathloss considering only the strongest arriving signal. The results are tabulated in Table 4.1.

Table 4.1 Outdoor Pathloss Exponents for 2.0 - 4.0 GHz

Type	n	σ (dB)
LOS	1.9	0.70
NLOS – All multipath	4.2	2.39
NLOS – strongest Path	4.5	2.44

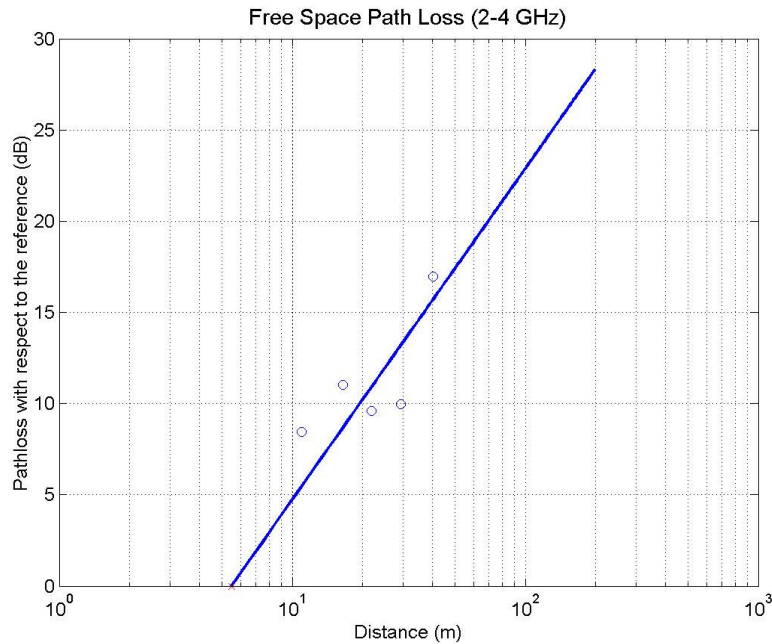


Figure 4.2: 2.0 – 4.0 GHz LOS Pathloss referenced to free space including all locations

The results indicate that in an LOS environment the pathloss approaches that of free space – with the NLOS pathloss being significantly larger. In the latter case, the number of multipath obtained are dependent upon sensitivity of the receiver to extract the weaker multipath from the noise.

The large variance obtained can be attributed to the differing characteristics of the locations. It is also important to note that in some occasions the positions of the transmitter and receiver are setup to force a reflection off a surface – either smooth or rough in nature. It is experimentally realized in a power limited regime the only way to receive a signal was an arrangement with the antenna facing a reflecting surface.

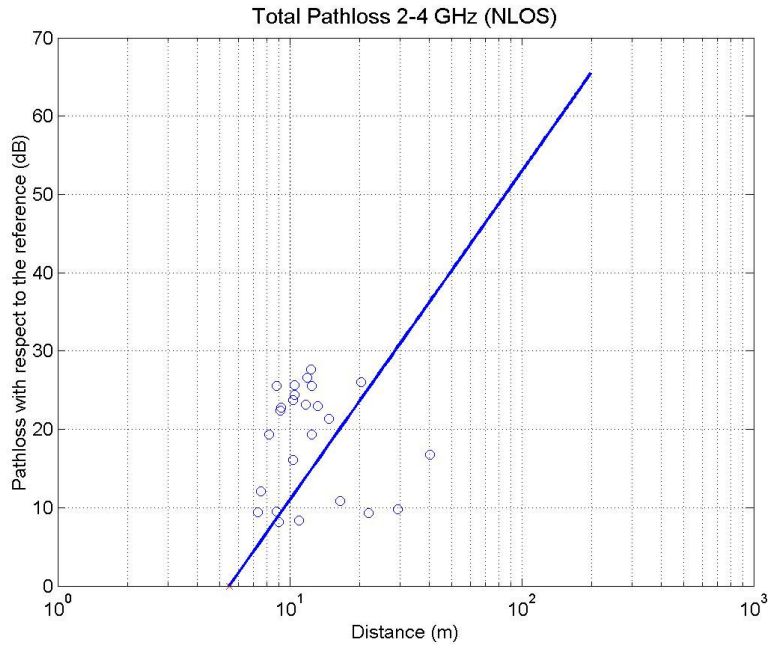


Figure 4.3 2.0 – 4.0 GHz NLOS Pathloss using all received energy for all locations

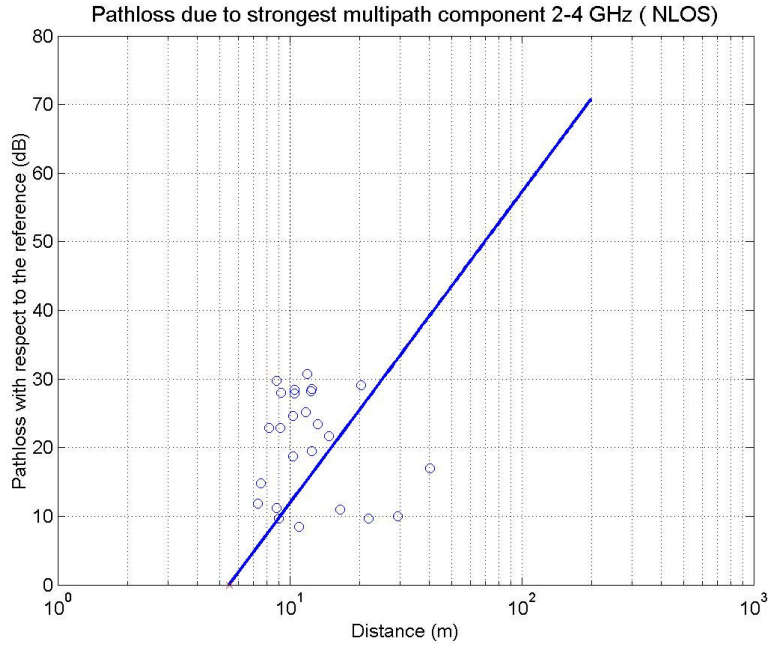


Figure 4.4 2.0 – 4.0 GHz NLOS Pathloss using only the strongest component for all locations

4.1.2 6-7 GHz

The LOS pathloss exponent for 2.0 – 4.0 GHz and 6.0- 7.0 GHz are close to being equal. However, the pathloss exponent for 2.0 – 4.0 GHz NLOS is greater than that measured for 6.0 – 7.0 GHz. The standard deviation of the pathloss exponent at 6.0 – 7.0 GHz is significantly greater than that at 2.0 – 4.0 GHz. The results are tabulated in Table 4.2.

Table 4.2 Outdoor Pathloss Exponents for 6.0 - 7.0 GHz

Type	n	σ (dB)
LOS	1.9	0.65
NLOS - Total Energy	2.89	2.54
NLOS - Largest Component	2.92	2.85

The difference in the 6.0 – 7.0 GHz pathloss exponent when the total energy is considered compared with the pathloss when only the largest multipath component is considered is much smaller as compared to other frequency bands. This suggests that either the largest multipath component occupies a significant portion of the received energy or there is very few other significant multipath. Figure 4.5 shows the LOS pathloss. Figure

4.6 and Figure 4.7 gives the pathloss for the NLOS case where all the energy and only the largest multipath component are considered.

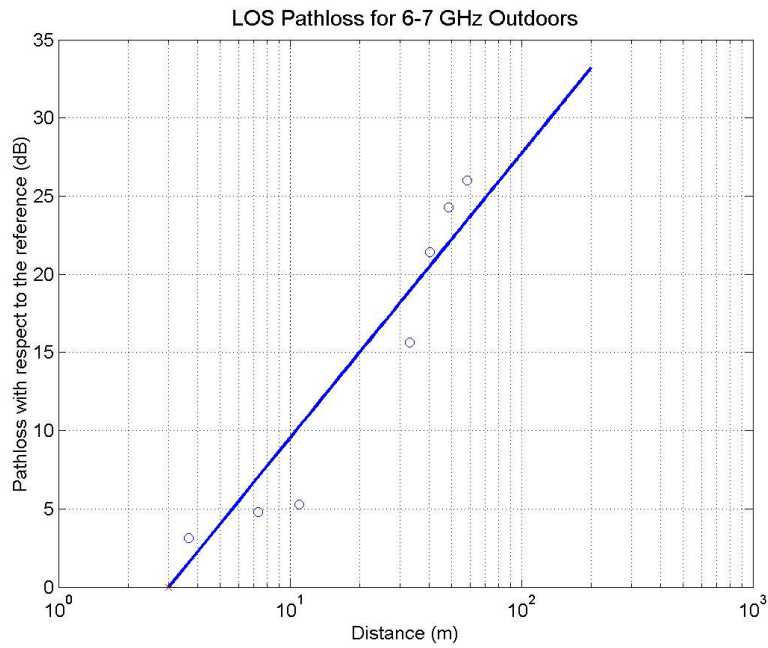


Figure 4.5 LOS Pathloss for all locations

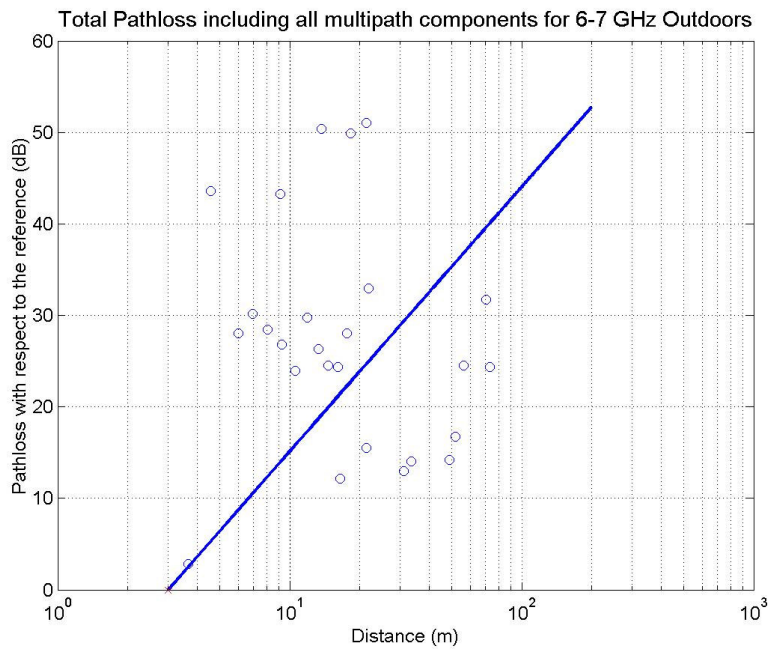


Figure 4.6 NLOS Pathloss with total received energy for all locations

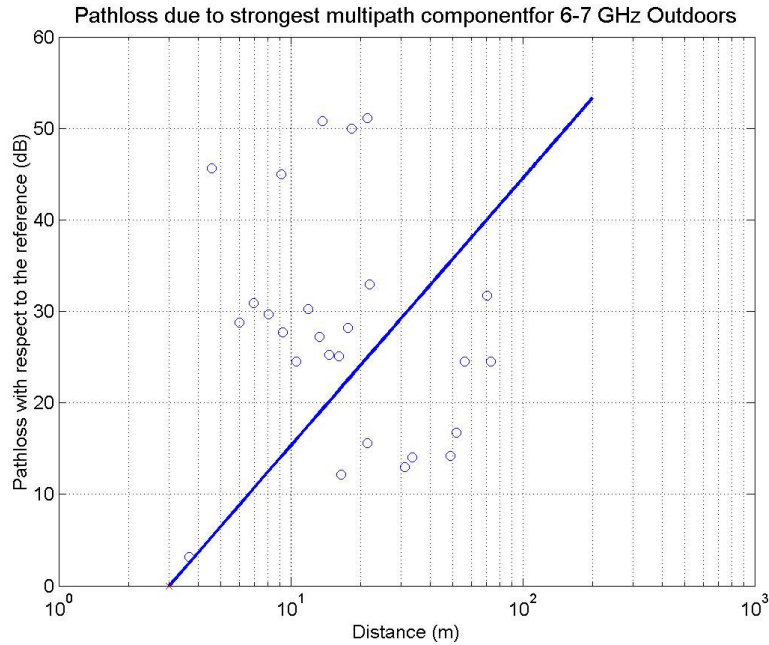


Figure 4.7 NLOS Pathloss with only strongest multipath for all locations

4.1.3 1-2 GHz

The LOS path follows the free space pathloss characteristics and the NLOS results are characteristic for typical cellular type NLOS environments.

Table 4.3 Outdoor Pathloss Exponents for 1.0 - 2.0 GHz

Type	n	σ (dB)
LOS	1.9	0.79
NLOS – All multipath	3.0	1.45
NLOS – Largest multipath	3.2	1.48

The results obtained for all three cases are graphically illustrated in Figure 4.8, Figure 4.9, and Figure 4.10. Figure 4.8 is the pathloss for all the outdoor LOS paths, Figure 4.9 is the pathloss for the outdoor NLOS paths with the energy from all multipath components, and Figure 4.10 is the pathloss for the NLOS paths considering only the strongest multipath.

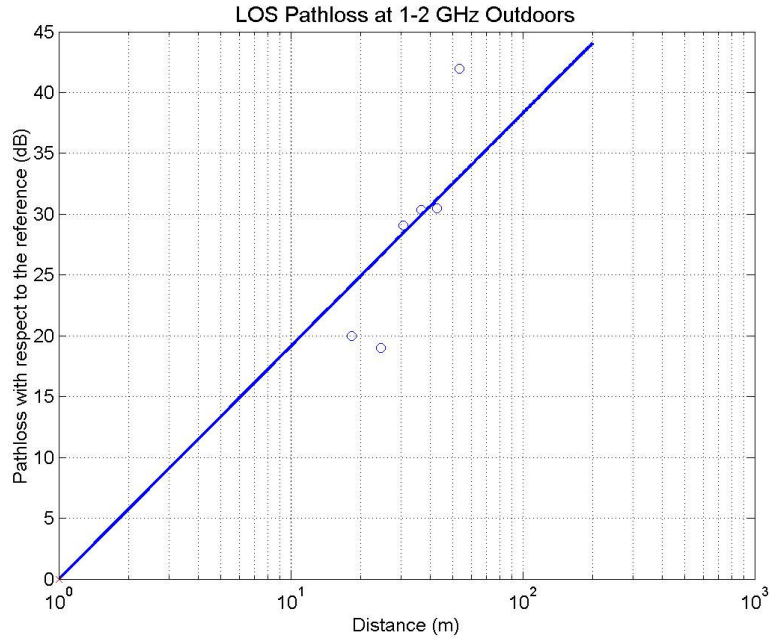


Figure 4.8 1.0 – 2.0 GHz Outdoor LOS Pathloss

It appears that compared to the 6-7 GHz results the 1-2 GHz band seems to suffer a lower NLOS pathloss. This would indicate that given the same bandwidth the pathloss seems to be directly proportional to the frequency. This is along the lines of the result which would have been obtained using the classical Friis equation where the pathloss would increase with an increase in frequency.

Comparing the results with those obtained for the 2-4 GHz a higher pathloss is obtained at that band points. This indicates that a larger bandwidth increases the receiver noise, decreasing the sensitivity. It is also noted that all the LOS data tends to fall the free space pathloss of 2.0.

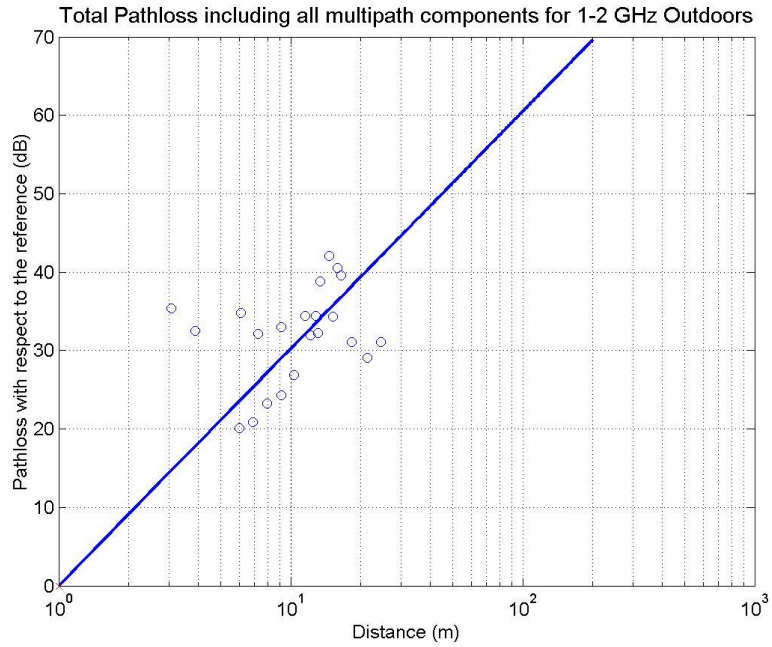


Figure 4.9 1.0 – 2.0 GHz NLOS Pathloss including all multipath components

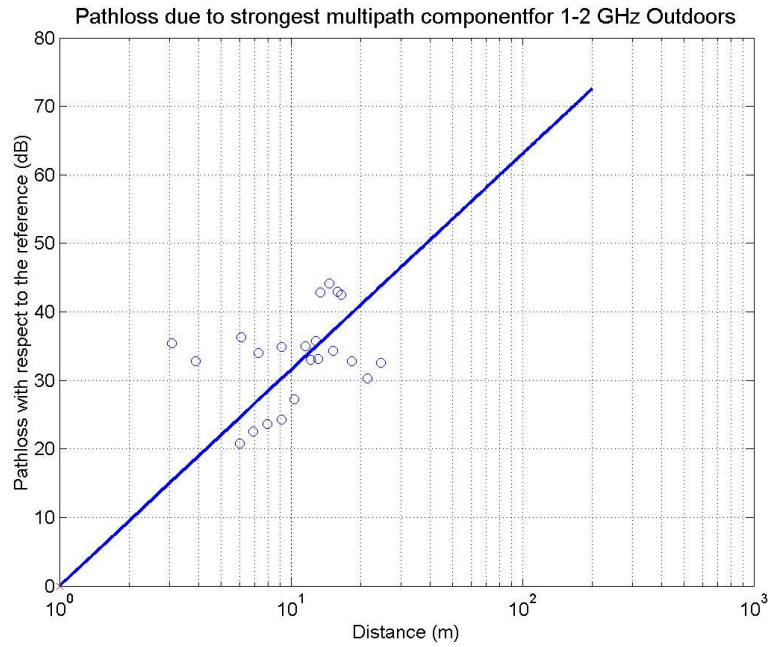


Figure 4.10 1.0 – 2.0 GHz NLOS Pathloss considering only the strongest multipath component

4.2 Power Delay Profile (PDP) and Time Dispersion Parameters

4.2.1 2-4 GHz

4.2.1.1 Power Delay Profile

Figure 4.11 shows a Burchard Hall power delay profile for the 2.0 – 4.0 GHz band. The multipath components tend to arrive in discrete time intervals rather than continuously. Figure 4.12 is the received pulse and it is possible to discern a multipath component out to approximately 50 ns.

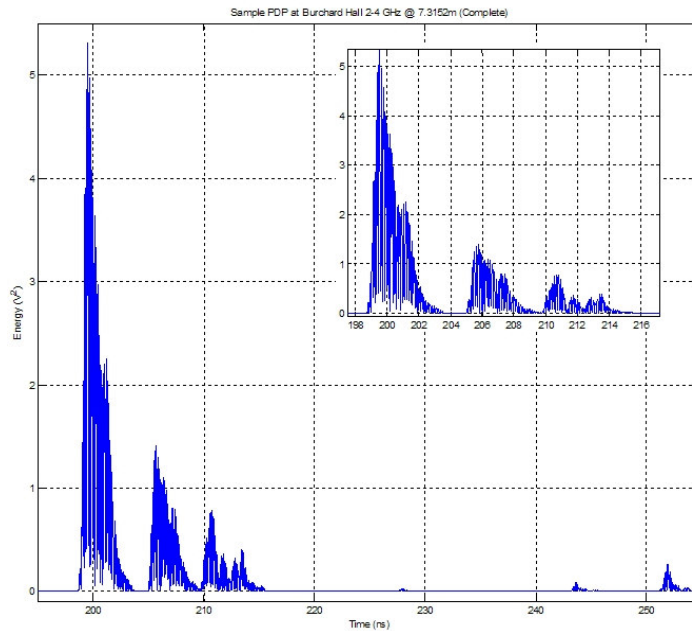


Figure 4.11 Burchard Hall 1, discrete clusters of multipath (inset – zoomed in version)

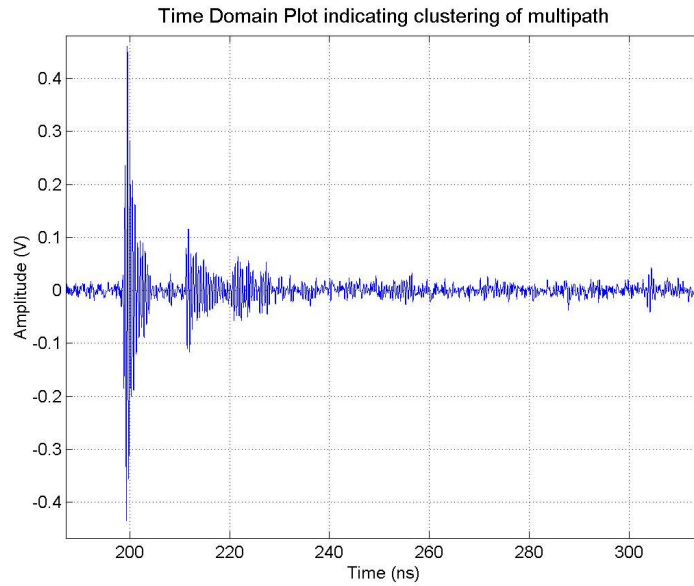


Figure 4.12 Burchard Hall 1, Clustering of Multipath in Time Domain

4.2.1.2 Small Scale Time Parameters

Small-scale time parameters are computed for both the LOS and NLOS data. The results obtained for each location and the overall small-scale parameters are tabulated in Table 4.4 below.

Table 4.4 Small Scale Time Parameters for 2.0 – 4.0 GHz outdoors

Location	Mean Excess Delay – (τ ns)	RMS Delay Spread (σ ns)	Excess Delay Spread (20dB) ns
Burchard Hall 1	6.16	5.80	63.5
Burchard Hall 2	1.57	10.59	69.2
Burchard Hall 3	6.55	4.04	36.7
Cowgill Hall	7.94	3.77	90.2
Hancock Hall	9.16	1.21	28.6
Average	9.64	5.16	52.87

4.2.2 6-7 GHz

4.2.2.1 Power Delay Profile

The 6.0-7.0 GHz PDP's show the presence of a maximum of three multipath components. This is significantly fewer than observed in other bands. However the multipath components arrive at distinct time intervals and are resolvable. Depending upon the configuration and arrangement, a weak direct component is obtained that may have

been due a direct path through concrete followed by a single bounce off a good reflector. (Figure 4.13)

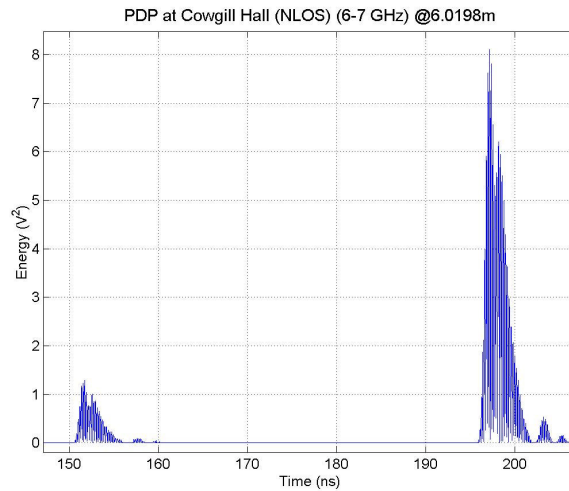


Figure 4.13 PDP at Cowgill Hall at 6.0198m. Note the early arriving pulse

4.2.2.2 Small Scale Time Parameters

Small Scale time parameters are obtained at each location. Table 4.5 contains the results. At some locations we obtain just a single path that results in no delay spread. The number of multipath components tend to decrease with increasing frequency.

Table 4.5 Small Scale Time Parameters for 6.0 – 7.0 GHz

Location	Mean Excess Delay ($\bar{\tau}$ ns)	RMS Delay Spread (σ ns)	Excess Delay Spread (20dB) ns
Burchard Hall 1	7.02	-	13.3
Burchard Hall 2	5.80	2.38	11.4
Burchard Hall 3	34.40	15.69	86.0
Cowgill Hall	22.6	1.80	45.1
Hancock Hall	8.40	1.37	22.2
Average	15.64	4.25	35.6

4.2.3 1-2 GHz

4.2.3.1 Power Delay Profile

Due to the low transmitter power and the directional antennas, only a few multipath components are observed. The presence of multipath seems to be dependent on the

presence of a strong reflector in the vicinity. The Cowgill Hall and Hancock Hall “canyon” produce strong reflections.

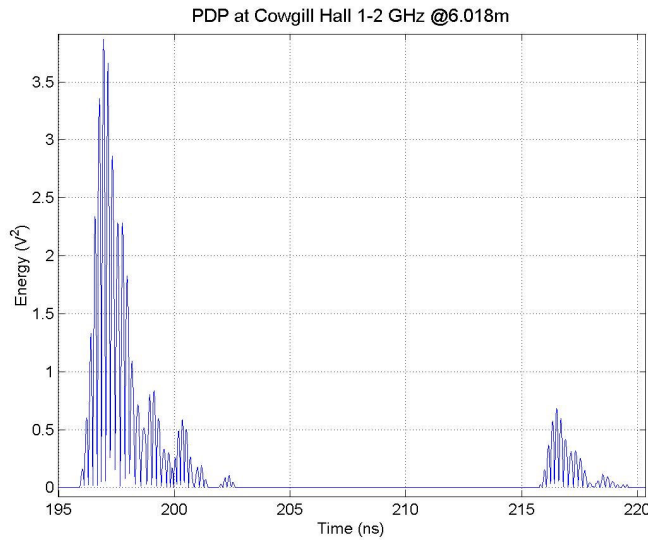


Figure 4.14 Power delay profile at Cowgill Hall

4.2.3.2 Small Scale Time Parameters

The delay spread is computed for both the LOS and NLOS data. The results obtained for each location and the overall small-scale parameters are tabulated in Table 4.6.

Table 4.6 Small Scale Time Parameters for outdoor 1.0 – 2.0 GHz

Location	Mean Excess Delay – $\bar{\tau}$ ns	RMS Delay Spread σ ns	Excess Delay Spread (20dB) ns
Burchard 1	17.53	5.21	36.35
Burchard 2	29.38	10.36	61.49
Cowgill	38.538	19.18	95.59
Average	28.48	11.58	64.47

We obtained the largest mean excess delays and the smallest excess delay spread of all the bands in the 1.0 – 2.0 GHz regime. The small rms delay spread indicates that the first few multipath components constitute a major portion of the received energy.

4.3 Characterization of Multipath Components

4.3.1 2-4 GHz

Three to five multipath components are detected depending upon the location and distance from transmitter. In the case of obstructed paths, most of the received energy is via reflections and there could be an absence of a dominant path as indicated in Figure 4.15.

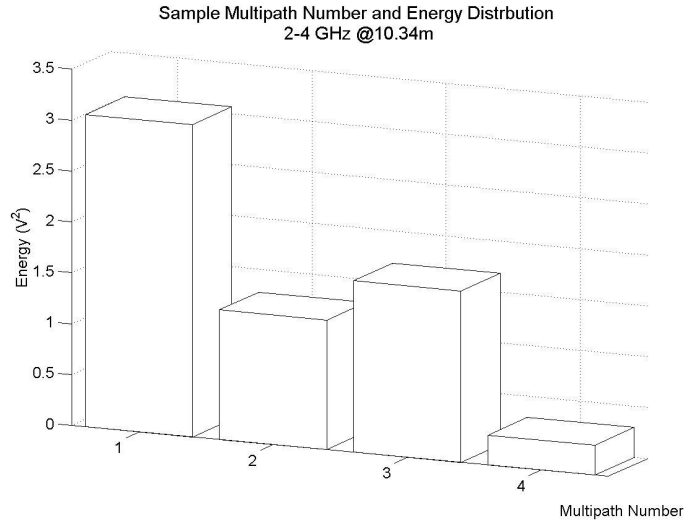


Figure 4.15 Burchard Hall 1, Multipath Number and Energy at 10.34m NLOS

In comparing the strongest multipath component to the total received energy, the strongest component in some cases can be as much as 50% of the total received energy over all the multipath components. This is graphically illustrated in Figure 4.16 which shows the ratio of the total energy to the strongest component of the signal at different distances from the transmitter.

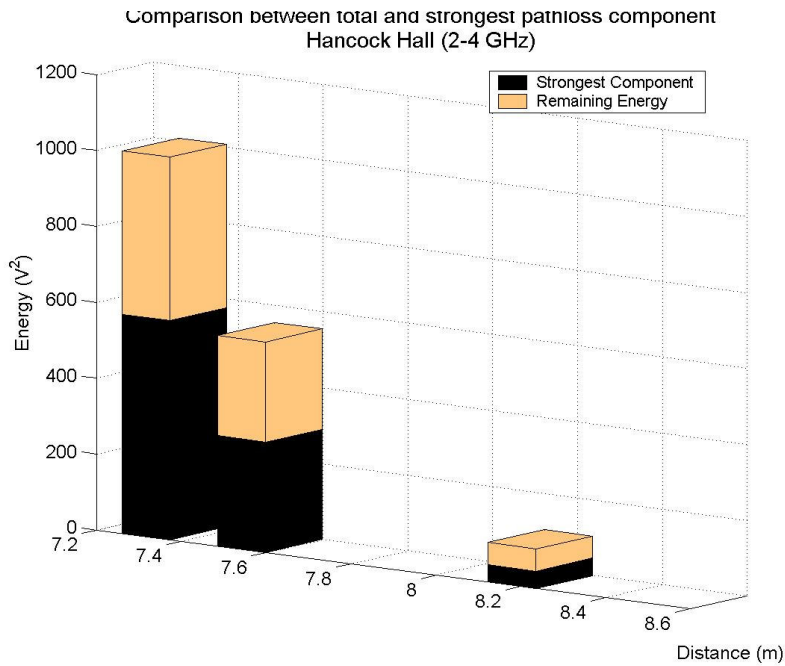


Figure 4.16 : Strongest Multipath is >50% of total Energy Received

4.3.2 6-7 GHz

As noted earlier, we see very few multipath components as compared to 2.0 - 4.0 GHz. Figure 4.17 shows the energy in the various multipath observed at Cowgill Hall Note that this path had very little directly ray energy. Figure 4.18 compares total received energy to the energy in the strongest component for the Burchard 1 location.

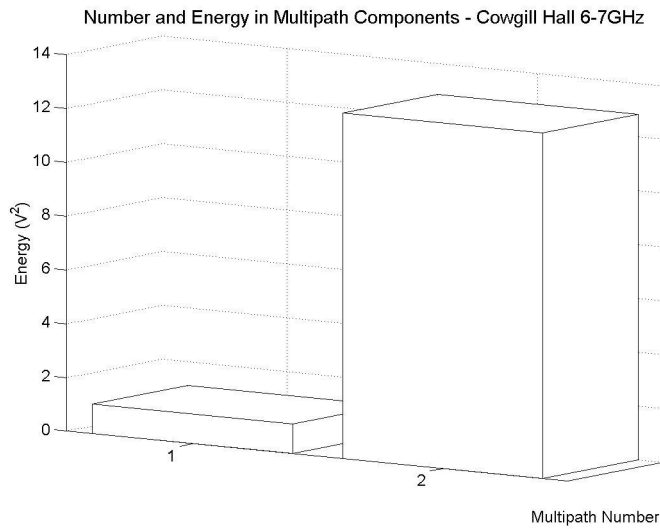


Figure 4.17 Number and energy of observed multipath at Cowgill.

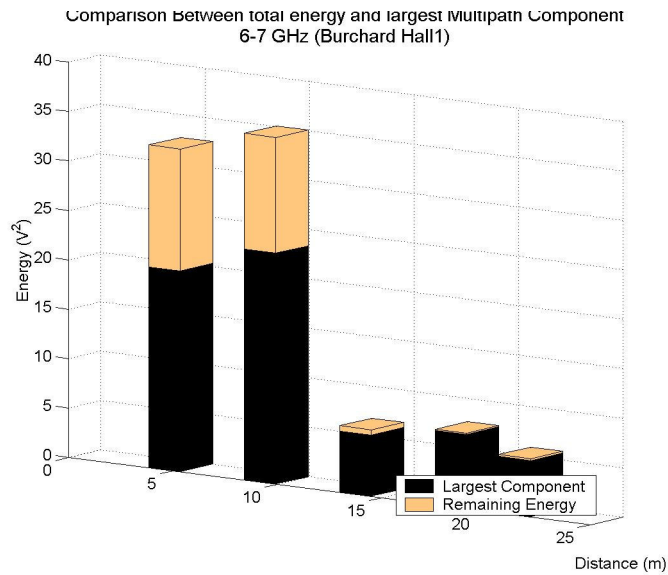


Figure 4.18 Comparison between strongest multipath component and total energy received at Burchard 1.

4.3.3 1-2 GHz

In many locations, only a single weak attenuated signal is obtained and in the presence of good reflectors only one or a maximum of two multipath components is observed. The primary arriving signal constitutes the majority of the energy in the signal. This can also be attributed to the higher threshold (7 standard deviations) required due to interference and fewer pulses being averaged (5 instead of 10) reducing the sensitivity of the system. The results are shown in Figure 4.19 and Figure 4.20. Figure 4.19 indicates the presence of two multipath components where the first multipath component is the most significant of the two.

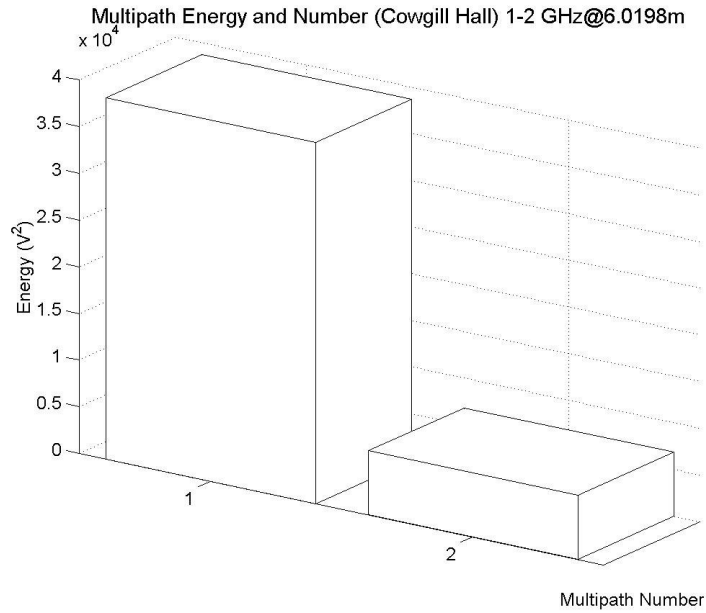


Figure 4.19 Number and Strength of Multipath at Cowgill Hall

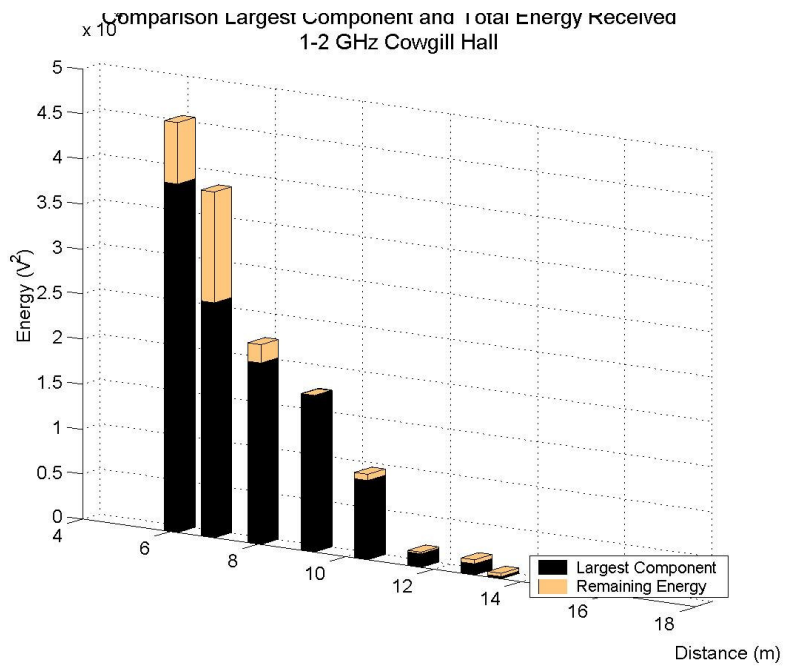


Figure 4.20: Largest Component and Total Energy of all Multipath at Cowgill Hall

5 Outdoor-to-Indoor Measurements

Outdoor to indoor measurements are carried out to study the propagation of UWB signals into buildings. The transmitter is placed outside the building and the receiver placed at various locations inside. These measurements are carried out in three buildings on the VA Tech campus: the Modular Building, Durham Hall and Randolph Hall. The modular Building is a small wood framed building and Durham and Randolph Halls are conventional concrete, stone, and steel academic buildings. The UWB pulse propagates through a range of materials in these buildings. The path length is of the order of 10's of meters. The measurements are made in two bands: 200 – 400 MHz with omni-directional disccone antennas and 6.0 – 7.0 GHz with the Vivaldi antennas.

The majority of outdoor to indoor propagation studies [29] [30] have been oriented towards determining indoor coverage for a wireless system with an outdoor base station. The primary consideration is the attenuation offered by the external walls and the partitions of the building. In the present study, we evaluate the feasibility of UWB under the same circumstances. Pathloss and multipath characteristics are discussed.

5.1 Pathloss

The pathloss calculations for the outdoor-to-indoor measurements computations incorporate two factors – the penetration loss suffered by the signal in propagating through the outer wall and the indoor pathloss between the wall and the receiver. Indoor pathloss is a result of either multiple reflections within a passage or direct penetration through the inner walls.

5.1.1 200-400 MHz

5.1.1.1 Modular Building

The pathloss exponent is computed using both the strongest pulse and the total energy over the entire multipath. The pathloss exponent is calculated using the data from all measurement locations. The results are indicated in Table 5.1.

Table 5.1 Pathloss at Modular Building

Energy	n	σ (dB)
Strongest Pulse	2.7	0.86
Total Energy	1.9	0.71

When the total energy is considered, the pathloss exponent approaches a value less than 2 since it is possible to collect energy from multiple reflections indoors. However, when the strongest pulse is considered, the path loss exponent is larger. This is typical of obstructed paths. The increase in the exponent can be seen in Figure 5.1 and Figure 5.2.

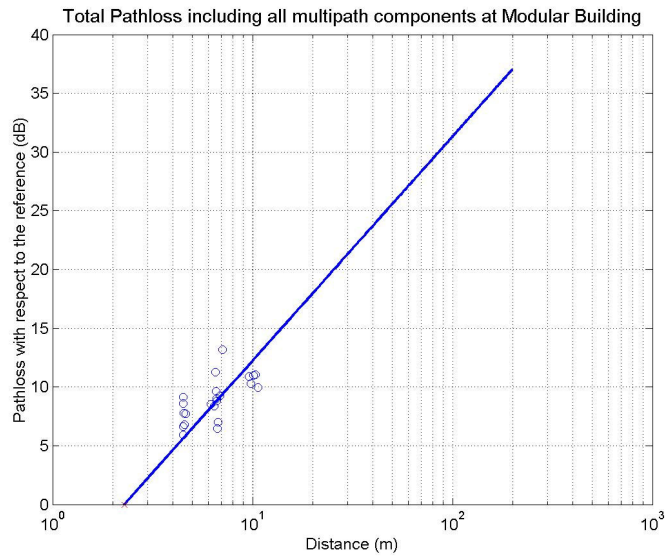


Figure 5.1 Total Energy Pathloss in Modular Building



Figure 5.2 Pathloss of Strongest Multipath Component in Modular Building

The values obtained seem to indicate the structure of the building provides very little loss to the UWB signal. The modular building has wooden framework and many windows. The inner walls and partitions are also wood based. This provides a low level of attenuation to the UWB pulse resulting in lower penetration loss. The total pathloss – consisting of the indoor pathloss along with the penetration loss is lowered.

5.1.1.2 Durham and Randolph Hall

In Durham and Randolph Halls, the pathloss exponent and its standard deviation resemble those of a NLOS path. This can be attributed to the fact that the concrete and brick walls attenuate the signals more than the wood and aluminum siding of the modular building. The pathloss exponent is calculated using the data from all measurement locations. The results of the pathloss calculation are tabulated in Table 5.2.

Table 5.2 Path Loss exponents and Standard Deviation for Durham Hall and Randolph Hall

Location	Energy	N	σ (dB)
Durham Hall	Total	3.9	0.91
	Strongest	4.4	0.94
Randolph Hall	Total	3.2	0.32
	Strongest	3.9	0.77

Total energy pathloss in Durham Hall is shown in Figure 5.3 and the pathloss for the strongest component in Durham Hall is shown in Figure 5.4. The total energy pathloss in Randolph Hall is shown in Figure 5.5 and the Randolph Hall strongest component pathloss is shown in Figure 5.6.

As can be seen from Figure 5.3 and Figure 5.4 since the pulse is propagated through the hallway the directional antenna is sufficient to collect most of the energy in the pulse.

Total Pathloss including all multipath components at Durham Hall

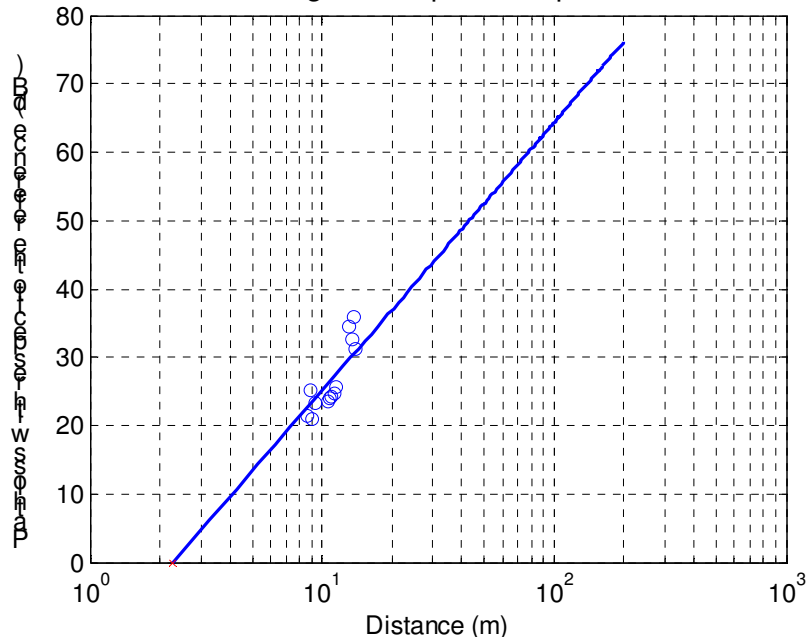


Figure 5.3 Durham Hall Total Energy Pathloss

Pathloss due to strongest multipath component at Durham Hall

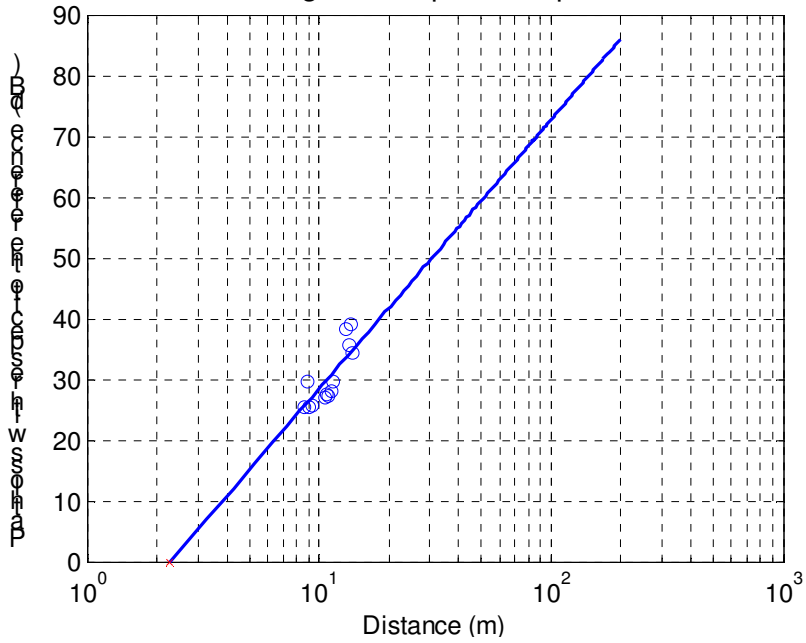


Figure 5.4 Durham Hall Pathloss with Strongest Multipath only

Total Pathloss including all multipath components at Randolph Hal

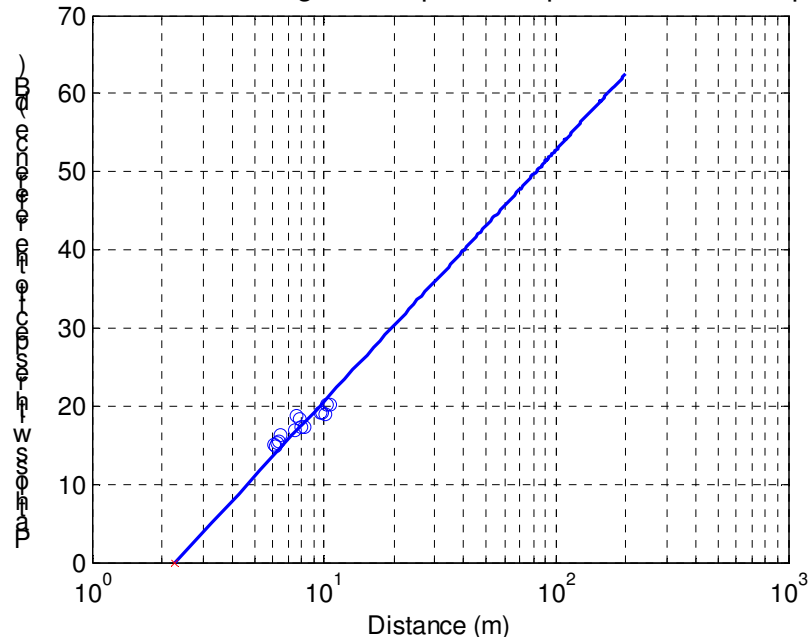


Figure 5.5 Randolph Hall Total Energy Pathloss

Pathloss due to strongest multipath component at Randolph Hall

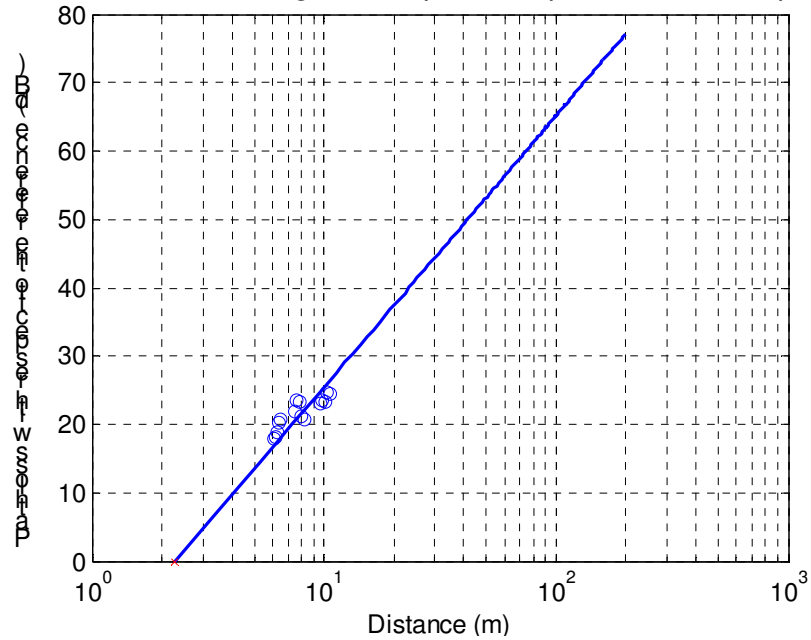


Figure 5.6 Randolph Hall Pathloss with Strongest Multipath only

5.1.2 6-7 GHz

Pathloss loss is computed for both the strongest component multipath and the total received energy for both Durham Hall and the Modular Building. The results are tabulated in Table 5.3.

Table 5.3 6.0 – 7.0 GHz Pathloss Exponents

Location	Energy	n	σ (dB)
Modular Building	Total Energy	5.4	1.22
	Strongest Path	6.4	1.37
Durham Hall	Total Energy	4.4	0.69
	Strongest Path	5.6	1.25

The signals in the Modular Building appear to be attenuated to a far greater extent than those at Durham Hall. One possible reason could be that in the Modular Building, the signal is forced to propagate *through* the wall, while in Durham hall, the pulse can propagate via windows, doors etc. into the hallways where the measurements were taken. Both measurement locations exhibit a loss exponent consistent with NLOS paths. The pathloss is calculated with respect to the LOS reference. Zero dB in Figure 5.7, Figure 5.8, Figure 5.9, and Figure 5.10 is the LOS reference loss.

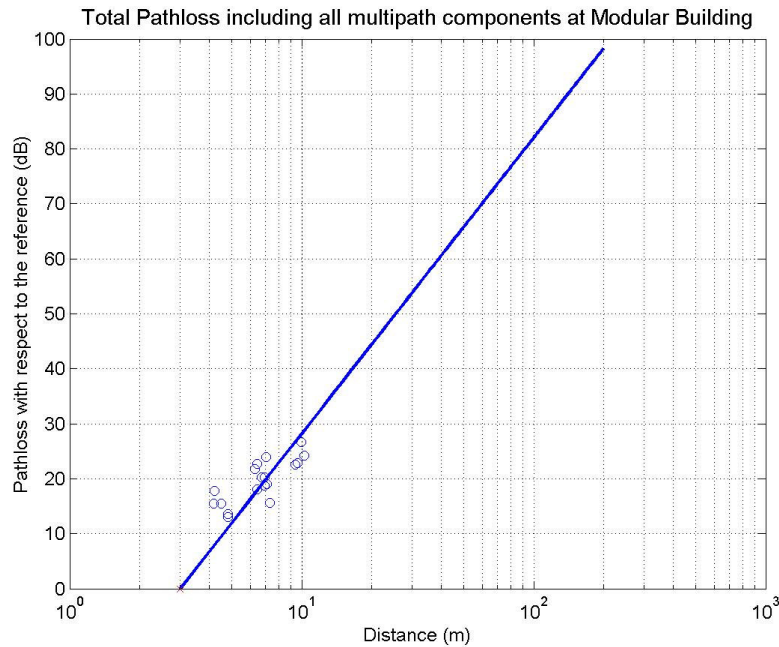


Figure 5.7 Total Pathloss at Modular Building

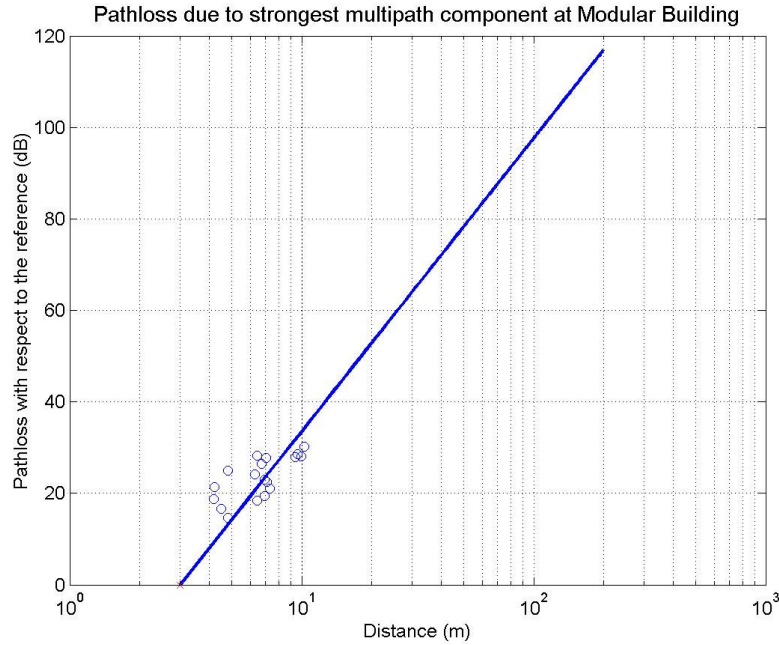


Figure 5.8 Strongest Path Pathloss at Modular Building

The lower value of n in Durham Hall than the value of n in the Modular Building is unexpected. It is expected that n would increase in the concrete and stone Durham Hall. In an effort to understand this phenomenon, the Durham Hall measurements are divided into short-range measurements up to approximately 10 meters and the longer-range measurements. For the short measurements with the directional Vivaldi antennas, we anticipate that the signal must come directly through the glass and metal walls in the entry hall. The windows are coated with a “low – ϵ ” tin oxide coating. However as we progress through the corridor, the receiver sees a more indoor environment. There are additional paths and the antenna intercepts more reflected energy. This results in the pathloss exponent decreasing to factor in the indoor propagation. Table 5.4 is a comparison of the pathloss exponent at various ranges. Figure 5.11, Figure 5.12, Figure 5.13, and Figure 5.14 show the pathloss exponents for the long and short-range calculations.

Table 5.4: Comparison of pathloss exponents in Durham Hall.

Type	Energy	n
------	--------	---

All Outdoor-to-Indoor Measurements	Total	4.25
All Outdoor-to-Indoor Measurements	Strongest	5.54
Short Range ~ 10 meters	Total	2.89
Short Range ~ 10 meters	Strongest	3.29
Long Range > ~ 10 meters	Total	2.93
Long Range > ~ 10 meters	Strongest	3.35

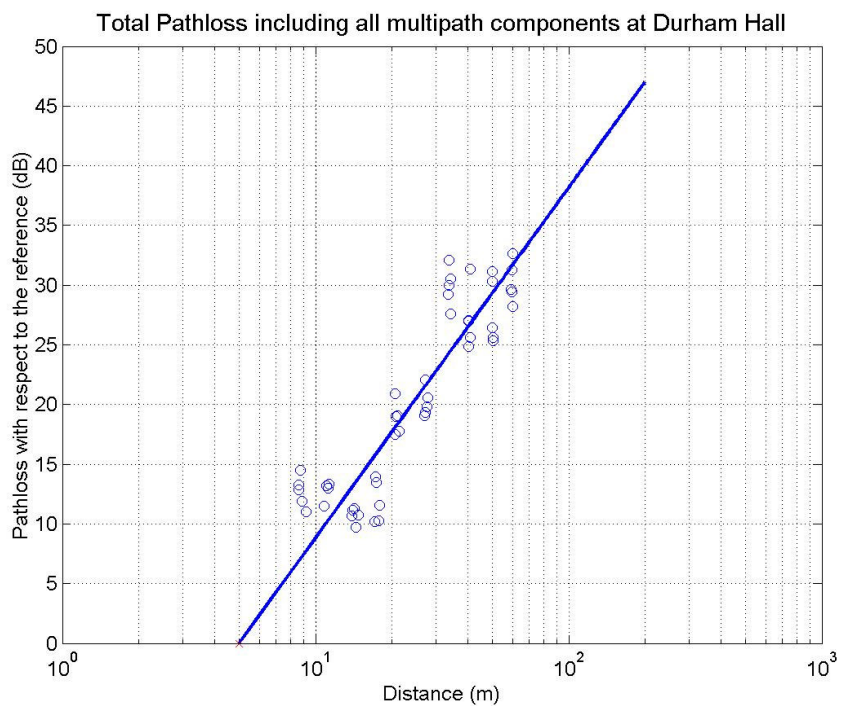


Figure 5.9 Total pathloss at Durham Hall employing all measurements.

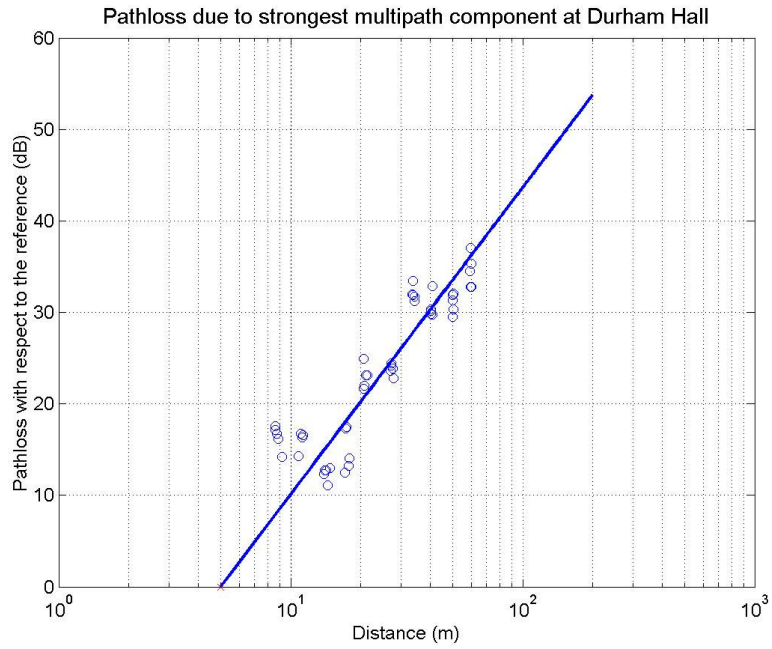


Figure 5.10 Strongest multipath component pathloss at Durham Hall employing all measurements..

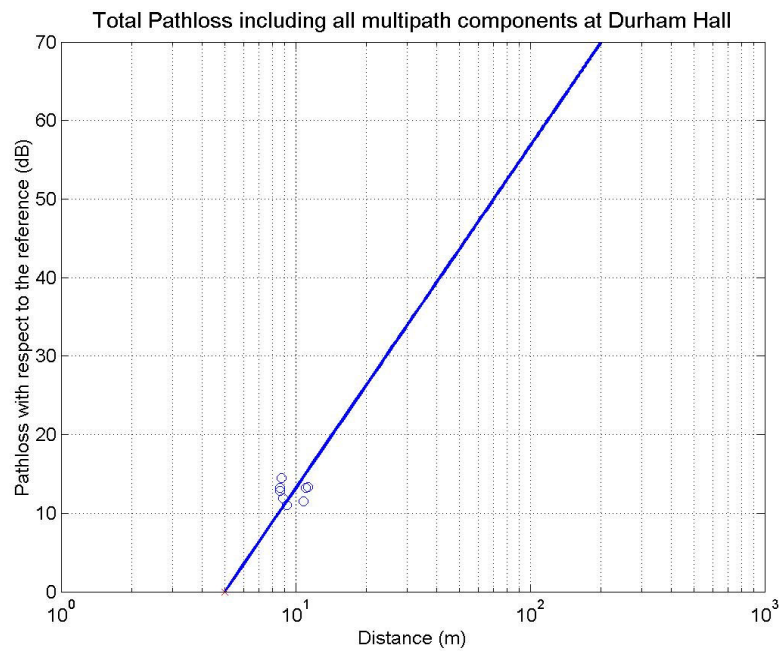


Figure 5.11 Durham Hall pathloss at short range employing all multipath components

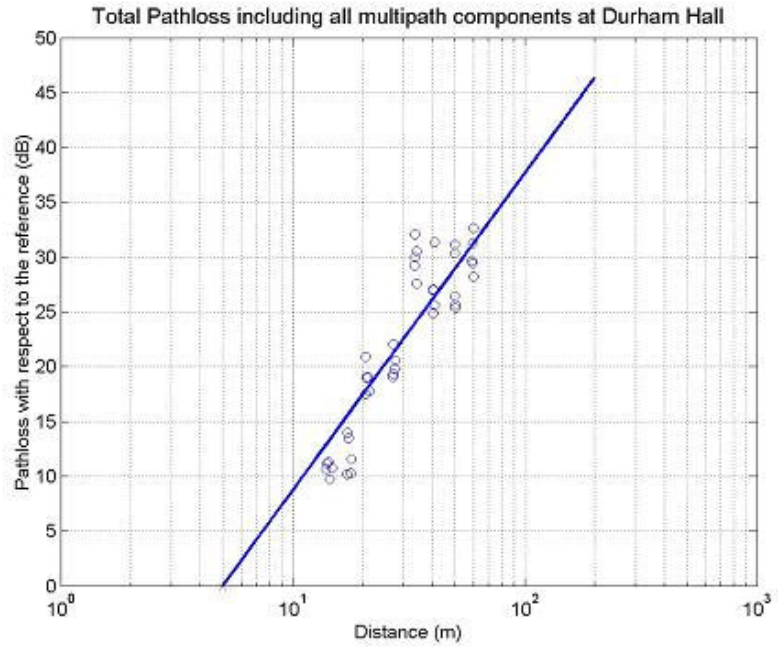


Figure 5.12 Durham Hall pathloss at long range employing all multipath components

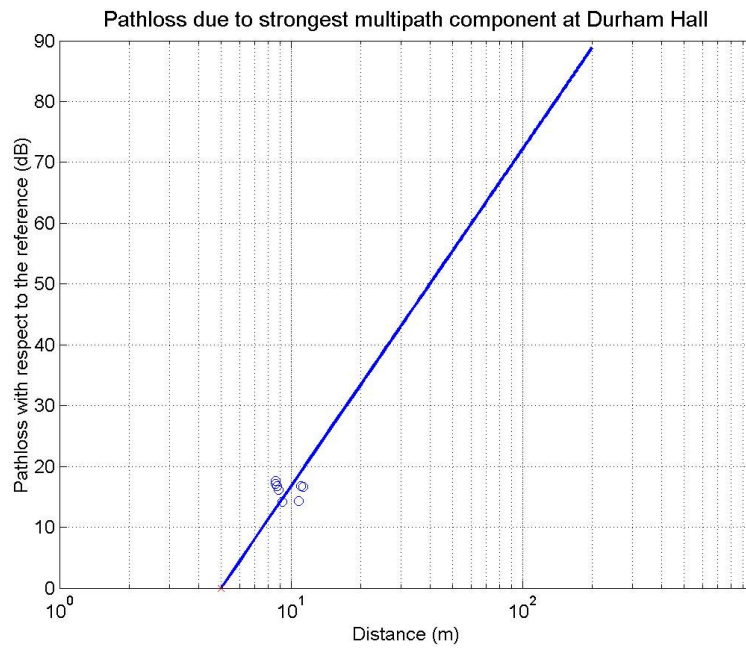


Figure 5.13 Durham Hall pathloss at short range employing only the strongest component

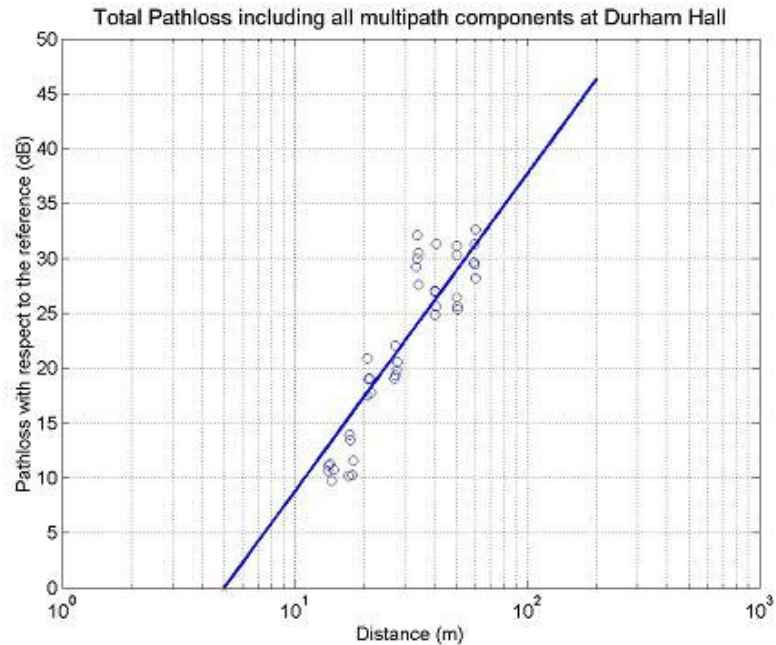


Figure 5.14 Durham Hall pathloss at long range employing only the strongest component

Another factor that should be taken into consideration is the type of antennas used in the measurement. While the lower frequency band has omni-directional antennas with corresponding lower gain they are able to receive a larger number of multipath over shorter distances. The directional antennas used at higher frequencies obtain a greater range at the expense of fewer multipath components for an extended range.

5.2 Characterization of the Multipath

The multipath analysis is conducted on similar lines as the outdoor campaign. Due to the smaller distances involved and the presence of many potential indoor reflecting surfaces a larger number of detectable multipath are realized. These are characterized on the basis of their small-scale time parameters.

5.2.1 200-400 MHz

5.2.1.1 Power Delay Profile

The incoming signal is correlated with the reference signal to generate a power delay profile (PDP). The threshold for the correlated output is set at 20dB below the strongest pulse. This defines the dynamic range of our system. A sample PDP from the Modular

Building is shown in Figure 5.15 with PDP's from Durham and Randolph Hall shown in Figure 5.16 and Figure 5.17 respectively.

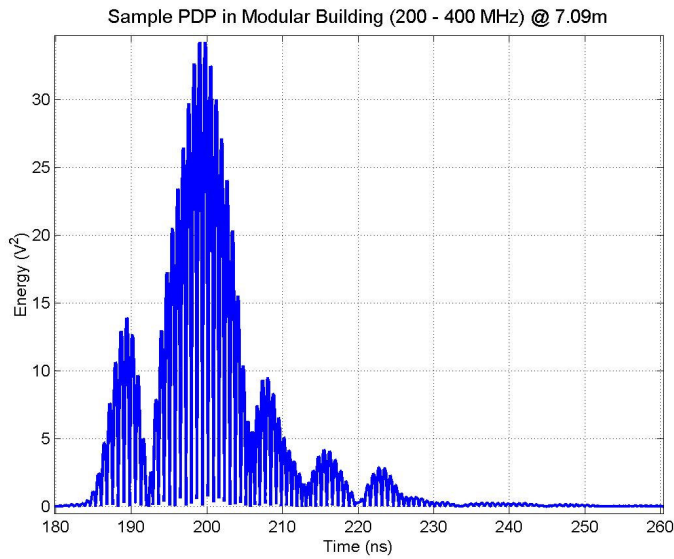


Figure 5.15 Sample Power Delay Profile from the Modular Building

Eight to ten resolvable multipath components are detected. In the case of the Modular Building and Durham Hall, the first arriving components are not the strongest. This is typical of NLOS paths. The distribution appears to be exponential. The main pulse appears to be made up of more than one resolvable multipath.

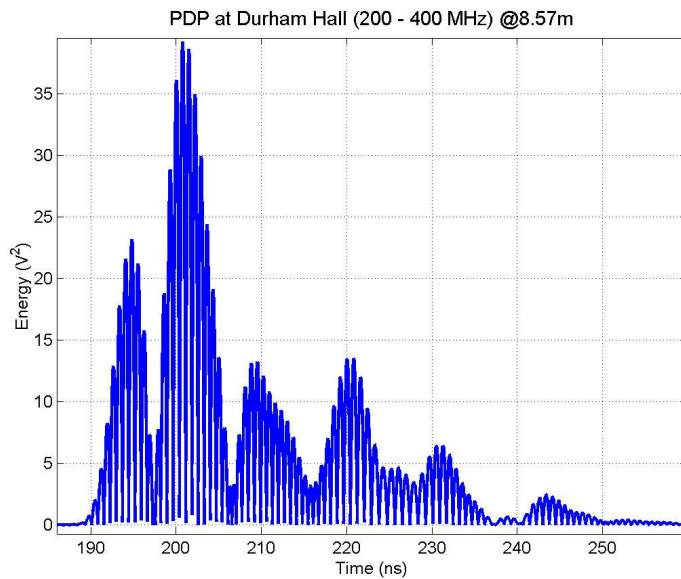


Figure 5.16: Sample Power Delay Profile from Durham Hall.

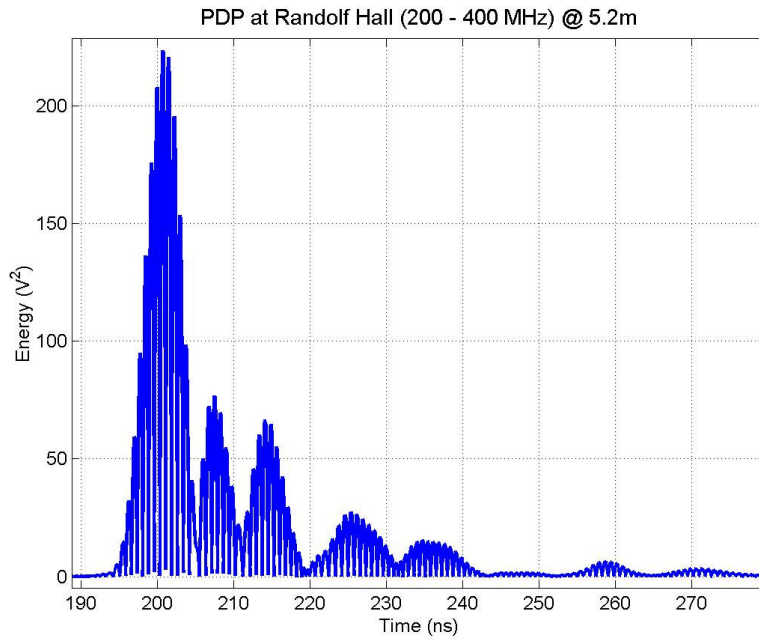


Figure 5.17 Sample Power Delay Profile from Randolph Hall

5.2.1.2 Small Scale Time Parameters

Two sets of the small-scale time parameters are computed for each location. For the first set, the transmitter is placed indoors, just inside the outer wall (the outdoor position of the transmitter would be on the outer side of this wall). Comparison of the two sets of measurements gives an insight into the propagating mechanism of the signal. For the second set, the transmitter is placed outdoors and the measurements repeated. The results obtained are tabulated in Table 5.5.

Table 5.5 Small Scale Time Parameters

Location	Mean Excess Delay (τ ns)	RMS Delay Spread (σ ns)	Excess Delay Spread (20dB) ns
Modular Bldg.	15.06	10.22	106.25
Modular Bldg Ref.	18.31	13.11	136.69
Durham Hall	15.96	11.23	108.70
Durham Hall Ref.	18.35	13.76	133.33
Randolph Hall	17.21	13.14	130.60
Randolph Hall Ref.	18.08	12.49	123.84

Table 5.5 shows that the mean excess delay and the rms delay spread are small compared with the excess delay spread. The strong multipath tend to arrive within a short time of the first arriving pulse; however there are multipath components with far smaller energy which arrive after numerous reflections.

5.2.1.3 Multipath Characterization

The energy of individual multipath components is extracted and plotted verses time giving a time distribution of the multipath. Plots of the number and strength of the multipath at each of the outdoor-to-indoor locations are given in Figure 5.18, Figure 5.19, and Figure 5.20. The energy in the strongest multipath component is compared with the total received energy in Figure 5.21, Figure 5.22, and Figure 5.23. A significant portion of the received energy is contained in the weaker multipath components.

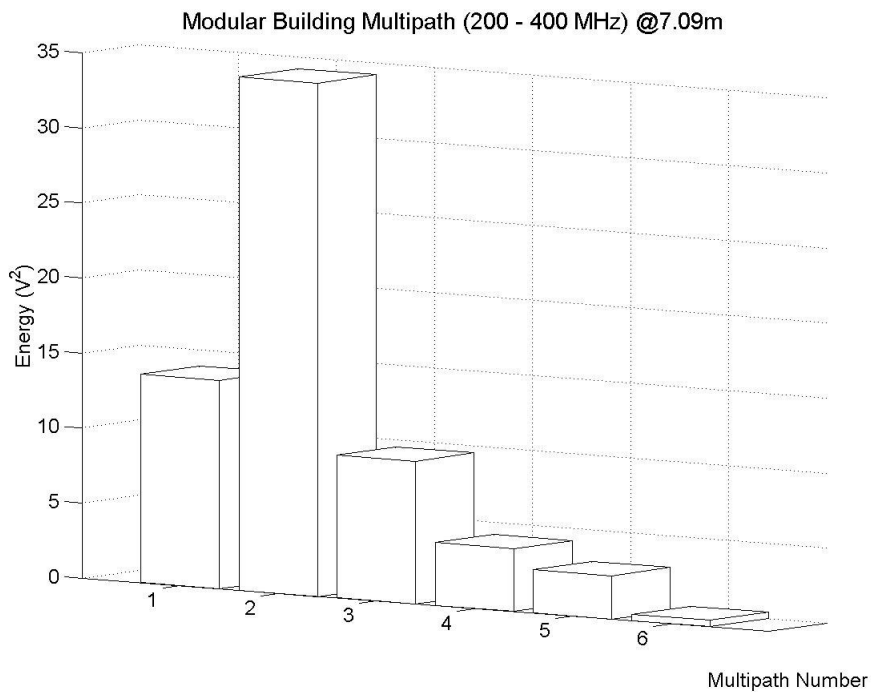


Figure 5.18 Modular Building Multipath Time Distribution

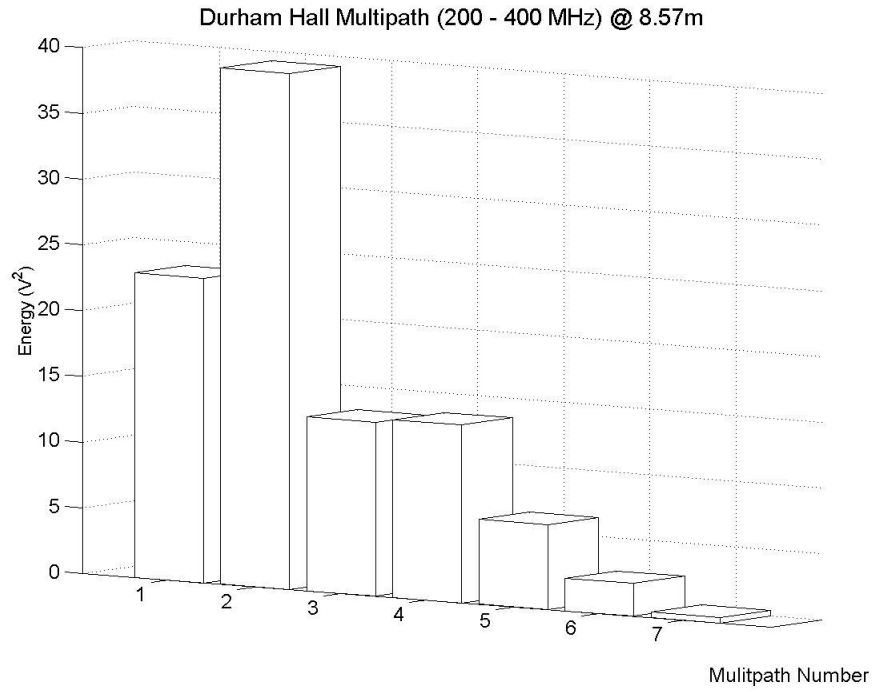


Figure 5.19 Durham Hall Multipath Time Distribution

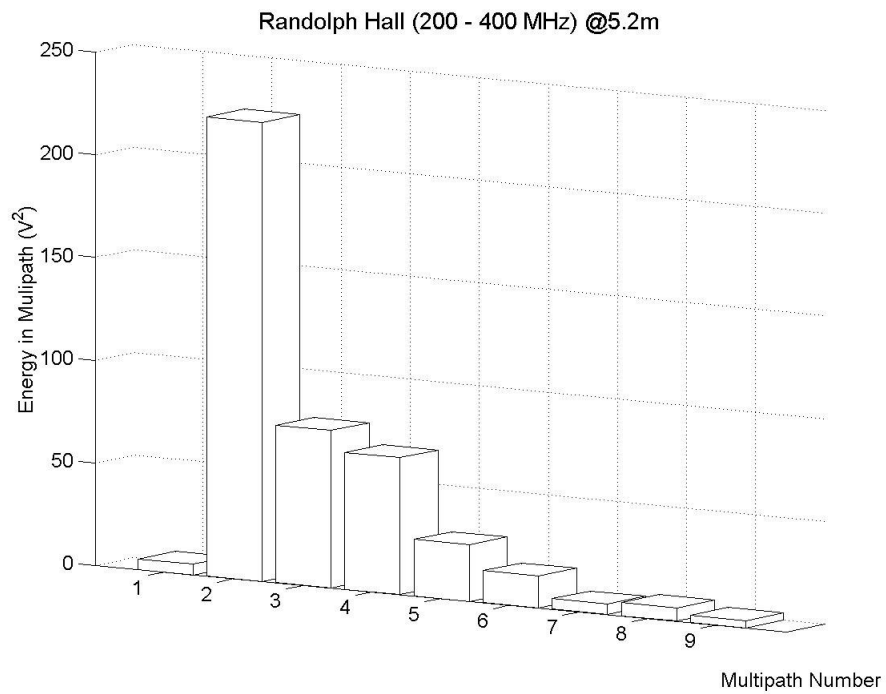


Figure 5.20 Randolph Hall Multipath Time Distribution

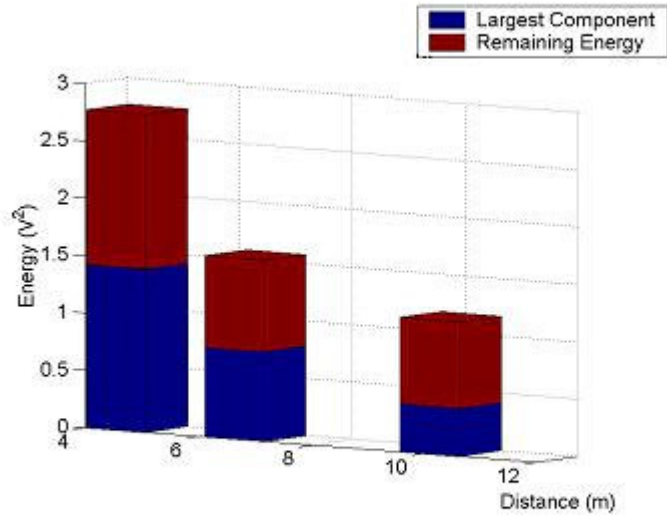


Figure 5.21 Comparison of Total Energy with Largest Multipath Component at the Modular Building

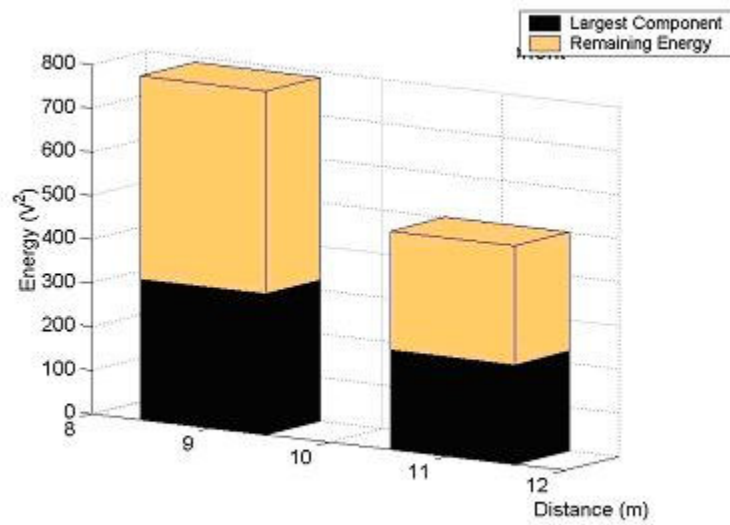


Figure 5.22 Comparison of Total Energy with Largest Multipath Component at Durham Hall

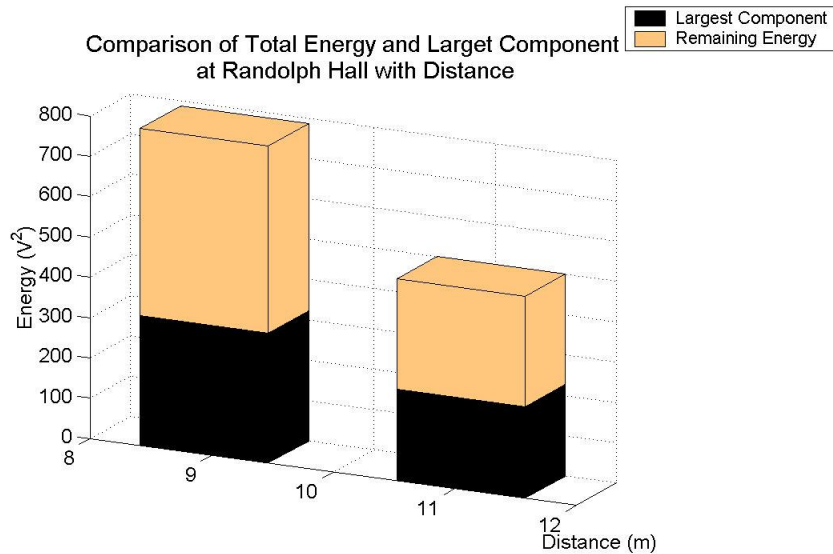


Figure 5.23 Comparison of Total Energy with Largest Multipath Component at Randolph Hall

5.2.2 6-7 GHz

5.2.2.1 Power Delay Profile

6.0 – 7.0 GHz power delay profiles (PDP) are shown in Figure 5.24 and Figure 5.25. Both locations show an average of 4-5 multipath components. The 200 – 400 MHz measurements show up to 7 multipath components. It is likely that the loss is higher at 6.0 – 7.0 GHz. Higher loss coupled with directional antennas result in fewer detectable multipath.

It was not always possible to resolve individual multipath. Either the sounder did not have adequate time resolution or the multipath is a result of non-specular reflections. There seems to be evidence of a continuum. There would possibly be many surface structures of the same order as the wavelength in question. This would potentially give rise to scattering and diffraction producing a continuum in the multipath. An example of this is shown in Figure 5.26 and Figure 5.27. This measurement was obtained in the Modular Building.

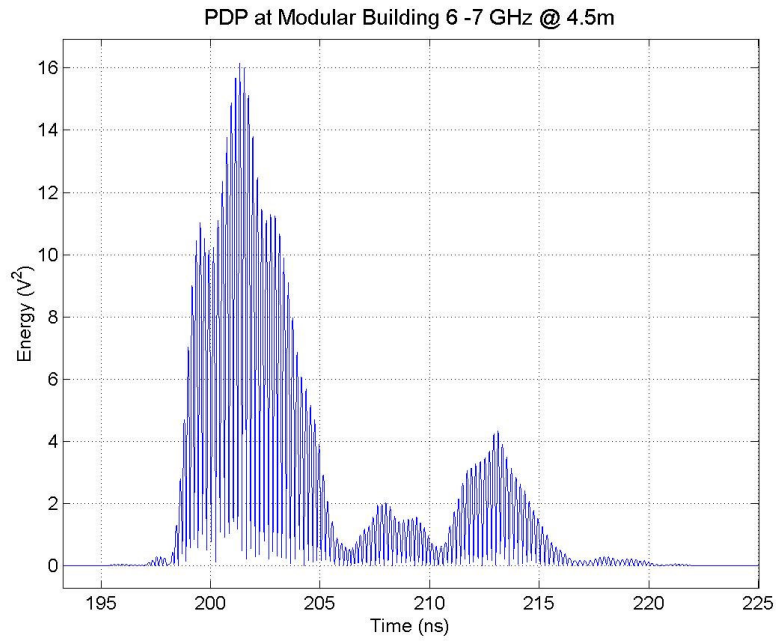


Figure 5.24 Power Delay Profile at the Modular Building

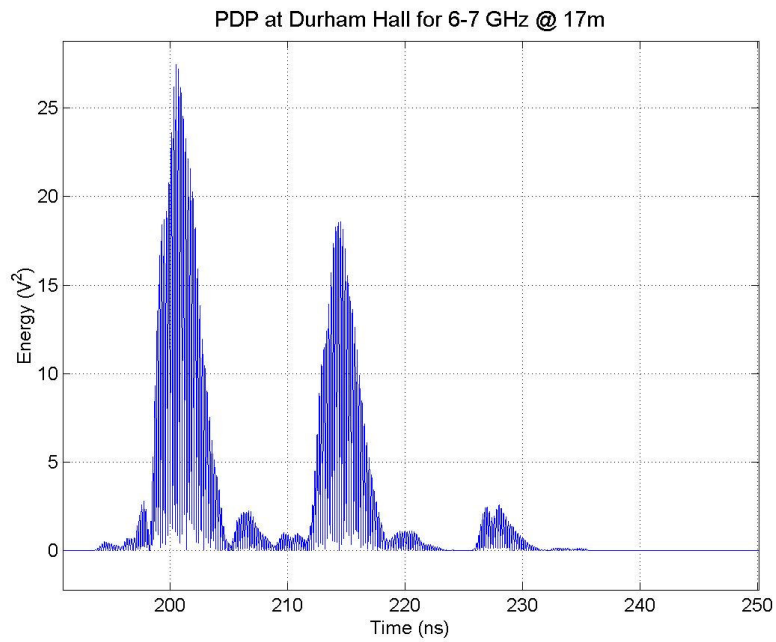


Figure 5.25 Power Delay Profile at Durham Hall

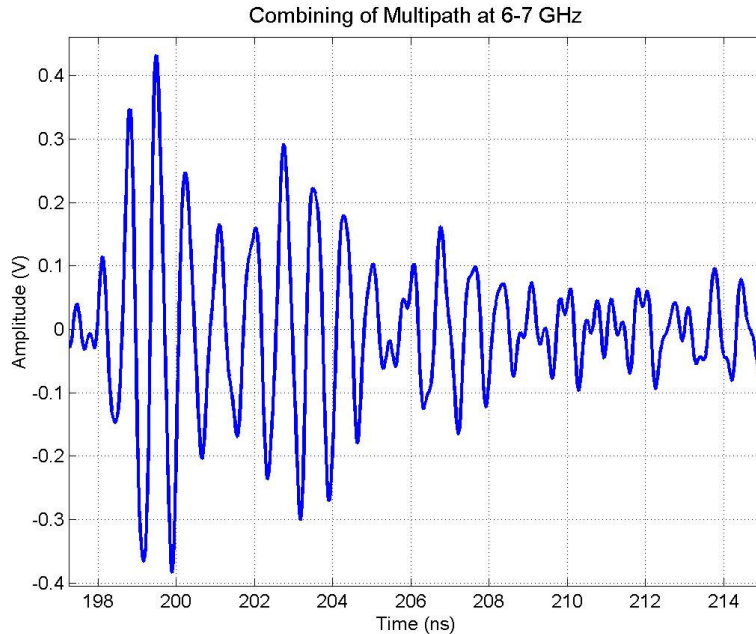


Figure 5.26 Combining of successive multipath components

5.2.2.2 Small Scale Time Parameters

Table 5.6 contains the small-scale time parameters for the 6.0 – 7.0 GHz indoor-to-outdoor measurements.

Table 5.6: Small Scale Time Parameters

Location	Mean Excess Delay – τ ns	RMS Delay Spread σ ns	Excess Delay Spread (20dB) ns
Modular Building	9.07	3.43	33.10
Durham Hall	15.54	8.32	75.81

The delays obtained in the 6-7 GHz band are significantly less than the delays for the 200 – 400 MHz band. This can be explained by the fact that there are fewer multipath components and the presence of higher attenuation at 6.0 – 7.0 GHz as compared to 200 – 400 MHz. Also the small mean excess delay with respect to the excess delay spread indicate that most of the prominent multipath components occur within a short time period following the first arriving pulse.

5.2.2.3 Multipath Characterization

As noted above, the measurements at 6.0 – 7.0 GHz yield far fewer multipath components as compared to the 200 – 400 MHz measurements. Directional antennas are used for the 6.0 – 7.0 GHz measurements, which improve the range due to an increased gain and discriminate against the off axis multipath. Another possible explanation for fewer multipath components is higher attenuation at the higher frequency. The typical distribution of the number of multipath at 6.0 – 7.0 GHz and their respective energies are given in Figure 5.27 and Figure 5.28.

Figure 5.29 and Figure 5.30 show the total received energy and the energy in the strongest multipath component as a function of range. The plots show the strongest multipath component comprises approximately 50% of the total energy received. Given that there are a maximum of 4 significant multipath components, a two or possible three-finger rake receiver could be used.

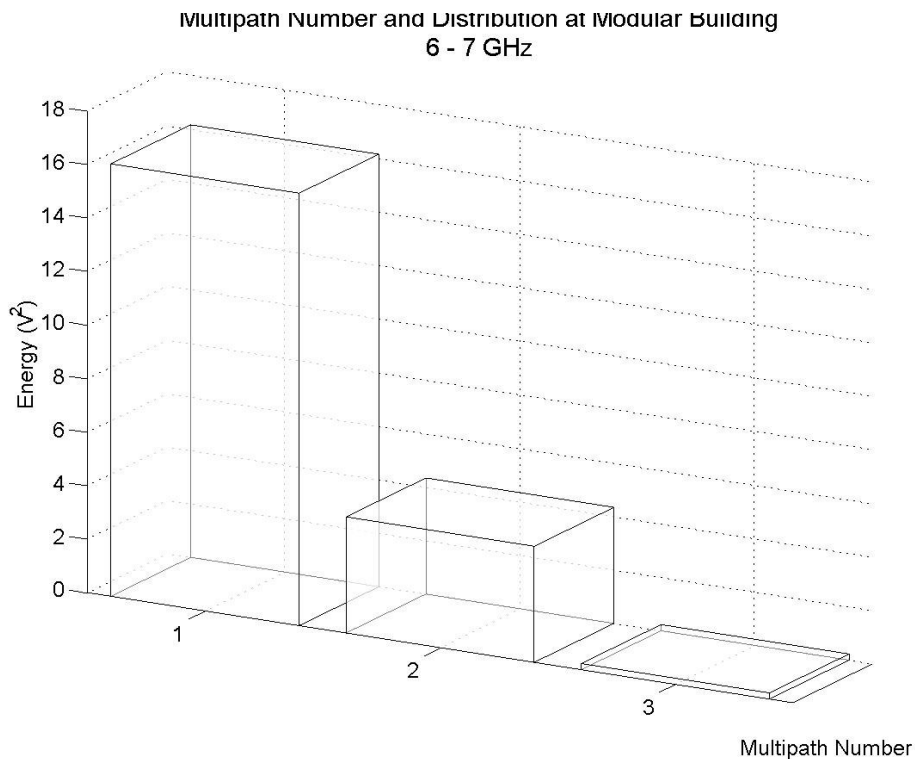


Figure 5.27 Plot of Energy and Number of Multipath Components in the Modular Building

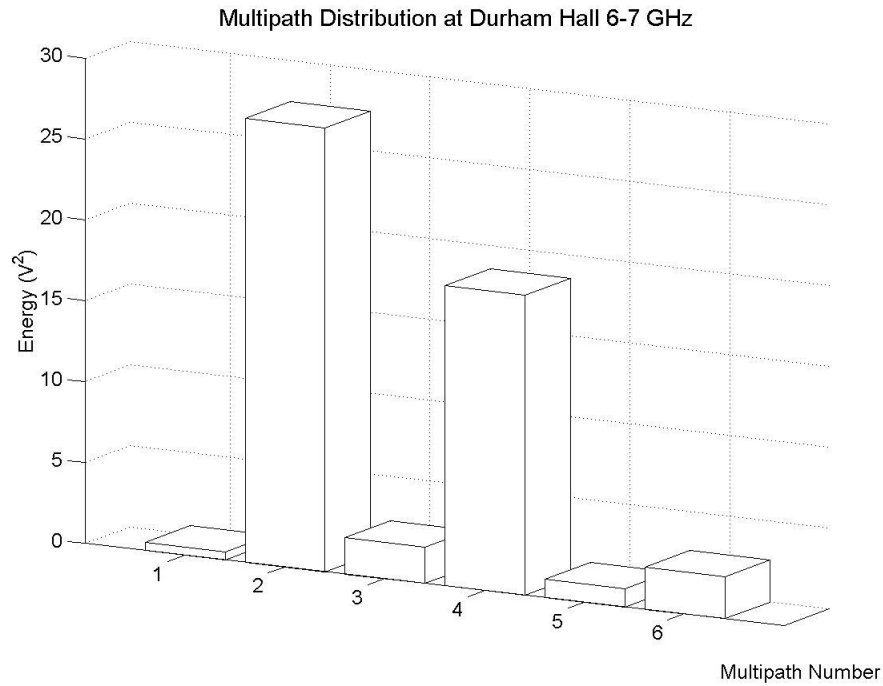


Figure 5.28 Plot of Energy and Number of Multipath Components in Durham Hall

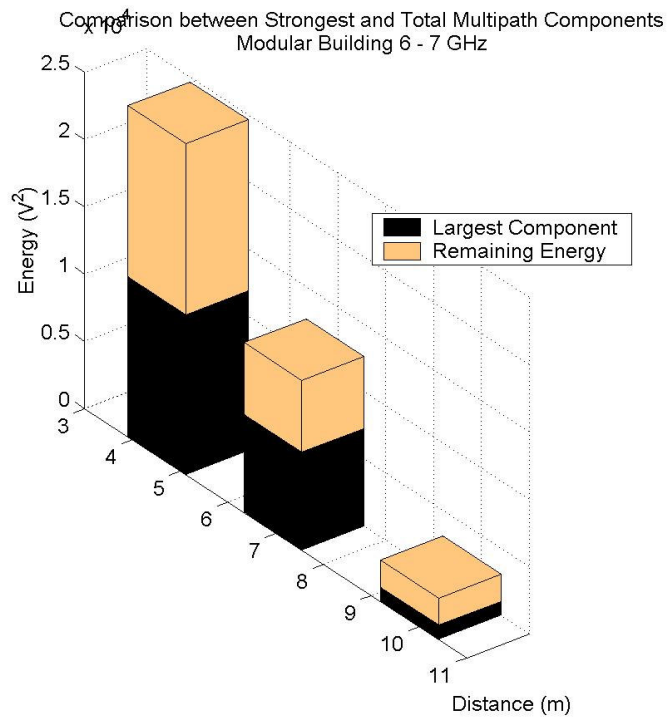


Figure 5.29 Relation of Total Energy and Strongest Multipath Component in the Modular Building

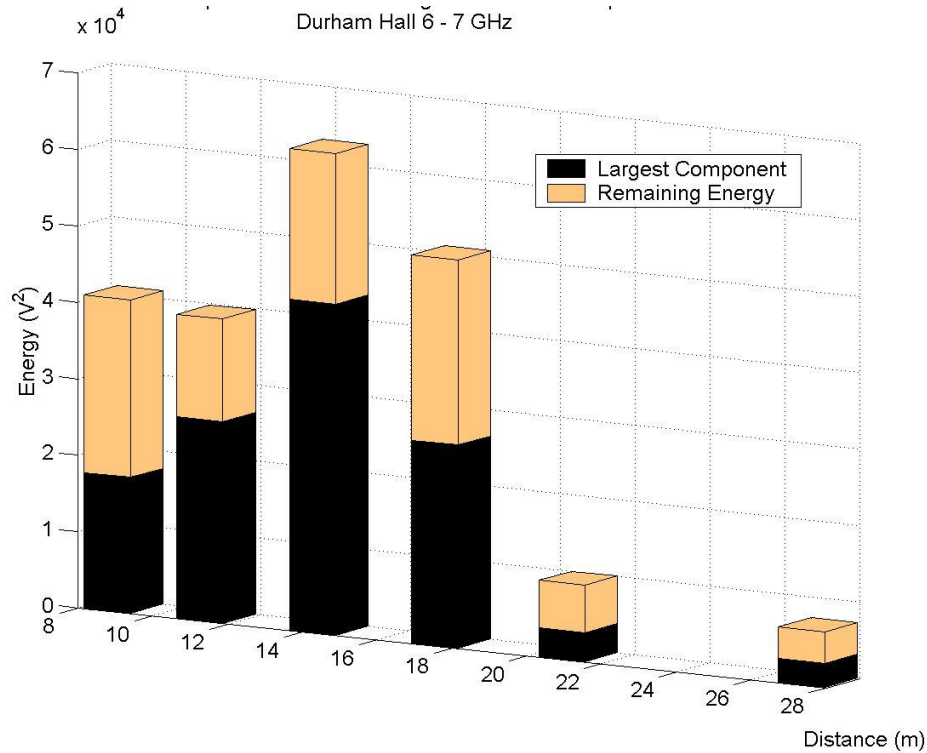


Figure 5.30 Relation of Total Energy and Strongest Multipath Component in Durham Hall

5.3 Penetration Loss

5.3.1 200-400 MHz

The pathloss of the reference indoor measurement is compared with a measurement taken just on the opposite side of the outdoor wall. The building penetration loss is computed from these two measurements. The computed wall loss is tabulated in Table 5.7.

Table 5.7 Summary of Penetration Loss (200 – 400 MHz)

Location	Penetration Loss (dB)
Modular Building	2.08
Durham Hall	10.92
Randolph Hall	4.01

The modular building is predominantly a wooden structure and provides the least attenuation while the double concrete walls and limestone of Durham Hall and the brick and concrete framework of Randolph Hall exhibits significantly higher loss.

5.3.2 6-7 GHz

The penetration loss for both the Modular Building and Durham Hall is higher for 6.0 – 7.0 GHz than for 200 – 400 MHz. The results are tabulated in Table 5.8.

Table 5.8 Penetration Loss at 6.0 – 7.0 GHz

Location	Penetration Loss (dB)
Modular Building	9.65
Durham Hall	11.93

The difference in penetration loss in Durham Hall at the two frequency bands under consideration is not of the order of the difference observed in the modular building. This may be attributed to the frequency dependent characteristics of the material of the respective walls. It indicates that the rate of attenuation with frequency is greater for wood as compared to concrete.

6 Evaluation of the Empirical Ultrawideband Parameters

In this chapter we will evaluate and compare the UWB parameters obtained from both the outdoor and the outdoor-to-indoor measurements with measurements obtained both from other UWB measurements and other narrowband measurements in similar frequency bands. One of the difficulties faced during this study was the absence of other measurement campaigns in the UWB regime. It is possible that there have been other studies conducted primarily by defense-related concerns whose results are classified or proprietary commercial information.

However, in order to validate the results, the parameters are compared against similar results from the limited UWB literature and available narrowband CW campaigns. The results in the sub-gigahertz segment are compared against measurements in the 200-400 MHz range. The 1-2 and 2-4 GHz measurements are evaluated against the ISM and cellular band results. The results obtained at the 6.0-7.0 GHz band were compared with results obtained in campaigns undertaken in the 802.11a band at ~5.5 MHz. Though not an exact comparison, we can evaluate parameters of pathloss, time dispersion parameters and penetration loss against these measurements.

6.1 Outdoor Measurements

Currently there is only one major reference [8] that describes outdoor UWB propagation. This is focused on rural terrain and it used a baseband system with a bandwidth of 1.3GHz. This section compares reported results from narrowband and ‘wideband’ systems with the results obtained by our UWB measurement campaign. The parameters, which are highlighted, are the pathloss exponent and the small-scale time parameters that define the multipath, namely the mean excess delay, rms delay spread and the excess delay spread. For each of the three bands, our results are compared with the results published at frequencies in and around the band in question.

The systems used for comparison are mainly cellular and wireless LAN applications. Most of the systems are able to transmit well over 500m [18] and have bandwidths from 1 KHz [19] to 200 MHz [20]. Average transmitter power ranging from 30dBm [21] to 47dBm [30], which resulted in greater range and sensitivity due to the lower bandwidth.

The results used for the comparison are mainly of measurements in locations ranging from residential environments [19] to urban built up areas [23].

6.1.1 Pathloss

The UWB pathloss is compared with the pathloss obtained in other studies. The comparisons are grouped by environment and frequency band. The reported narrowband results below 2 GHz are grouped together for comparison with the 1.0 – 2.0 GHz UWB band, narrowband results between 2-5 GHz were compared with the 2.0 – 4.0 GHz UWB measurements, and frequencies over 5 GHz were compared with the 6.0-7.0 GHz band. The comparison is presented in Table 6.1, Table 6.2, and Table 6.3.

Table 6.1 Comparison of outdoor path loss exponents obtained by various researchers with our UWB path loss exponents in the 1.0 – 2.0 GHz band.

Reference	Type	Pathloss Exponent
Devasirvatham (850 MHz) [21]	Urban	2.75
Seidel (900 MHz)[18]	Urban	3.0
Paez (1800 MHz) [24]	Suburban	2.45
Patwari (1800 MHz) [20]	Suburban	2.8
Hendrickson (1814 MHz) [25]	Urban	3.0
Devasirvatham (1900 MHz) [19]	Urban NLOS	5.0
VA Tech UWB	Suburban LOS	1.91
VA Tech UWB	Suburban NLOS	3.02

Table 6.2 Comparison of outdoor path loss exponents obtained by various researchers with our UWB path loss exponents in the 2.0 – 4.0 GHz band.

Reference	Type	Pathloss Exponent
Devasirvatham (2.11 GHz) [19]	Urban NLOS	4.8
Healey (2.4 GHz) [26]	Suburban	2.532
VA Tech UWB	Suburban LOS	1.81
VA Tech UWB	Suburban NLOS	4.18

Table 6.3 Comparison of outdoor path loss exponents obtained by various researchers with our UWB path loss exponents in the 6.0 – 7.0 GHz band.

Reference	Type	Pathloss Exponent
Kim (5 GHz) [27]	Urban LOS	1.98
Zhao (5.3 GHz) [28]	Suburban LOS	2.5

Zhao (5.3 GHz) [28]	Suburban NLOS	3.4
VA Tech UWB	Suburban LOS	1.82
VA Tech UWB	Suburban NLOS	2.82

From the tabulated results, it appears that the pathloss exponent follows the trend as the narrowband results, especially in the NLOS cases. In the 6.0 – 7.0 GHz band, the pathloss seems lower than that obtained in the lower frequency bands. This is along the lines of the classical decrease in pathloss with increase in frequency.

6.1.2 Small Scale Time Parameters

The large bandwidth offered by UWB permits the resolution of individual multipath components. The sensitivity of the measurement system limits detection of multipath components greater than 20dB below the strongest arriving signal. The limited sensitivity and the use of directional broadband antennas tend to reduce the delay spread to the order of nanoseconds. This reduced sensitivity is a limitation of the measurement system and it is suspected to be one of the main challenges in UWB receiver design. The delay spreads are also tabulated depending upon the respective bands of consideration. This is tabulated in Table 6.4, Table 6.5 and Table 6.6.

Table 6.4 Comparison of outdoor delay spread reported by various researchers with our UWB path loss exponents in the 1.0 – 2.0 GHz band.

Reference	Type	RMS Delay Spread
Seidel (900 MHz)[18]	Urban	19.6 μ s
Hendrickson (1814 MHz) [25]	Urban	75ns
Paez (1800 MHz) [24]	Suburban	22ns
Patwari (1800 MHz) [20]	Suburban	200ns
Devasirvatham (850 MHz) [21]	Urban	110ns
Win (1.3 GHz) [8]	Rural	14.49ns
Durgin (1920 MHz) [29]	Suburban (Short range)	33.25ns
Devasirvatham (1900 MHz) [23]	Urban NLOS	475ns
VA Tech UWB	Suburban	28.48ns

Table 6.5 Comparison of outdoor delay spread reported by various researchers with our UWB path loss exponents in the 2.0 – 4.0 GHz band.

Reference	Type	RMS Delay Spread
-----------	------	------------------

Paez (2.45 GHz) [24]	Suburban	25ns
VA Tech UWB	Suburban LOS	5.15ns

Table 6.6 Comparison of outdoor delay spread reported by various researchers with our UWB path loss exponents in the 6.0 – 7.0 GHz band.

Reference	Type	RMS Delay Spread
Zhao (5.3 GHz) [35]	Suburban NLOS	25ns
Kim (5 GHz) [27]	Urban LOS	6.25ns
VA Tech UWB	Suburban	4.25ns

The UWB rms delay spreads are much lower than a number of other measured results. However, a few narrowband researchers [28][29] do obtain similar results.

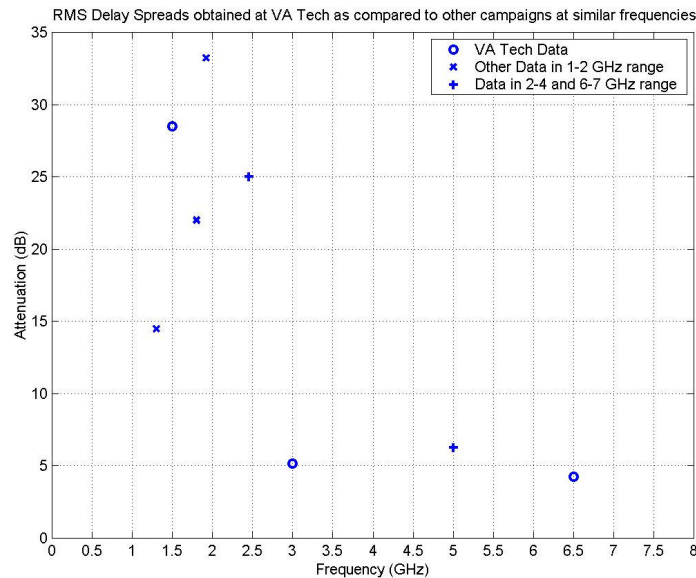


Figure 6.1 Variation in RMS Delay spread obtained for UWB versus other campaigns

The multipath distribution in narrowband systems tends to be more continuous than discrete. This is due to the limited time resolution on most narrowband measurement systems. A maximum of 5 – 6 resolvable multipath components are observed compared to the 20 or more, which have been reported by some narrowband measurements [22]. Most of the narrowband measurements that reported larger number of multipath components operated with a highly sensitive receiver with a lower noise floor. Ultrawideband signals with a bandwidth in the gigahertz band resulted in a receiver with lower sensitivity that limited the number of multipath obtained over the noise.

6.2 Outdoor-to-Indoor Penetration Loss

Penetration loss has been studied in the PCS and cellular bands in the USA [31], [32] along with measurements carried out in the 5GHz Unlicensed National Information Infrastructure band (UNII)[33][34]. Most of the measurements are classical narrowband CW measurements. An extensive literature survey found no work reported in outdoor-to-indoor UWB propagation. Most of the narrowband studies [34], [35] suggest that the propagation mechanisms including penetration loss through the walls are dependent upon several factors –

- Electrical parameters of the materials (ϵ_r , σ)
- Composition – either single or multilayered that may result in multiple reflections
- Presence of windows and other artifacts
- Frequency of operation
- Angle of incidence
- Polarization of the antenna

Table 6.7 tabulates the penetration loss reported by various researchers. The outdoor to indoor results from our UWB measurements are included for comparison. The results obtained in our campaign are in the range reported by [33], [34], [35], [36], [37] and [38]. For concrete walls, the trend is increasing loss with increasing frequency. A similar trend is reported in [35] where CW narrowband measurements were conducted from 900 MHz to 18 GHz.

We measure lower loss for UWB than that reported for narrowband systems. This is the result of a larger bandwidth and the possibility of multiple paths. In addition, the walls appear to act like a filter selectively attenuating a few frequencies while allowing other frequencies to pass through. In the case of narrowband systems all the frequencies that comprise the signal could face attenuation – while UWB offsets this by its bandwidth. This is shown in Figure 6.2. It can be seen that in the modular building certain frequencies around 300MHz are attenuated. However the same measurement in Durham Hall shows a greater loss, which is the result of the higher penetration loss and pathloss.

Table 6.7 Comparison of Measured Penetration Loss

Material Penetration Loss (dB)

	Plasterboard/ wood	Concrete
Hoppe (230 MHz) [32]	-	10
Silva (840 MHz) [37]	3.5	-
Tanis (880 MHz) [38]	-	19.2
Toledo (900 MHz) [31]	-	14.2
Zhang (900 MHz) [35]	2.5	10
Aguirre (912 MHz) (Floor 1) [36]	5.833	14
VA Tech (200-400MHz)	2.1 (Modular Building)	10.9 (Durham Hall)
Karlsson (5.8GHz) [34]	-	15.5
Schwengler (5.85 GHz) [40]	-	13.2
Muqaibel (5.0 GHz) [41]	2.11	13.62
Durgin (5.85 GHz) [33]	-	16.3
Aguirre (5.99 GHz) [36]	12.0833	16
Zhang (6 GHz) [35]	7	12
VA Tech (6 – 7 GHz)	9.7 (Modular Building)	11.9 (Durham Hall)

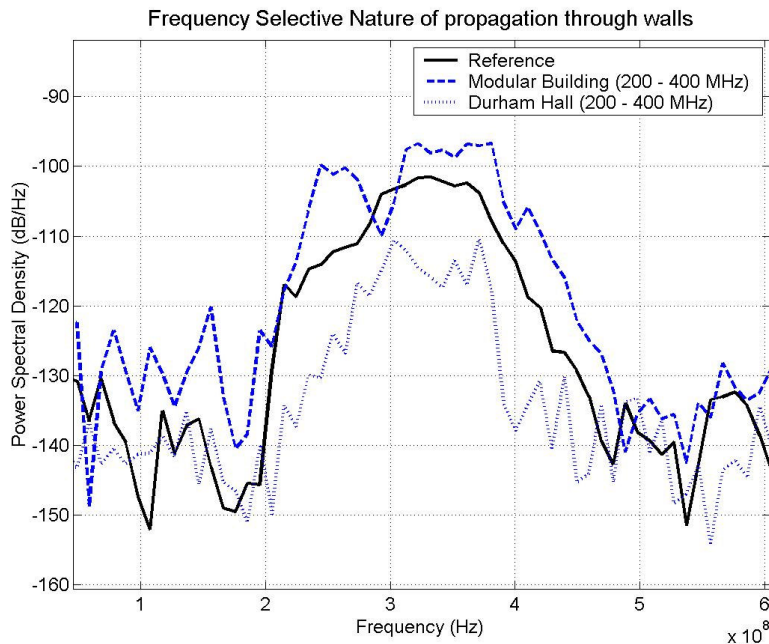


Figure 6.2 Frequency selective transmission

Another important aspect reviewed in the literature [34], [33] is the effect of windows and other similar structures on the total received signal strength. Depending on the type of opening, the difference in penetration loss could be anything from 1.2dB for a simple window to more than 20dB for glass coated with metal oxide film. Given the structure of

Durham Hall where the transmitter was placed outside the glass doors and there was presence of a large number of floor-to-ceiling metal oxide coated glass panels a higher penetration loss can be also partly ascribed to this factor.

It is suggested [36] that if there is significant correlation between the penetration losses at different frequencies, then the penetration loss at other frequencies can be determined by extrapolation via linear regression as determined by Eqn. 6.1.

$$y(f_2) = x(f_1) + \alpha + N(0, \sigma) \quad \text{Eqn. 6.1}$$

where f_2 is the frequency at which penetration loss is to be determined

f_1 is the frequency at which penetration loss has been estimated

α is a linear regression fit factor

$N(0, \sigma)$ is a zero mean Gaussian random variable with standard deviation of σ dB

where the correlation coefficient is given by Eqn. 6.2.

$$\rho(f_1, f_2) = \frac{E[(f_1 - m_1)(f_2 - m_2)]}{\sigma_1 \sigma_2} \quad \text{Eqn. 6.2}$$

where m_1 and m_2 are the mean

σ_1 and σ_2 are the standard deviation of the penetration loss.

However in the case of UWB, this may not be valid. Considering the bandwidths in question, either the total bandwidth or the fractional bandwidth may have to be incorporated in order to reasonably extrapolate the penetration loss. The correlation coefficient $\rho(f_1, f_2)$ would have to be relatively constant over the entire bandwidth ($f_1 - f_2$) in question for the formula to be valid.

Evaluating results from [35], it can be seen that in the case of a concrete wall with glass windows, the penetration loss seems to follow a linearly increasing trend. However given that only two frequency bands were measured it would be difficult to estimate the trend followed in the case of the Modular Building to verify the results obtained in [35]. A plot of the change in penetration loss with frequency for different materials is given in Figure 6.3. It indicates that the rate of penetration loss with frequency depends upon the nature of the material.

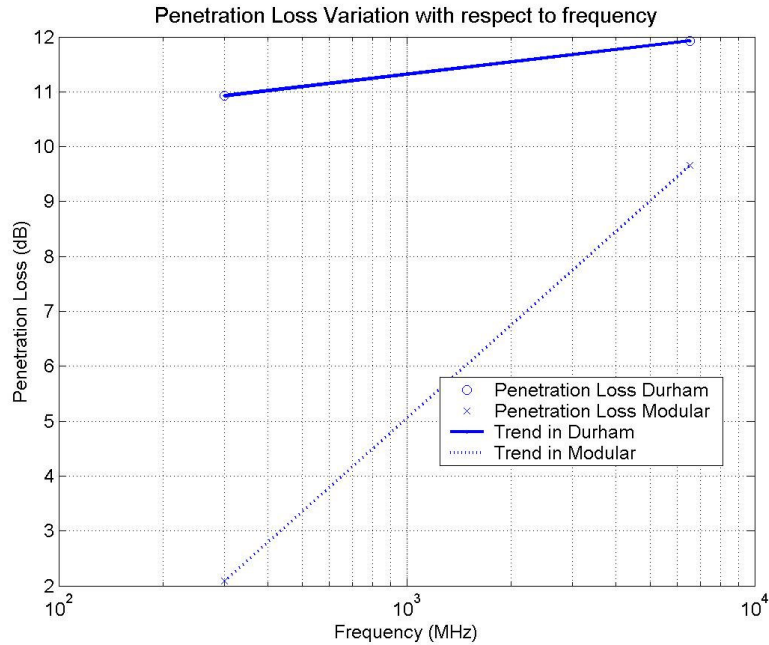


Figure 6.3 Variation of penetration loss with frequency in propagation through different materials

Table 6.8 tabulates reported pathloss exponents for narrowband measurements. The UWB pathloss exponents fall in a similar range.

Table 6.8 Comparison of Pathloss Exponents

Reference	Pathloss
Karlsson (5.85 GHz) (Concrete Wall) [34]	3.5
Durgin (5.85 GHz) (Brick Wall) [33]	3.4
VA Tech (6.0-7.0 GHz) (Concrete& Glass)	4.26
Toledo (900 MHz) (Concrete) [31]	5.3
Parson (900 MHz) (Concrete) [17]	4.0
VA Tech (200 – 400 MHz) (Concrete & Glass)	3.92

Studying the general trends in the absence of other UWB measurements, we note that the results obtained fall in the same range as the results obtained by comparative narrowband measurements. We also note that the UWB pathloss increases with frequency. A plot of the change in pathloss exponent with frequency is given in Figure 6.4 for the two frequency bands of 200-400 MHz and 6.0-7.0 GHz. From the two figures it seems that the rate of change in penetration loss with frequency has a bearing on the rate of change of pathloss with frequency for a particular material.

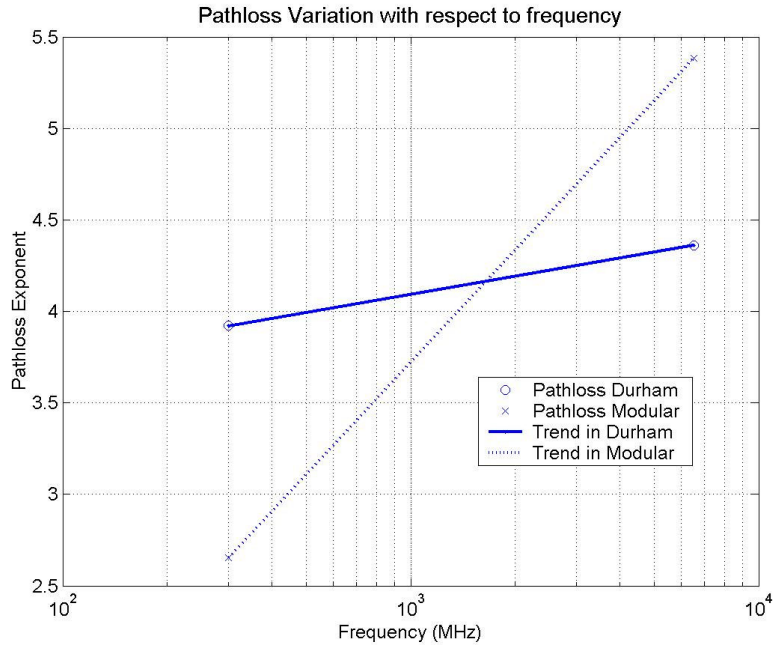


Figure 6.4 Trend indicating variation of pathloss vs. frequency in different materials

7 Conclusion

The research that was undertaken as part of the DARPA NETEX initiative served as a means to understand the propagation mechanism of Ultrawideband in outdoor regimes. Given the need of a greater range and also a more sensitive receiver operating under FCC emission guidelines, the task of designing the system to satisfy two complementary goals was by no means a trivial issue.

The results obtained however serve as good starting points for any further measurement campaigns in this realm. The work has provided the parameters required for the development of a comprehensive outdoor and outdoor-to-indoor UWB propagation model, which could be useful in the development of any standard. The results provide estimates of the pathloss and small-scale parameters derived from the power delay profile across different frequency bands that are included in the FCC specification. Penetration loss across two different bands over different materials is also discussed. It was noticed that UWB suffers a pathloss and penetration loss along the same lines of similar narrowband measurements. However in terms of the delay statistics it is seen that the delays obtained are lower than that of narrowband signals. Most of the multipath components are discrete and resolvable in nature.

However given the present limitations and the results obtained it would seem that outdoor UWB could best be deployed in the form of an ad-hoc mesh topology. In this scenario each node would be near to at least one other node, which would be in line-of-sight. In this fashion UWB could overcome the distance limitations where each node would act like a router to transmit/receive information from other nodes. Such a setup would inherently be LPI/LPD and would operate efficiently at low data rates. It has been seen that even if the peak power is high, depending upon the pulse repetition frequency the average power could be well below the noise floor.

Further research would be along the lines of developing higher layer protocols that use Ultrawideband as an overlaying technology over existing users. Studies need to be carried out with regards to analyzing the tradeoff of data-rate with distance and power. This would be required for all power budget analysis. Finally the development of highly sensitive impulse based receivers would have a far-reaching impact for both imaging and communications based applications.

8 Appendix

8.1 Appendix I - Sample Outdoor Setup with sets of received data

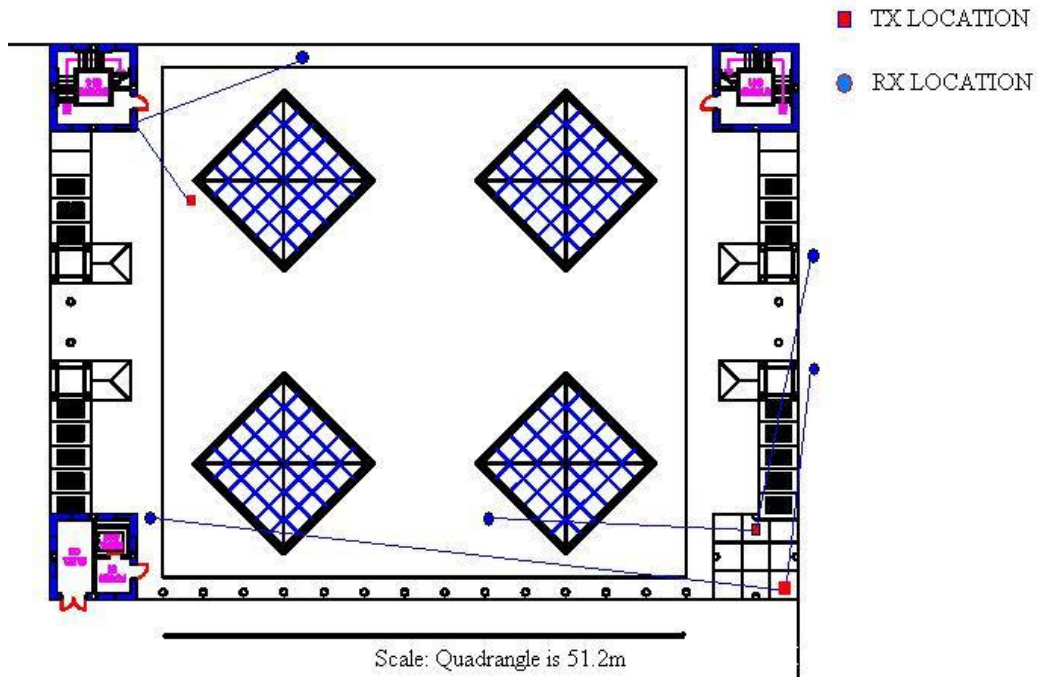


Figure 8.1 Burchard Hall Measurement Locations



Figure 8.2 Burchard Hall measurement location. This picture is the transmitter location in the lower right of Figure 8.1



Figure 8.3 Location next to Cowgill Hall with a bounce path off Hancock. The Modular Building is to the left

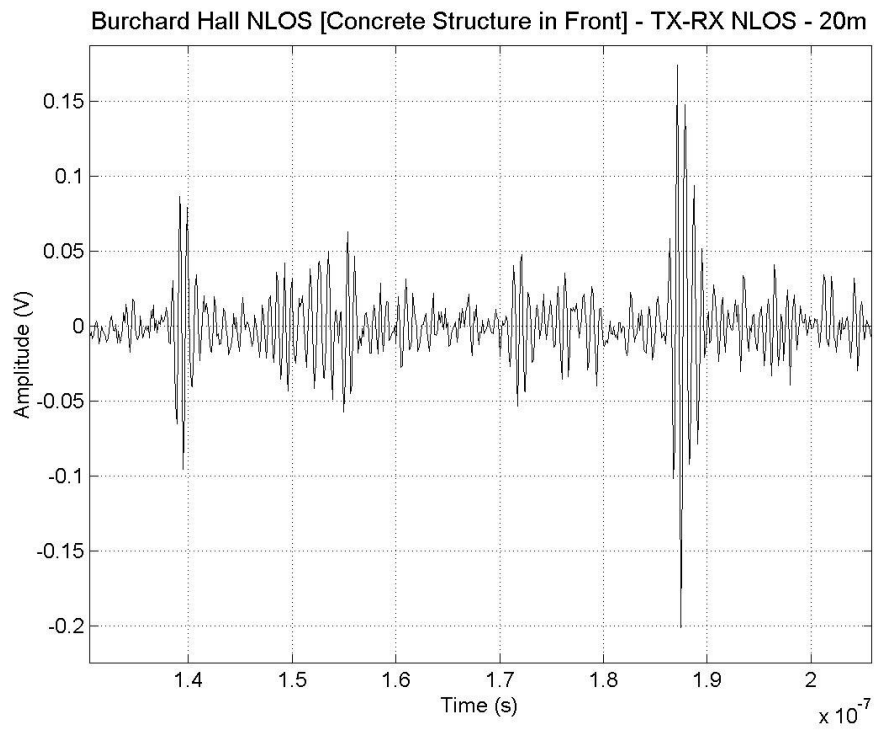


Figure 8.4 Burchard Hall NLOS path

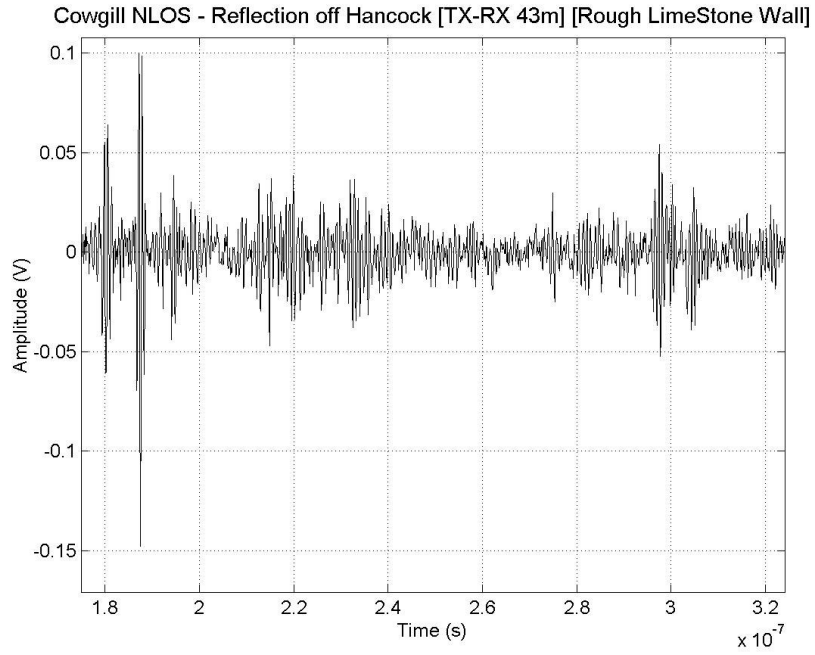


Figure 8.5 Cowgill Hall NLOS path. Multiple Multipath off Adjacent Walls - Canyon Environment

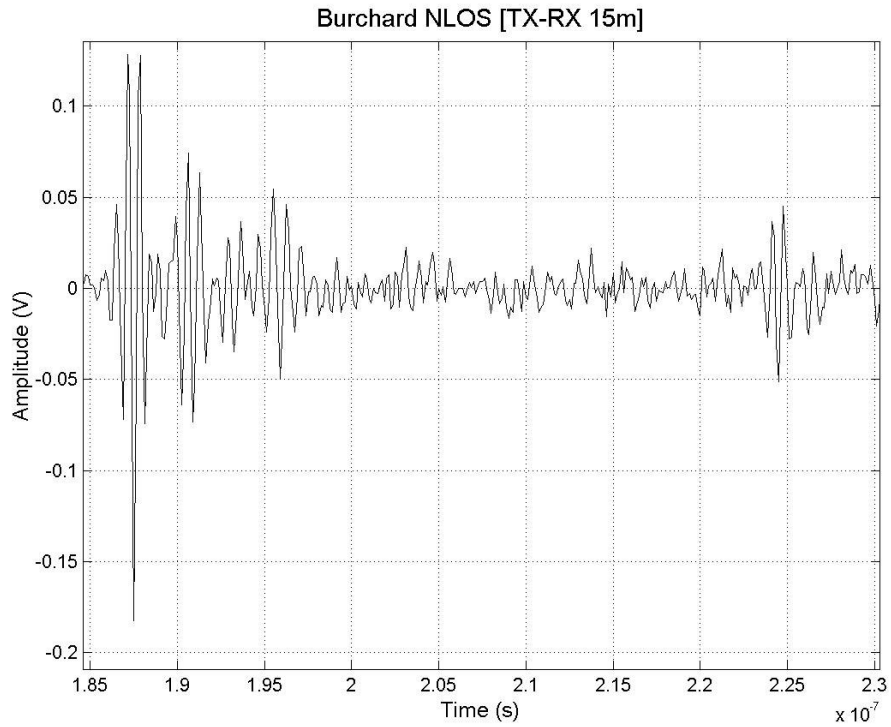


Figure 8.6 Burchard Hall NLOS, note the resolvable multipath components

8.2 Appendix II – Outdoor-to-Indoor Measurement Locations

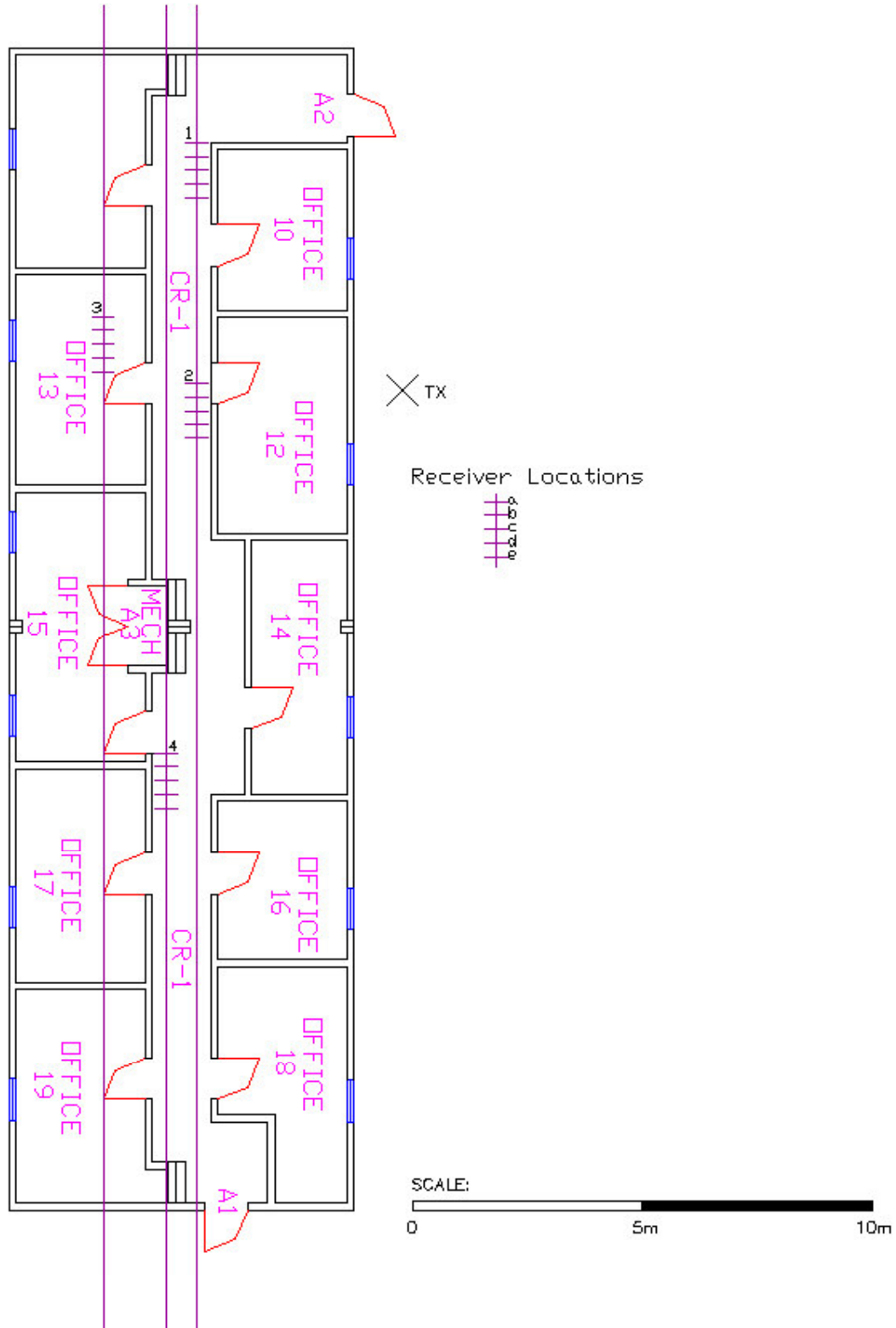


Figure 8.7 Modular Building Transmitter and Receiver Locations. The transmitter location is the X to the right of the building and the receiver is placed a various locations down the center hall. The receiver locations are approximately 0.3 meters apart

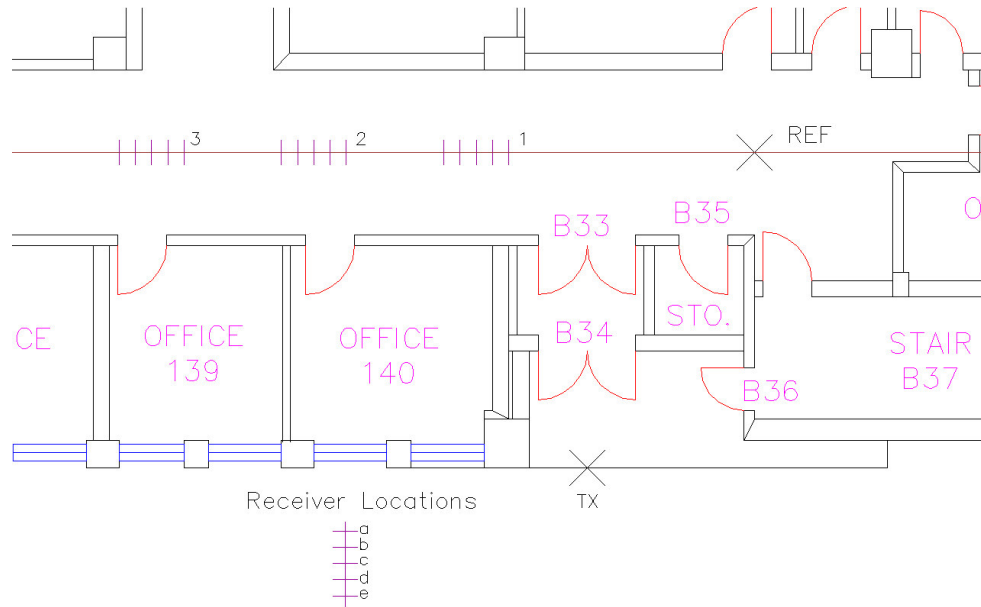


Figure 8.8 Randolph Hall Transmitter and Receiver Locations. The transmitter location is the X in the right center and the receiver is placed a various locations down the center hall on the same level as the transmitter. The reference measurement was taken at the “REF” X at the center right. The receiver locations are approximately 0.3 meters apart

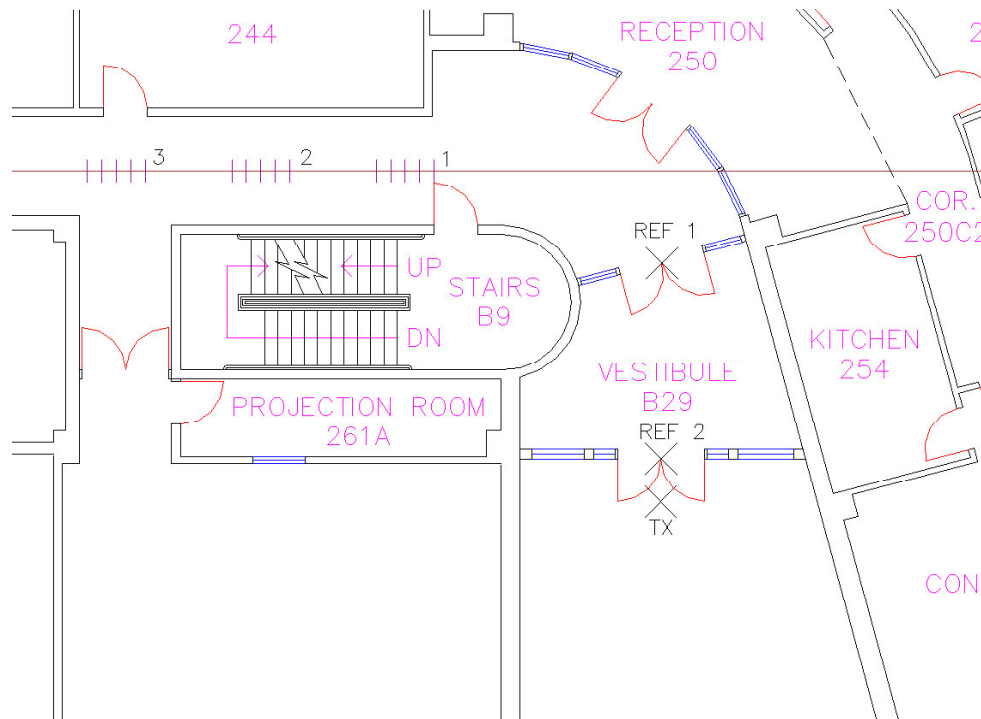


Figure 8.9 Durham Hall Transmitter and Receiver Locations. The transmitter location is the X in the lower right and the receiver is placed a various locations down the center hall on the same level as the transmitter. Two reference measurements were taken. These are located at REF 1 and REF 2 in the vestibule. The receiver locations are approximately 0.3 meters apart

8.3 Appendix III - Outdoor Measurement Locations

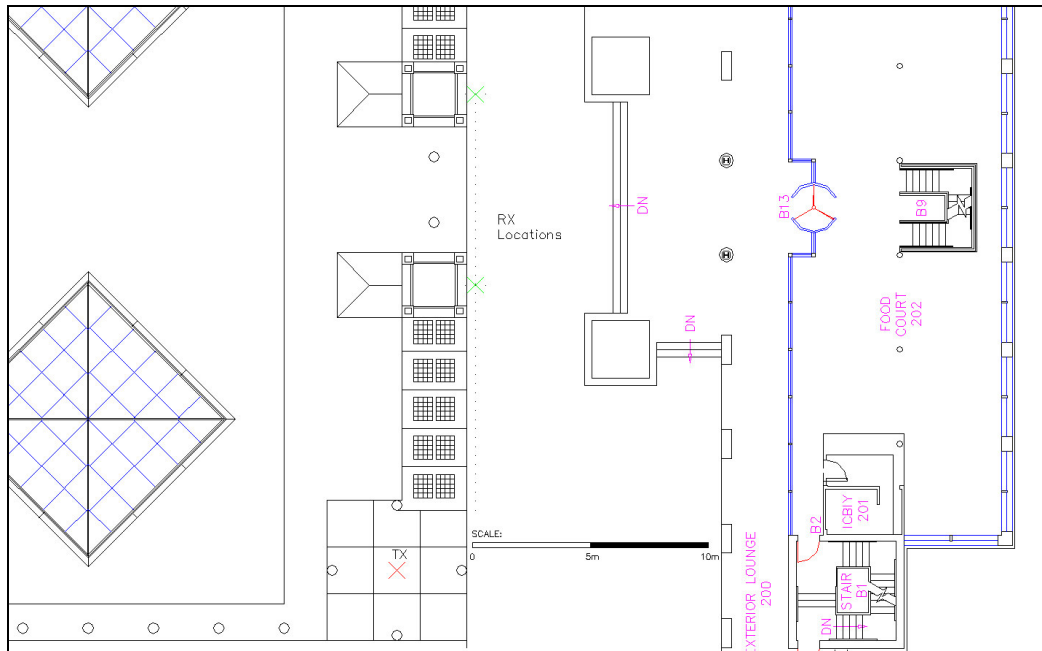


Figure 8.10. Burchard hall Location 1 The receiver is placed next to the two air handlers on top of Burchard (green crosses), and it faces parallel to the path. The transmitter is placed on top of the unfinished stairwell (red cross, lower left) so that the path from the transmitter to receiver is blocked by the air handlers

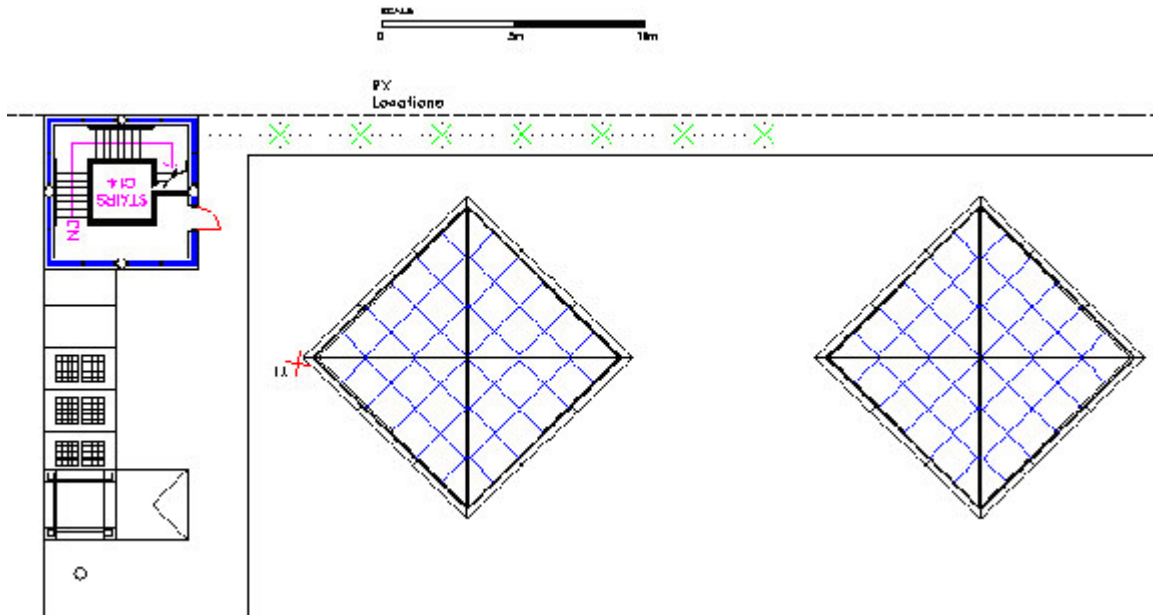


Figure 8.11 Burchard 2 location. Transmitter is placed next to the skylight, facing the stairwell (red cross, center left). The receiver (green crosses) starts 1.5 meters back from the stairwell and moves in 1.5 meter increments. The receiver antenna is facing the stairwell. This gives a line of sight signal that is much weaker than the first multi-path. Most of the received signal comes from the bounce off the stairwell

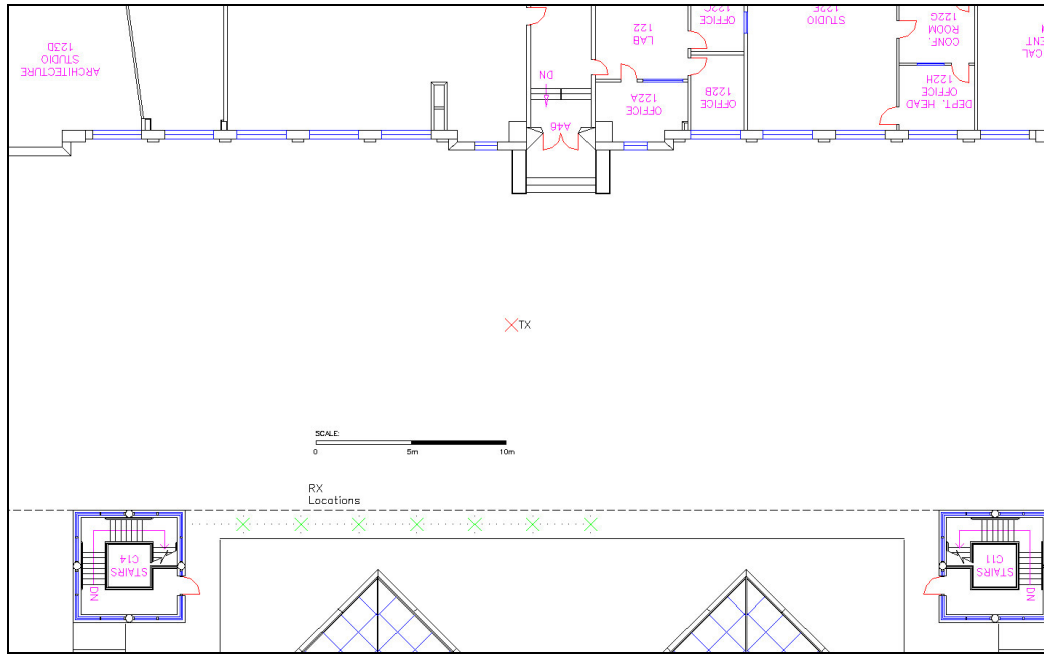


Figure 8.12 Burchard Hall Location 3. The transmitter (red cross, center) is placed between Burruss Hall and Burchard Hall, facing Burchard. The receiver (green crosses, lower center) moves along the same track as in Burchard 2, except that the antenna is now facing Burruss

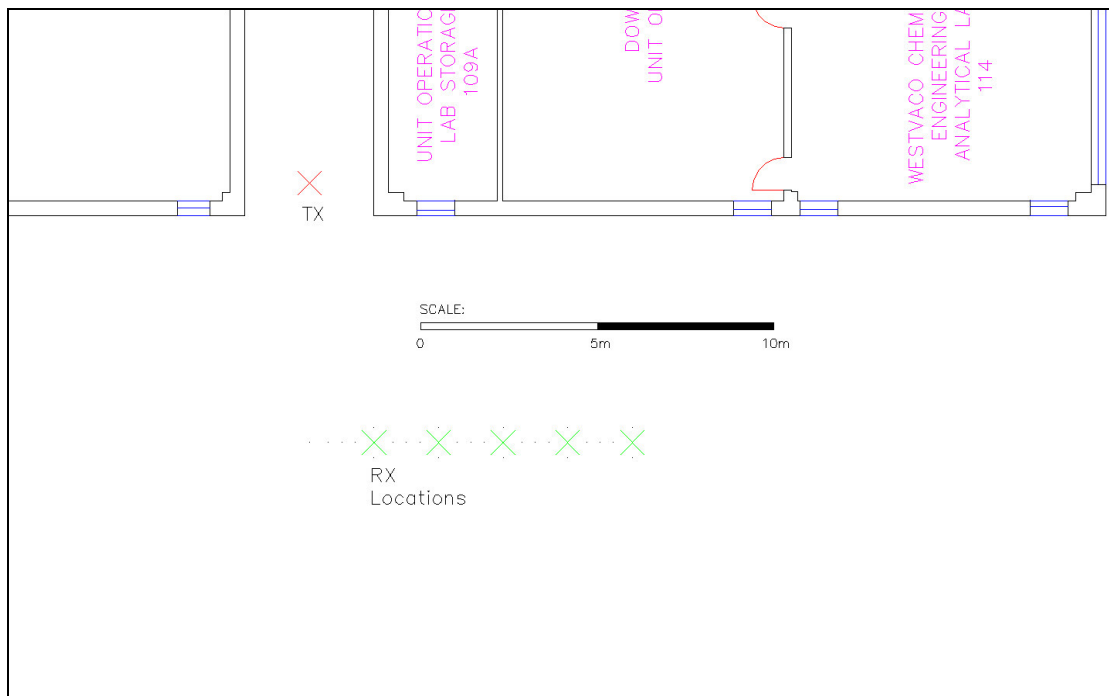


Figure 8.13 Hancock Hall The transmitter (red cross, center) and receiver (green crosses, front center) are placed perpendicular to each other 7.2 meters apart. The receiver moves back 1.5 meters at a time eventually being blocked from the transmitter by Hancock Hall

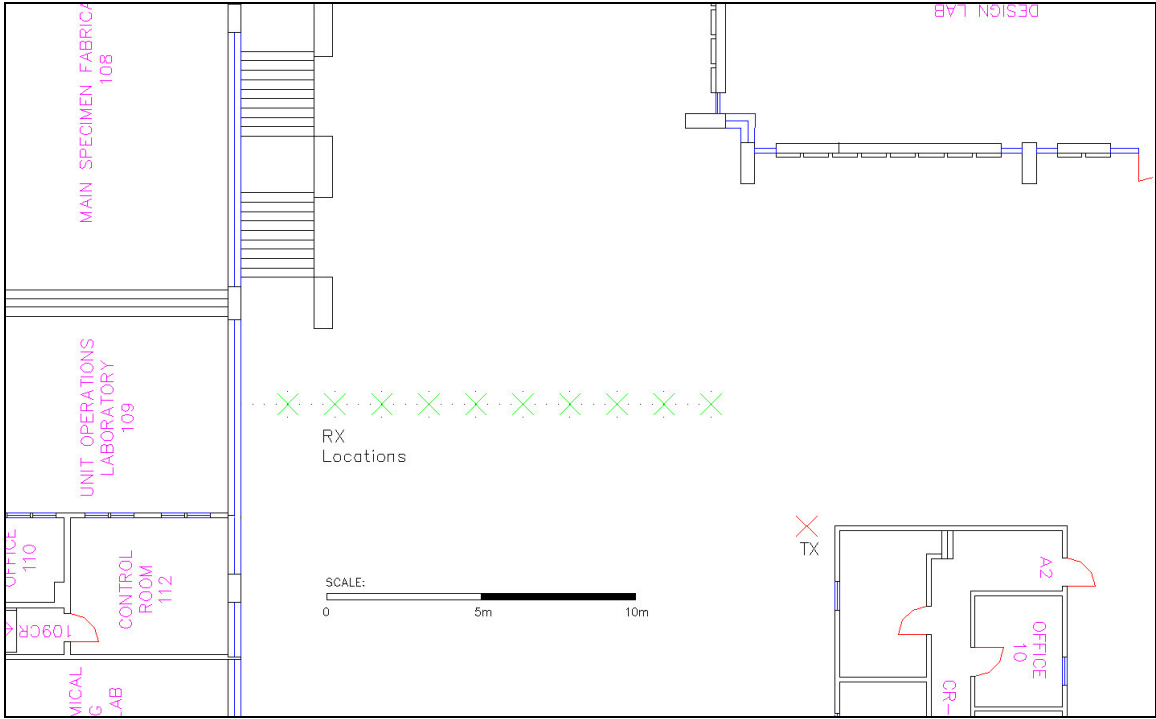


Figure 8.14 Cowgill location. The transmitter (red cross, upper right) and the receiver (green crosses, center) are placed beside each other facing the wall of Hancock. The receiver is moved closer to Hancock 1.5 meters feet at a time. The first multi-path is the strongest as the line of sight signal is received in the side and back lobes of the receiver antenna

9 References

1. Harmuth, H.F, 'Propagation of Non-sinusoidal Electromagnetic Waves (Advances in Electronics and Electron Physics – Supplement 18), Academic Press 1986
2. Authorization of Ultrawideband Technology, First Note and Order, Federal Communications Commission, February 14, 2002
3. Win, M.Z., Scholtz, R.A, 'Impulse radio: how it works' Communications Letters, IEEE, Volume: 2 Issue: 2, Feb. 1998, Page(s): 36 –38
4. Siwiak, K., 'A path link model for Ultrawideband pulse transmissions', VTC 2001, spring, Vol. 2, Page(s): 1181-1183
5. Cassioli, D., Win, M.Z., Molisch, A.F., 'A Statistical Model for the UWB Indoor Channel', IEEE VTC Spring 2001, Vol. 2, Page(s): 1159-1163
6. Welborn M., McCorkle J., 'The importance of Fractional Bandwidth on Ultra-Wideband Pulse design', Communications, 2002. ICC 2002. IEEE International Conference on, Volume: 2, 28 April-2 May 2002, Page(s): 753-757, vol.2
7. Molisch, A.F., Foerster, J.R., Pendergrass, M., 'Channel Models for Ultrawideband Personal Area Networks', IEEE Wireless Communications, Dec. 2003, Page(s): 14-21
8. Win, M.Z.; Ramirez-Mireles, F.; Scholtz, R.A.; Barnes, M.A., 'Ultra-wide bandwidth (UWB) signal propagation for outdoor wireless communications', Vehicular Technology Conference, 1997 IEEE 47th, Volume: 1, 4-7 May 1997, Page(s): 251 -255 vol.1
9. Sanders F., NTIA Report 01-383, January 2001
10. Hamalainen M., Hovinen V., Tesi R., Iinatti J.H.J, Latva-aho M., '*On the UWB System Coexistence with GSM900, UMTS/WCDMA, and GPS*', Selected areas in communication, IEEE Journal on, Vol.20, Issue 9, Dec. 2002, pp 17
11. Sheng H., Orlik P., Haimovich A.M., Cimini L.J Jr., Zhang J., '*On the Spectral and Power Requirements for Ultra-Wideband Transmission*', Communications, 2003. ICC '03. IEEE International Conference on , Volume: 1 , 2003, Page(s): 738 –742

12. Han, Jeongwoo and Cam Nguyen, 'A New Ultra-Wideband, Ultra-Short Monocycle Pulse Generator With Reduced Ringing,' IEEE Microwave and Wireless, Components Letters, Vol. 12, No. 6, June 2002, pp 206 – 208
13. Shlivinski, E. Heyman, R. Kastner, "Antenna Characterization in the Time Domain," IEEE Antennas and Propagation Magazine, Vol. 45, No. 7, July 1997
14. J. A. N. Noronha, T. Bielawa, C. R. Anderson, D. G. Sweeney, S. Licul, and W. A. Davis, "Designing Antennas for UWB Systems," Microwaves & RF, June 2003
15. S. Licul, J. A. N. Noronha, W. A. Davis, D. G. Sweeney, C. R. Anderson and T. Bielawa, "A Parametric Study of Time-Domain Characteristics of Possible UWB Antenna Architectures", VTC Fall 2003
16. T. S. Rappaport, Wireless Communications: Principles and Practice 2nd edition, tice Hall PTR, Upper Saddle River, NJ, 2002
17. Parsons, J.D., 'The Mobile Radio Propagation Channel', John Wiley & Sons, 1992
18. Seidel, S.Y., 'Pathloss and multipath delay statistics in four European cities for 900MHz cellular and microcellular communications', IEEE Elect. Letters, vol.26, Issue 20, Sept. 1990, pp. 1713-1715
19. Devasirvatham, D.M., Murray, R.R., Arnold, H.W., Cox, D.C., 'Four-frequency CW measurements in residential environments for personal communications', 3rd Annual Intl. Conf. on Universal Personal Comm., Oct. 1994, pp. 140-144
20. Patwari, N., Durgin, G.D., Rappaport, T.S., Boyle, R.J., 'Peer-to-peer low antenna outdoor radio wave propagation at 1.8GHz', 49th IEEE VTC, vol.1, May 1999, pp. 371-375
21. Devasirvatham, D.M., Murray, R.R., 'Time delay spread measurements at two frequencies in a small city', IEEE MILCOM, vol. 3, Nov. 1995, pp. 942-946
22. Wepman, J.A., Hoffman, J.R., Loew, L.H., Tanis, W.J. II, Hughes, M.E., 'Impulse response measurements in the 902-928 and 1850-1990 MHz bands in macrocellular environments', 2nd Intl. Conf. on Universal Personal Communications, vol. 2, 1993, pp. 590-594
23. Devasirvatham, D.M., Banerjee, C., Murray, R.R., Rappaport, D.A., 'Two-frequency radiowave propagation measurements in Brooklyn', 1st ICUPC'92, Oct. 1992, pp. 01.05/1 – 01.05/5

24. Paez, I., Loredó, S., Valle, L., Torres, R.P., 'Measuring broadband radio channel parameters using a simple experimental set-up', 13th IEEE Intl. Symp. PIMRC, vol.1, Sept. 2002, pp. 473-477
25. Hendrickson, C., Gerace, G., Yerkes, C., Forgy, J., 'Wideband wireless peer to peer propagation measurements', 33rd Asilomar Conf. on Signals, Systems and Computers, vol. 1, Oct. 1999, pp. 183-189
26. Healey, A., Bianchi, C.H., Sivaprasad, K., 'Wideband outdoor channel sounding at 2.4GHz', IEEE – APS, Nov. 2000, pp. 95-98
27. Kim, K.H., Kim, J.H., Yoon, Y.J., Seok, J.H., Lim, J.W., Shin, Y.S., 'A study on the outdoor propagation channel model for the 5GHz WLAN service', IEEE APS Symposium, vol. 4, 2003, pp. 915-918
28. Zhao, X., Kivinen, J., Vainikainen, P., Skog, K., 'Propagation characteristics for wideband outdoor mobile communications at 5.3 GHz', IEEE JSAC, vol. 20, Issue 3, April 2002, pp. 507-514
29. Durgin, G.D., Kukshya, V., Rappaport, T.S., 'Wideband measurements of angle and delay dispersion for outdoor and indoor peer-to-peer radio channels at 1920 MHz.', IEEE Trans. on Antennas and Propagation, vol. 51, Issue 5, May 2003, pp. 936-944
30. Wepman, J.A., Hoffman, J.R., Loew, L.H., Tanis, W.J. II, Hughes, M.E., 'Impulse response measurements in the 902-928 and 1850-1990 MHz bands in macrocellular environments', 2nd Intl. Conf. on Universal Personal Communications, vol. 2, 1993, pp. 590-594
31. de Toledo, A.F., Turkmani, A.M.D, 'Propagation into and within buildings at 900, 1800 and 2300 MHz', IEEE VTC 1992, vol. 2, pp. 633-636
32. Hoppe, R., Wolfe, G., Landstorfer, F.M., 'Measurement of building penetration loss and propagation models for radio transmission into buildings', IEEE VTC, Fall 1999, vol. 4, pp. 2298-2302
33. Durgin, G., Rappaport, T.S., Hao, Xu., 'Measurements and models for radio path loss and penetration loss in and around homes and trees at 5.85GHz', IEEE Trans. on Communications, vol. 46, Issue 11, Nov. 1998, pp. 1484-1496

34. Karlsson, P., Bergljung, C., Thomsen, E, Borjeson, H., '*Wideband measurement and analysis of penetration loss in the 5GHz band*', IEEE VTC, Fall 1999, vol.4, pp. 2323-2328
35. Zhang, Y.P., Hwang, Y., '*Measurements of the Characteristics of Indoor Penetration Loss*', IEEE VTC, June 1994, pp: 1741-1744, vol. 3
36. Aguirre, S. Loew, L.H., Yeh, Lo, '*Radio propagation into Buildings at 912, 1920 and 5990 MHz using Microcells*', Universal Personal Communications, Third Annual Intl. Conf., 1994, pp. 129-134
37. Costa e Silva, J., Neto, A.G., Nogueira de Carvalho, J., Alencar, M.S., '*Determining the average penetration loss: measurement procedure and results*', SBMO/IEEE MTT-S, APS and LEOS – IMOC 1999, vol. 1, pp. 339-341
38. Tanis, W.J. II, Pilato, G.J., '*Building penetration characteristics of 880 MHz and 1922 MHz radio waves*', IEEE VTC 1993, pp. 206-209
39. Silva, J.S., Alegre, R., Fernandes, C.A., '*Window effect on wall penetration loss in mobile communications*', IEEE APS 2003, vol. 2, pp. 122-125
40. Schwengler, T., Gilbert, M., '*Propagation models at 5.8GHz-path loss and building penetration*', IEEE RAWCON 2000, pp. 119-124
41. Muqaibel, A. H, '*Characterization of Ultra Wideband Communications Channels*', Ph.D Thesis, Virginia Tech, 2003

Vita

Joseph Noronha graduated with a First Class from the University of Mumbai, India in 2001. From 2002 onwards he worked as a Graduate Research Assistant at the Center for Wireless Telecommunications, Virginia Tech under Dr. Dennis Sweeney in the area of Ultrawideband systems. He undertook an Internship with the Center for Remote Sensing Inc., Fairfax VA in 2003 and will be continuing with the firm after graduation specializing in Global Positioning Systems (GPS), software radio architectures and Smart Antennas.